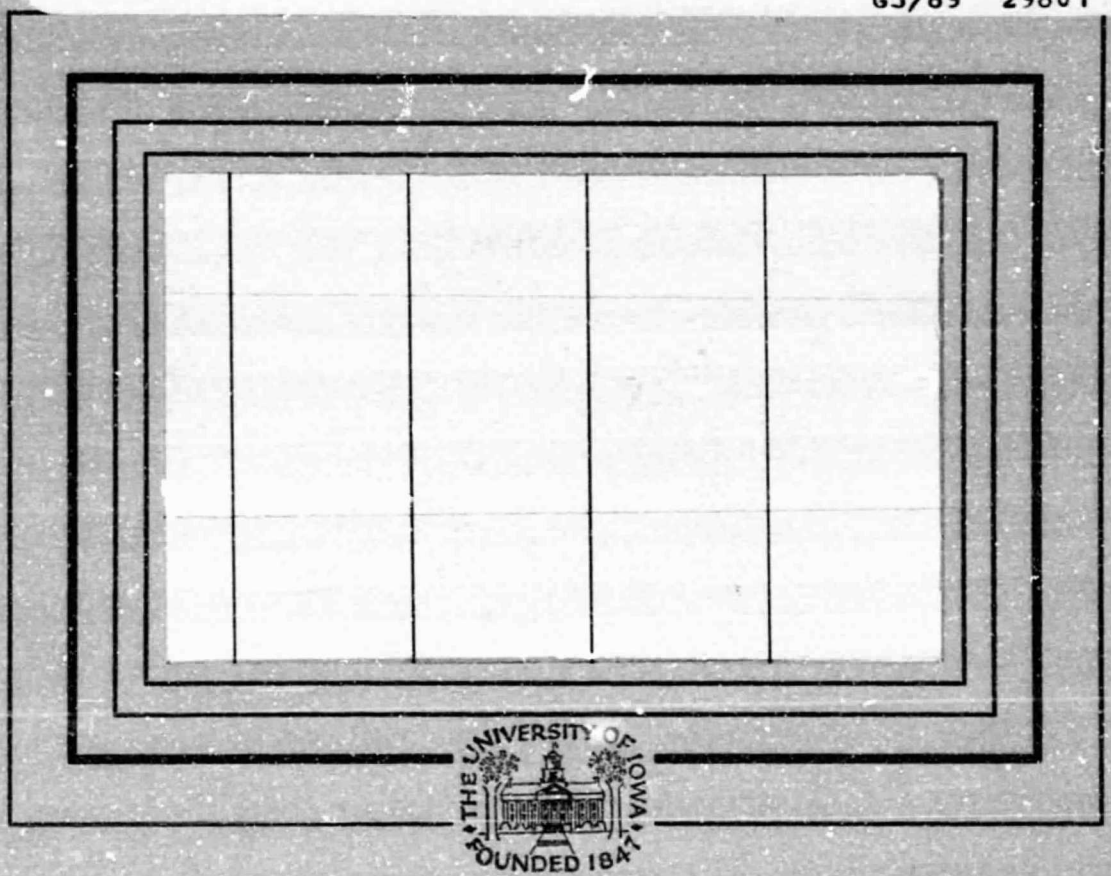

Department of Physics and Astronomy

THE UNIVERSITY OF IOWA

Iowa City, Iowa 52242

U. of Iowa 75-12

A Decametric Wavelength Radio Telescope for Interplanetary Scintillation Observations

by

WILLARD M. CRONYN* and STANLEY D. SHAWHAN**

*Space Environment Laboratory, NOAA, Boulder, Colorado 80302, and
Clark Lake Radio Observatory, Borrego Springs, California 92004

**Department of Physics and Astronomy, University of Iowa, Iowa City, Iowa 52242

March 1975

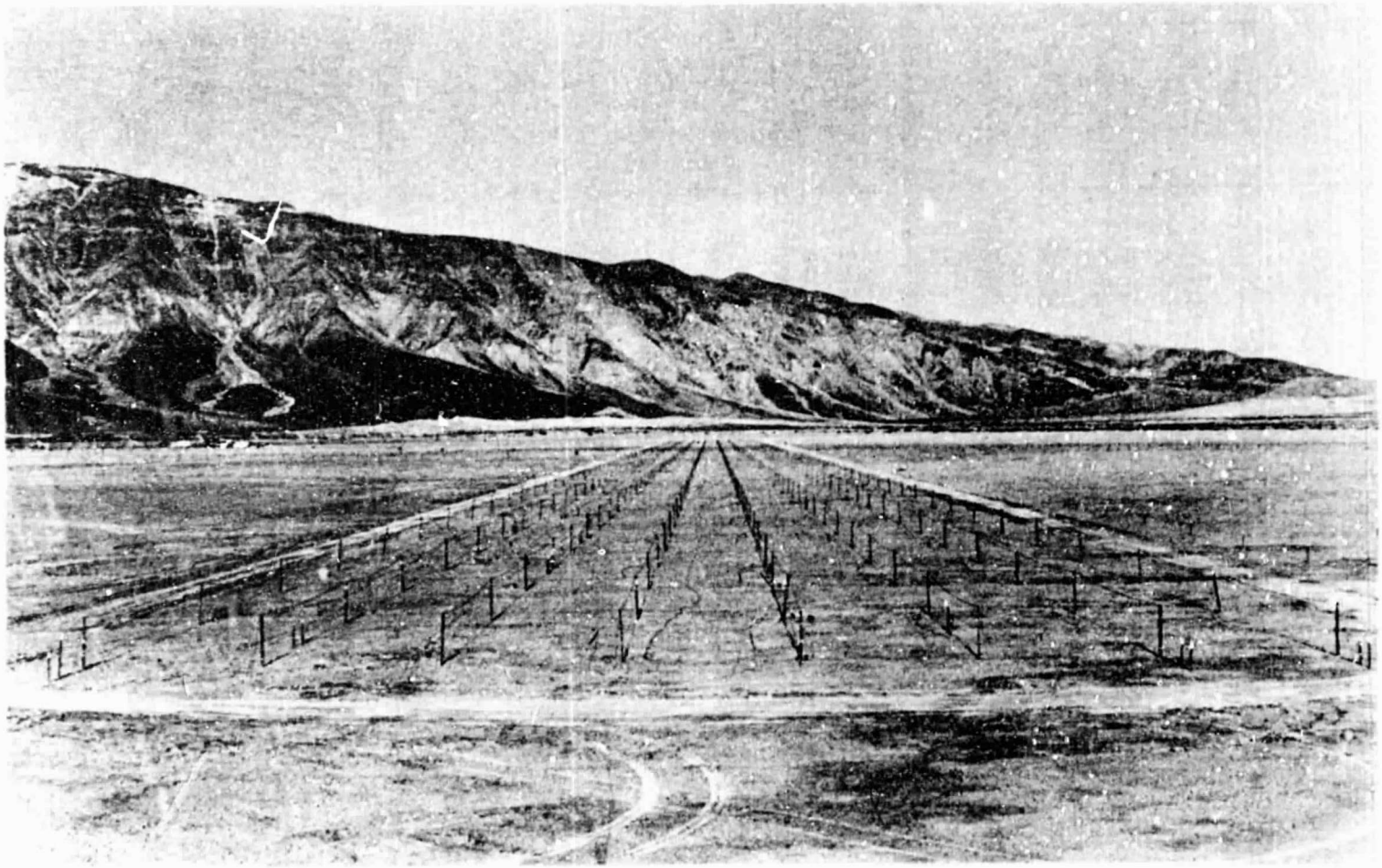

Frontispiece

Photograph of the COCOA-Cross Radio Telescope, looking East along the East-West arm. The poles supporting the coaxial cable are 2 meters high. The arm is 46 meters wide and 1200 meters long. The Santa Rosa Mountains can be seen in the background.

FOREWARD

This report has been prepared to serve as the final project report for NASA Purchase Request S-57016-A and as a progress report and detailed technical description of the Cocoa Cross Radio Telescope which has been funded in part by the Atmospheric Science Section of the National Science Foundation through Grant DES73-06559-A01 and by NASA Grant NGL-16-001-002.

ABSTRACT

A phased array, electrically steerable radio telescope, with a total collecting area of 18 acres (one of the largest in the world) has been constructed for the purpose of remotely sensing electron density irregularity structure in the solar wind. This Cocoa Cross radio telescope will locate, map, and track large scale features of the solar wind, such as streams and blast waves, by monitoring a large grid of natural radio sources subject to rapid intensity fluctuation (interplanetary scintillation) caused by the irregularity structure. Observations have verified the performance of the array, the receiver, the scintillation signal processing circuitry, and, most importantly, the basic scientific utility of the instrument.

TABLE OF CONTENTS

TABLE OF TABLES

1. INTRODUCTION

A decametric wavelength radio telescope, named the Cocoa Cross, to be dedicated to solar wind studies using interplanetary scintillation observations, has been constructed at the Clark Lake Radio Observatory, a University of Maryland facility in Borrego Springs, California. This report is an account of progress to date on construction and operation of the telescope, observations, and initial scientific results. This report describes progress to date as of January 1975.

It had been known for about ten years [Hewish et al., 1964] that small angular diameter natural radio sources display intensity fluctuations on a time scale of about one second. The intensity fluctuations develop because of random diffraction arising from scattering by irregular variations in the interplanetary electron density and are termed IPS (interplanetary scintillation).

Detailed analyses of day-to-day changes in IPS activity revealed associations between the activity and other solar wind phenomena. The emphasis to date in IPS observations oriented towards studies of the solar wind had been on three areas: (1) statistics of dynamical features, i.e., auto-correlation analyses of scintillation activity to find 27 day synodic

periodicities, cross-correlation of solar wind activity (as deduced from IPS measurements) and IPS activity, cross-correlation of IPS data with solar disc, space probe, and terrestrial data [Burnell, 1969; Houminer, 1971; Houminer and Hewish, 1972; Watanabe and Kakinuma, 1972; Houminer, 1973a; Coles et al., 1974]; (2) detailed analyses of specific solar wind events in which IPS data contributed to a self-consistent description involving a variety of solar-terrestrial and space probe data [Sharp and Harris, 1967; Wiseman and Dennison, 1972; Ward, 1974; Rickett, 1973; Watanabe et al., 1973a, b; Armstrong et al., 1973]; and (3) analyses of ambient solar wind parameters such as plasma density spectrum and solar wind speed dependence on solar latitude [Dennison and Hewish, 1967; Matheson and Little, 1971; Coles and Maagoe, 1972; Cronyn, 1972; Houminer, 1973b; Rickett, 1973; Coles et al., 1974]. However, no synoptic observational program of more than a few weeks' duration had ever been undertaken to locate, map, and track such structures [Wiseman and Dennison, 1972]. The reason was primarily a lack of suitable instrumentation, i.e., a radio telescope of large collecting area which could be dedicated to solar wind studies. We felt that an instrument that could observe a large number of sources (to serve as a background grid against which solar wind features could be observed) would make a significant contribution to an understanding of solar wind phenomena.

The instrument we proposed in 1972 which led to the NASA Purchase Request S-57016-A could, we estimated, observe at least 50 more-or-less randomly distributed IPS sources for which the line of sight trajectory passed no closer to the sun that 0.5 A.U. (Sources at smaller elongation angles would probably not scintillate due to a combination of non-zero angular size, increasing scattering strength, and the well-known IPS source resolution effect.) The operating frequency we chose, 34.3 MHz, is in the middle of an interference-free band at the Clark Lake Radio Observatory. It is high enough to preclude the occurrence of ionospherically propagated interference, but low enough to provide high sensitivity to the weakly scattering region beyond 1 A.U.

The scientific objectives are listed below as they appeared in the NASA proposal. They still stand as the current objectives although there are no plans to do any long baseline interferometry or multiple site observations. Presently the four major planets are being observed for dekametric emissions with which to at least set an upper limit (~1 flux unit). The sun is not being observed but the secondary observing program includes radio flare stars, pulsars, and x-ray stars.

2. SCIENTIFIC OBJECTIVES

2.1 Primary Objectives

Primary objectives of interplanetary scintillation observations:

(1) Monitoring scintillation activity parameters (index, spectral width, power law index) along a large number of trajectories through the interplanetary medium beyond 0.5 A.U. from the sun, disseminating such information in preliminary form on a real time basis and compiling activity compendia for future reference.

(2) Deducing the location of co-rotating streamers and other non-transient structural features of the interplanetary medium from gross scintillation activity and detailed analyses of IPS power spectra.

(3) Locating and tracking transient (non-co-rotating) features, such as blast waves and localized turbulent plasma structures, to study their evolution as a function of time and heliocentric distance, their interaction with Earth, Jupiter, and comets, their association with solar phenomena, and other aspects of the origin and dynamics of such features.

(4) Forecasting interception of both transient and non-transient features by space probes, Earth, Jupiter, and comets.

(5) Explicitly extending objectives (2) and (3) out of the ecliptic plane.

(6) Measuring the small-scale electron density fluctuation spectrum.

(7) Serving as the large collecting area end of very long baseline interferometry experiments oriented strictly toward studies of large scale irregularity structure of the interplanetary medium.

(8) Serving as the large collecting area station of multiple site total power, IPS observations to make direct measurements of the diffraction pattern velocity (i.e., the projection of the solar wind velocity onto the plane transverse to the source-observer ray trajectory).

2.2 Secondary Objectives

Secondary objectives requiring no more than 5 percent of the total observing time on the array:

(1) Solar observations.

(2) Planetary observations (Jovian emission and, if detected, emissions from other planets).

3. INSTRUMENTATION AND GENERAL FACILITY DESCRIPTION

3.1 Site Selection and Schedule of Progress to Date

A number of factors -- noise level, isolation, weather, terrain, available land area, and an established radio observatory -- made us decide to erect the array at the Clark Lake Radio Observatory, a University of Maryland facility located near Borrego Springs, California (see Figure 1). The major construction costs for the array were supported by the National Aeronautics and Space Administration (NASA), Goddard Space Flight Center. Construction was carried out through joint efforts of the Space Environment Laboratory (SEL) of the National Oceanic and Atmospheric Administration (NOAA) and the Department of Physics and Astronomy, University of Iowa. Continuing support has been provided through these two institutions and through the National Science Foundation under Grant DES73-06559. The array is now (January 1975) in full automatic, unattended 24 hour/day, 7 day/week operation. About 120 sources/day are being observed, of which more than 65 display IPS.

Figure 1. Clark Lake Radio Observatory and Vicinity in Southern California.

3.2 Antenna Element and Array Design

3.2.1 Element

The basic [Balsley-Ecklund, 1972] antenna element is shown schematically in Figure 2. It is made up of a number of half wavelength colinear sections of coaxial cable connected together; the inner conductor on each section is connected to the outer conductor (shield) on the next section and vice versa. Note the origin of the acronym "COCOA", COlinear COAxial, to describe the element. Balanced transmission line is connected to the adjacent pair of outer conductors at the center of the element. The result is a rectified sine wave current distribution on the element with the phase of the current essentially constant throughout its length. The elements are polarized east-west and supported approximately one-quarter wavelength above ground by 2" x 2" posts on "Parafil" rope, a unique rope with a black polyethylene outer jacket and polyester thread core which has superb UV and weather resistance. No metallic ground plane is used.

Element lengths were determined by the requirement that the array be capable of observing a source for ± 4° of meridian transit or about 30 minutes of time. The east-west arm elements are shorter than those in the north-south arm to avoid excessive grating lobe responses. Photographs of the elements are shown in Figures 3a, 3b, 3c, 3d, and 3e.

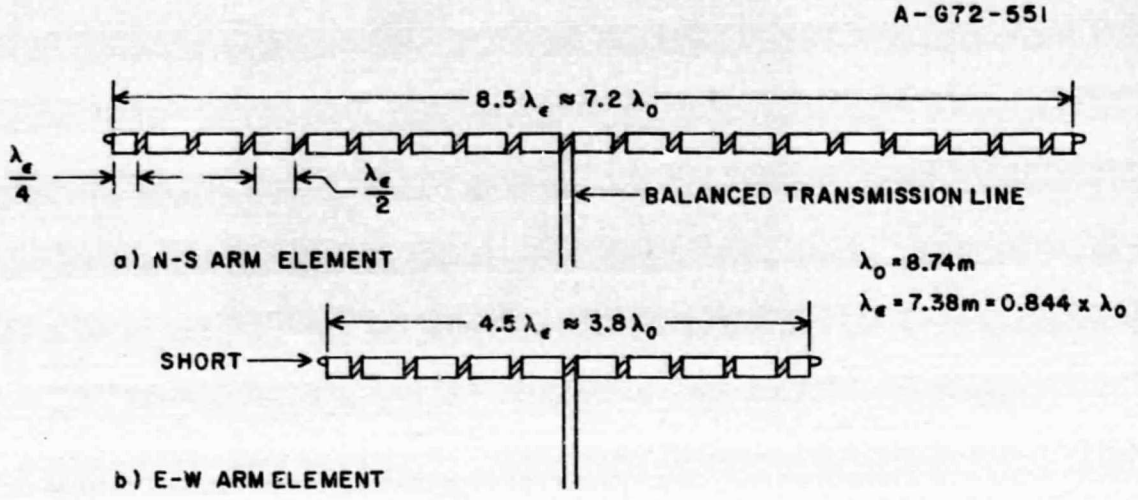

Figure 2. Simplified illustration of coaxial, colinear elements used in (a) north-south arm and (b) east-west arm of the scintillation array. Elements are supported 1.8 m above ground on messenger rope tied to 5 cm wooden support poles spaced about 16 m apart. Velocity factor and impedance of RG-62B cable are 0.844 and 93 ohms, respectively. Element impedances are (a) 85 ohms and (b) 160 ohms. Commercial and homemade 450 ohm ladder line is used to feed the elements; stubbing is required to tune out the resultant mismatch. λ_o = free space wavelength, λ_e = wavelength in coax.

Figure 3a. Antenna Element Center. Ladder line is attached to element pig-tails using "Nicopress" sleeves. Pig-tails are wrapped around outer shields of adjoining cable sections. Normally, center is encased in protective coating of epoxy.

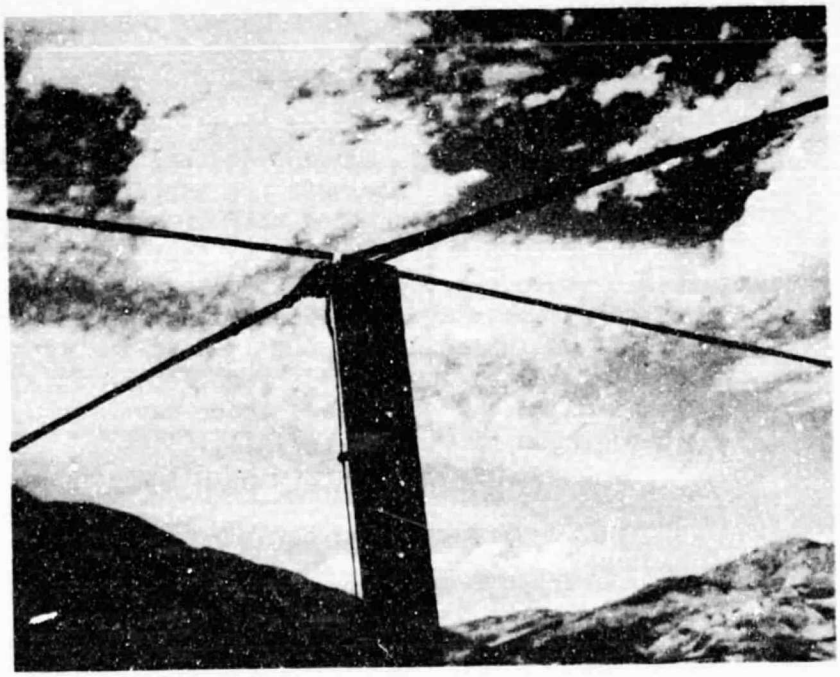

Figure 3b. Antenna Element Center. Ladder line and "Nicopress" crimp may be clearly seen. North-south "Parafil" rope is for guy support on redwood 2 x 2 post.

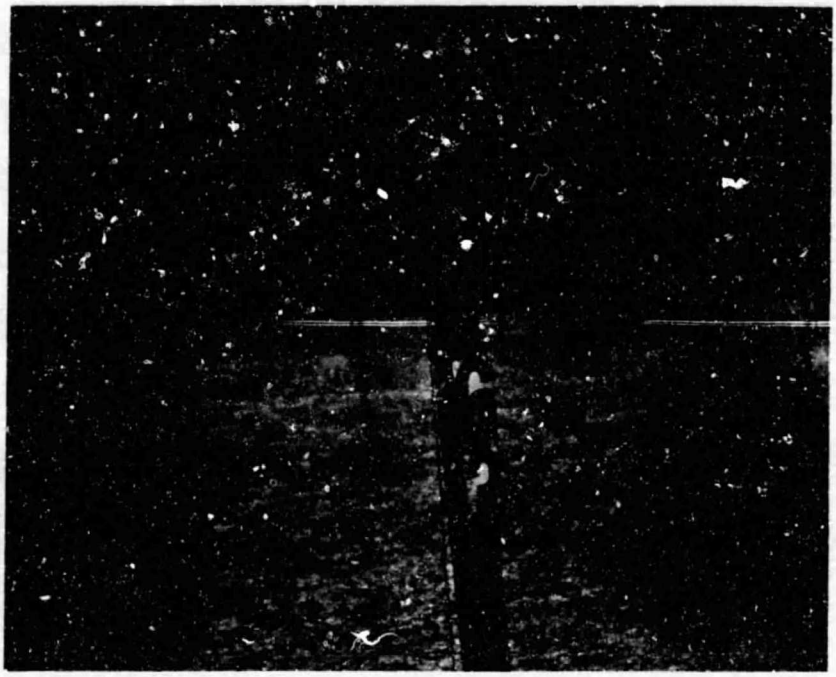

Figure 3c. Antenna Element Center. Number specifies location of pole in south arm. Ladder line is 18 gauge copperweld wire, 1 inch spacing to give characteristic impedance of 450 ohms. Line at lower left is part of impedance matching stub.

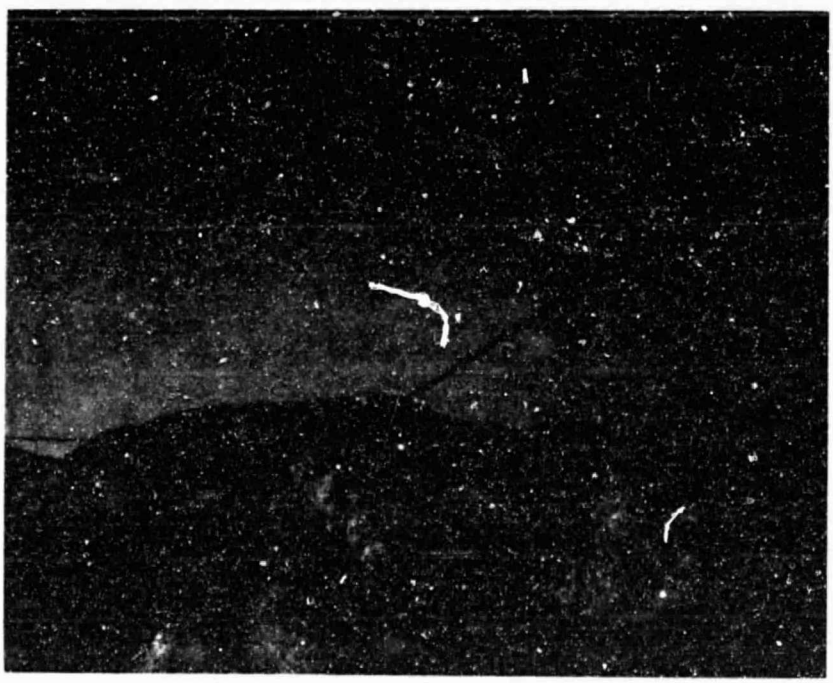

Figure 3d. Antenna Element Center. Arrow shows location of joint between adjoining sections.

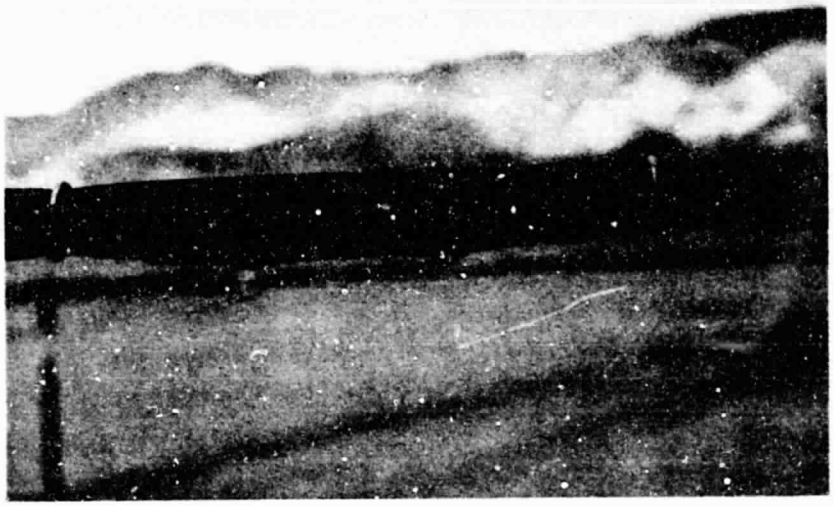

Figure 3e. Joint Detail. Inner and outer coax conductors are interchanged between adjoining sections. Hog-rings used for strain relief can be seen under the shrink fit tubing which seals the joint. Element is attached to "Parafil" rope with hog-rings.

This type of coaxial transmission line antenna element has been used successfully in at least two large antenna arrays: the 20 acre incoherent-scatter array of the Jicamarca Radar Observatory near Lima, Peru [Ochs, 1965] and an auroral radar array [Balsley and Ecklund, 1972]. The material and labor cost involved in fabricating this type of element is substantially lower than the wire-dipole type elements we originally proposed. It also had the advantage that it could be fabricated remotely (at the University of Iowa) and shipped to Clark Lake for field installation.

Although our element is quite similar to the Balsley-Ecklund element, there are several significant physical and electrical differences. The elements are terminated in quarter-wavelength shorted sections of coax rather than open-circuited half wavelength sections. We used RG-62B coaxial cable which has a higher velocity factor than most other types of coax (0.84 vs 0.66). We thus reduce the number (and hence fabrication cost) of individual half-wavelength sections (for a given collecting area) by about 25 percent, an important consideration since there are 4096 half-wavelength and 768 quarter-wavelength sections in the array.

The north-south element has an impedance of 85 ohms, essentially purely resistive at the design frequency, and a beamwidth of about 8° as determined from total power observations of radio sources. The impedance of the east-west element is about 160 ohms, also essentially purely resistive. Bandwidth of the element for a VSWR of less than 1.5 : 1 is 1.8 MHz.

3.2.2 Array

Configuration and Feed. The array has the "Mills' Cross" configuration shown in Figure 4. The total collecting area is about 7.2×10^4 m^2, making it one of the largest radio telescopes in the world, as indicated by Table 1. The complete east-west arm has a beam about 0.4° E-W x 11° N-S, while the north-south arm has a beam 0.6' sec (z) N-S x 8° E-W, z = zenith angle. In the normal (N-S) x (E-W) correlation mode the product beam is 0.6° sec (z) N-S x 0.4° E-W. Photographs of the array and construction details are shown in Figures 5a through 5f and in Figure 6. A list of technical specifications is given in Table 2.

The north-south arm feed system is shown in Figure 7a. It is basically a branch feed system (also known as "corporate" or "Christmas Tree" feed) in which pairs of elements are combined, then pairs of pairs, etc. The same procedure is followed in the east-west arm (Figure 7b).

Because of the relatively high attenuation through the feed system, it is necessary to amplify the output of each arm at the center of the arm to prevent any degradation of signal-to-noise ratio. The amplifiers were designed by Gerry Reeve of National Bureau of Standards (NBS) and feature excess noise temperatures of less than 140 °K, gain of over 30 db, and high stability. The amplifiers are placed in insulation-filled plastic pipe about 2 feet underground for thermal stability.

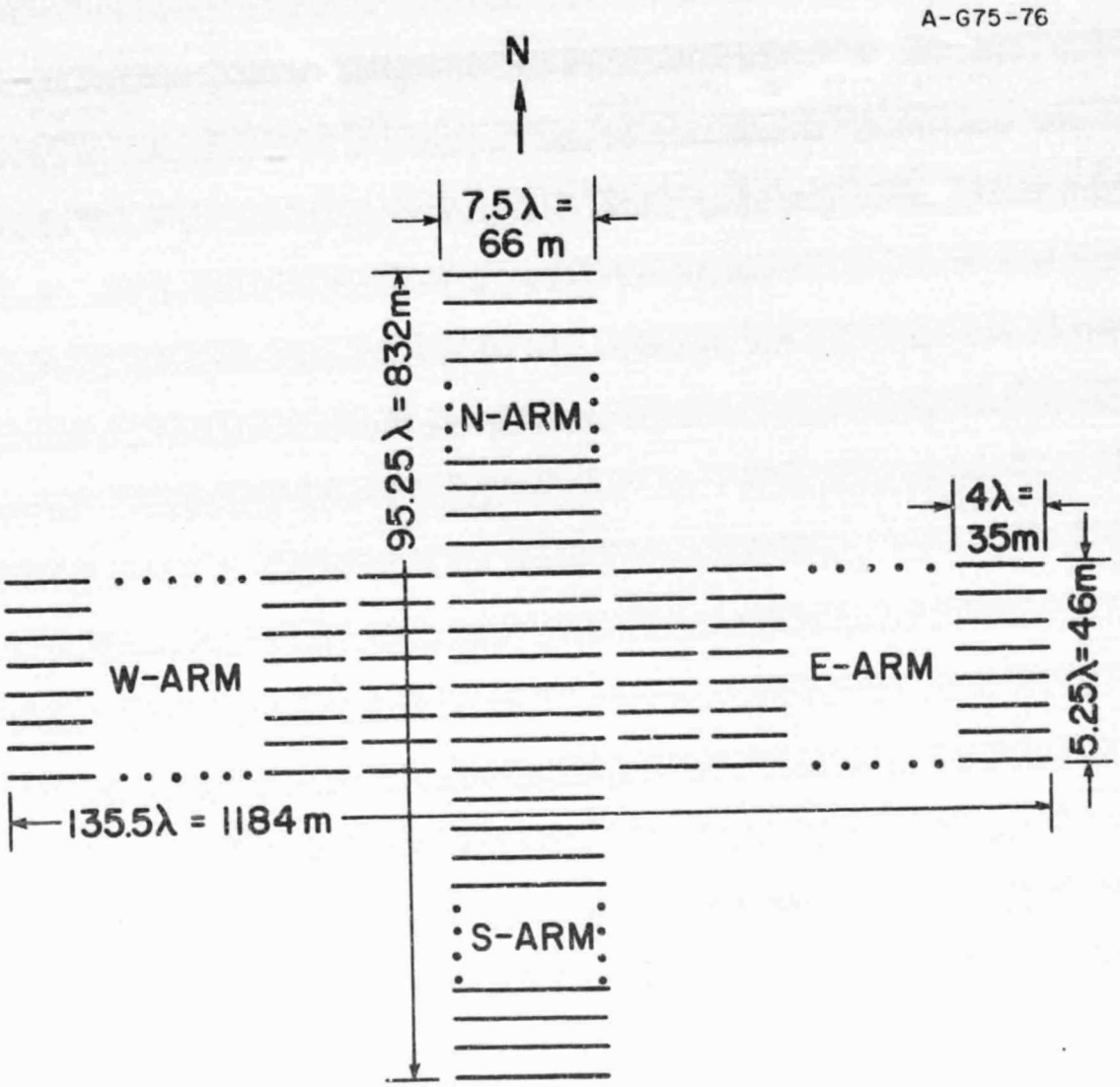

Figure 4. Pictorial sketch of Cocoa Cross layout with external dimensions. The elements are polarized E-W. The N-S arm consists of 128 elements and the E-W arm 256.

Table 1. Collecting Areas of the Largest Radio Telescopes and Radio Telescopes Used for Interplanetary Scintillation Observations.

Name and Location	Type of Telescope	Effective Collecting Area ÷ 10^4 m^2	Frequency (MHz)
Dominion Radio Astrophysical Obs. Penticton, B.C., Can.	Mills "T"**	19.5	10
	Mills "T"	6.5	22
Jicamarca Radio Obs. Lima, Peru	Square Filled*** Aperture	8.1	50
Serpukhov Radiophysical Station Serpukhov, U.S.S.R.	Twin Parabolic Cyl.	8.0	400
CLARK LAKE RADIO OBS. Borrego Springs, Calif.	"Mills" Cross (Iowa)*	7.2	34
	Mills "T" (U. Md.)	1.8 (at 34 MHz; area $\propto \lambda^2$)	15-130
UCSD, La Jolla, Calif.			
+ La Posta, Calif.	Square Filled Aperture*	0.4	73
+ Carlsbad, Calif.	Square Filled Aperture*	0.4	73
+ Desert Center, Calif.	Square Filled Aperture*	0.2	73
+ Borrego Springs, Calif.	Square Filled Aperture*	0.4	73
U. Bologna Obs. Medicina, Italy	"Mills" Cross	3.5	408
U. Florida Radio Obs. Dixie County, Fla.	Rectangular Filled Aperture	3.0	26
Arecibo Obs. Arecibo, P.R.	Spherical Reflector*	2.2 (at 317 MHz)	40-600
Mullard Radio Astro. Obs. Cambridge, England	Rectangular Filled Aperture	2.0	81
Molonglo River Obs. Hoskintown, N.S.W., Austr.	"Mills" Cross	1.7	111, 408
Catacamund Obs. Catacamund, India	Parabolic Cylinder*	0.95	325
Solar Physics Obs. Culgoora, N.S.W., Austr.	Circular Array*	0.6	80
+ Toyokawa Obs. Toyokawa, Japan	Dipole Array*	0.2	69
+ Fujigane Obs. Fujigane, Japan	Dipole Array*	0.1	69
+ Sugadaira Obs. Sugadaira, Japan	Dipole Array*	0.1	69

*Radio telescopes on which substantial amounts of observing time have been, or will be, allocated to IPS observations.
**No longer operational.
***Very little observing time has been allocated to radio astronomical studies.
+Groups of radio telescopes which are operated together to measure solar wind velocity from drifting IPS diffraction pattern.

Figure 5a. Truck caravan used for installing the 2" x 2" supporting posts. The leading ladder truck was equipped with a water tank and compressor to wet the clay ground and with a generator to power an electric drill with a 2" soil auger. Posts were then pounded into the holes.

Figure 5b. Jeep and jack-hammer assembly used to drive ground anchors into the ground. The anchors were used to tie off the Parafil ropes.

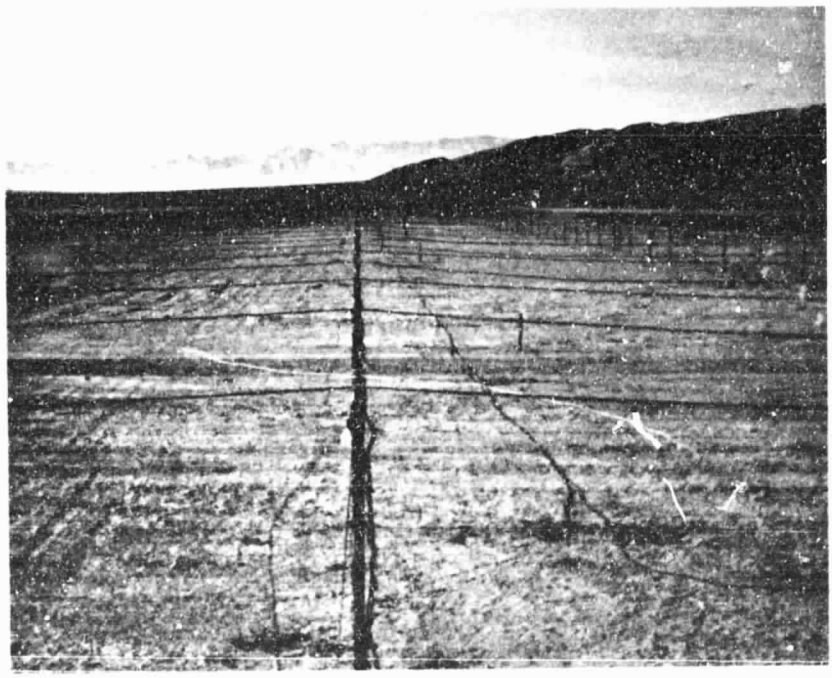

Figure 5c. View looking south from north end of north arm. Elements are supported on 8 foot redwood 2 x 2's placed in 20 inch deep holes. Five poles are used to support each element.

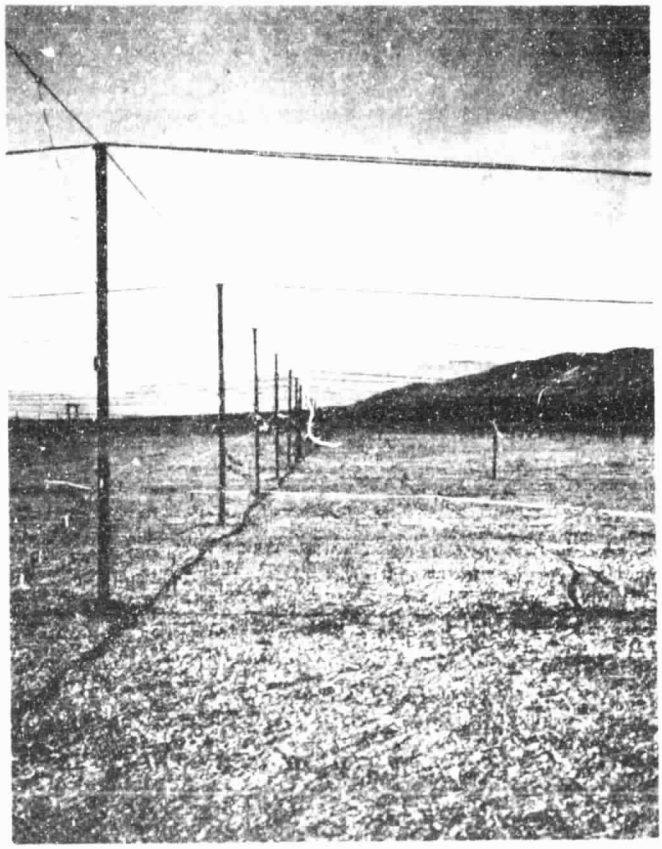

Figure 5d. Another view of the north arm looking south. The phasing fan is attached to line 1 (about 1/4 the way up the pole). The physical arm of line 2 can also be seen (white spacer latter line) on the foreground pole. Short pole at right center supports a line 5 8-way fan.

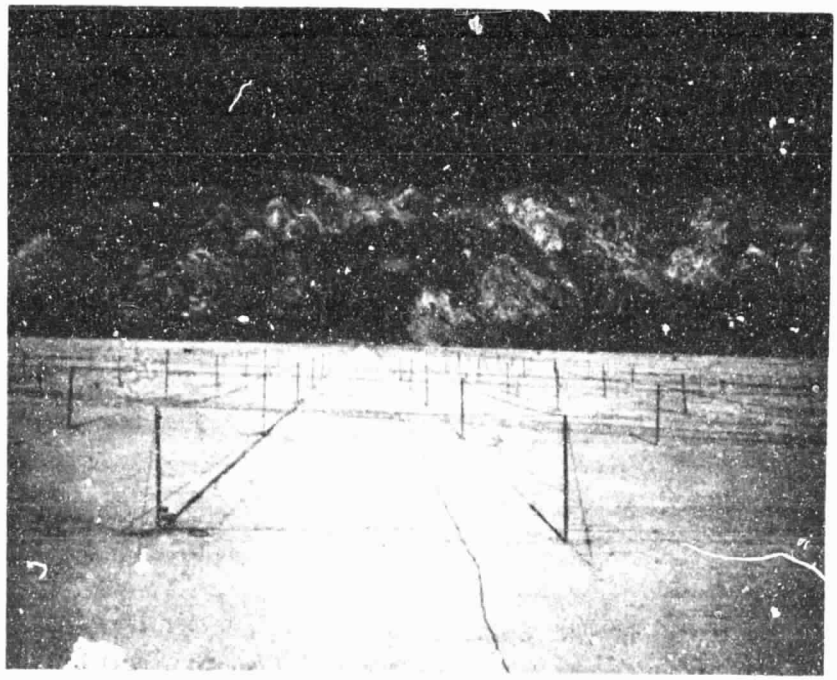

Figure 5e. View looking west from east end of east arm. The 8 east-west lines of elements can be seen.

Figure 5f. Looking north along east end of east arm. The upper north-south ladder line is line 2 for north-south phasing of the 8 element column. The bottom line is line 4 which connects the column to east-west lines located along the northern edge of the arm. The NOAA/U. of Iowa trailer can be seen in the distance.

Figure 6. Construction details for securing ends of "Parafil" messenger and support ropes. The hot-galvanized cast iron ground anchor, with its 12 gauge stainless steel anchor wire attached as shown, is driven about 2 feet into the ground with a compressed air jack hammer. The wire loop is secured with a "Nicopress" sleeve, as is the "Parafil" rope. The extremely high alkaline content of the soil makes the use of corrosion-resistant metals essential. Both the hardware and the overall installation technique were developed by the University of Maryland staff at Clark Lake.

Table 2. Parameters of the Cocoa-Cross Radio Telescope

A.	Array Type	Mills Cross	135.5λ EW x 95.25λ NW
B.	Linear Dimensions	NW Arm	66m EW x 832m NS
		EW Arms	1184m EW x 46m NS
C.	Antenna Elements	Type	Balsley-Ecklund Colinear-Coaxial
		Polarization	East-West
		Length	NS Arm 7.2λ EW Arm 3.8λ
		EW Beamwidth	NS Arm 8° EW Arm 15°
D.	Element Organization	NS Arm	128 elements spaced 0.75λ NS
		EW Arm	256 elements in 32 banks spaced 4λ EW with 8 elements per bank spaced 0.75λ NS
E.	Feed and Phasing	Branch feed, diode-switch-controlled tapped phasing lines with real-time delay control for wideband coherence	
F.	Steering	NS	± 60° from zenith, 33° ± 60° in declination
		EW	Meridian transit ± 10 minutes
G.	Beamwidth	NS Arm	8° EW x 0.6° secant (z) NS
		EW Arm	0.4° EW x 11° NS
		Composite	0.4° EW x 0.6° secant (z) NS
H.	Collecting Area	NS Arm	3.5×10^4 m^2
		EW Arm	3.7×10^4 m^2
		Total	7.2×10^4 m^2
I.	Array Response	$26°K/10^{-26}W/m^2$-Hz	(Uniform illumination)
J.	Center Frequency	34.3 MHz	(λ = 8.75 meters)
K.	Bandwidth	1 MHz maximum	

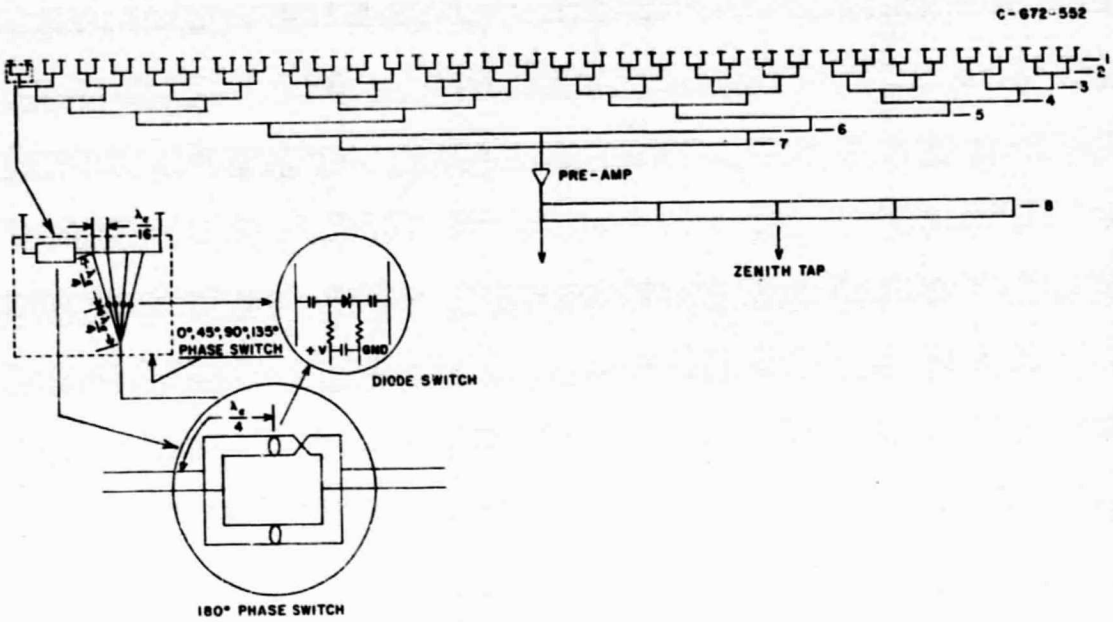

Figure 7a. Simplified schematic of branch feed system for north (or south) arm. All transmission lines are balanced open wire. Elements are oriented east-west. Diode switches are turned on for all phase tap lines except desired tap, thereby reflecting open circuits back to both the tapped line and the fan-in point. Signal travels down phase tap line on which diode switch has been turned off. Phasing switches on lines 1, 2, and 5 are 4 position, as shown; 3 and 4 are 8 position; 6 is two position (at each of the 3 delay taps). Relative phase increment of n-position switch is 180°/n. Taps on lines 7 and 8 are for incremental real time delay equalization sufficient for 1 MHz bandwidth.

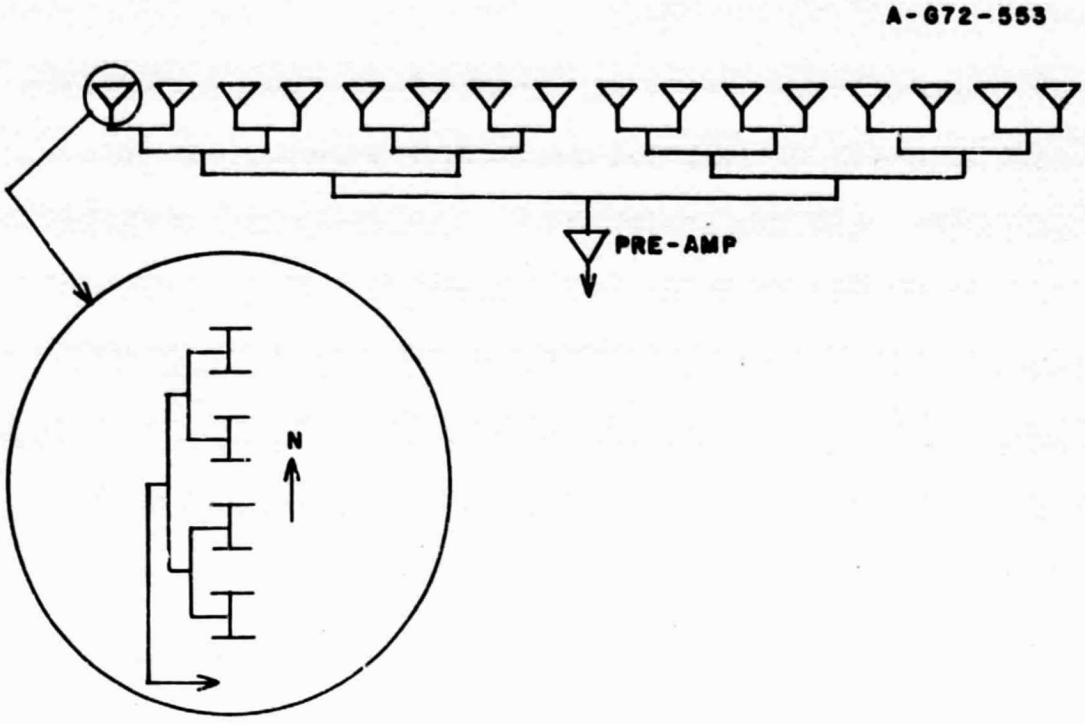

Figure 7b. Simplified schematic of branch feed system for east (or west) arm. Each north-south column of 8 elements is combined in a north-south branch feed, as shown in insert. The 16 columns are then combined in the east-west branch feed system for each half of the east-west arm. The north-south column feeds and east-west feed have the same type of beam steering phase switches as the north-south feed shown in Figure 7a. No provision for real time delay equalization is necessary because of the restricted east-west steering ($\pm$ 4° of meridian).

Phasing System and Beam Steering. Beam steering is accomplished by changing the point at which the signals from a pair of elements (or a pair of pairs, etc.) are combined and delivered to the next transmission line hierarchy. The signals are combined in relative phases of 0°-180° $\times$ (1 - 1/n) provded by the tapped line and another 180° provided by a phase-reversal switch. Details of the phase switches are shown in the circled inserts in Figure 7a. Real time delays in the north-south arm are large enough over the $\pm$ 60° zenith angle coverage for a (maximum) system bandwidth of 1 MHz that real time delay equalization is required as shown.

Photographs of both tapped phasing lines and reversing switches are shown in Figures 8a to 8f. Measured VSWR is less than 1.1 : 1 for the different tap points.

All observations until about 1 June 1974 were made by using the toggle switch control box (shown in Figure 9) which controlled the phasing fan diode switches. Each toggle switch turned on or off all the diode switches on any one fan position in a hierarchy, i.e., each line 1 toggle switch in the north-south arm controls 64 diode switches, each line 2 toggle switch controls 32 diode switches, etc. The toggle switch settings are computed for each beam position by the beam steering program "ALLIN1", a sample of which is shown in Figure 10.

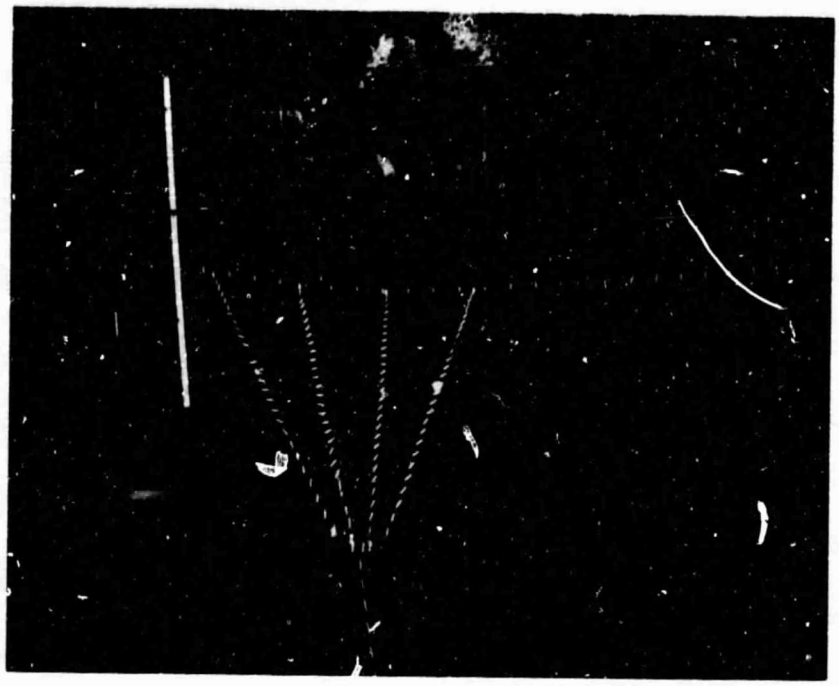

Figure 8a. Four-way north-south phasing fan on line 3 in east arm. The line 3 reversing switch can be seen to the right of the fan, and a line 1 reversing switch to the left near the bottom. This photograph, and Figures 8b and 8c, were taken after an unusually heavy rain which fell in early January, 1974, and inundated the "dry" lake with more than 3.5 inches of water.

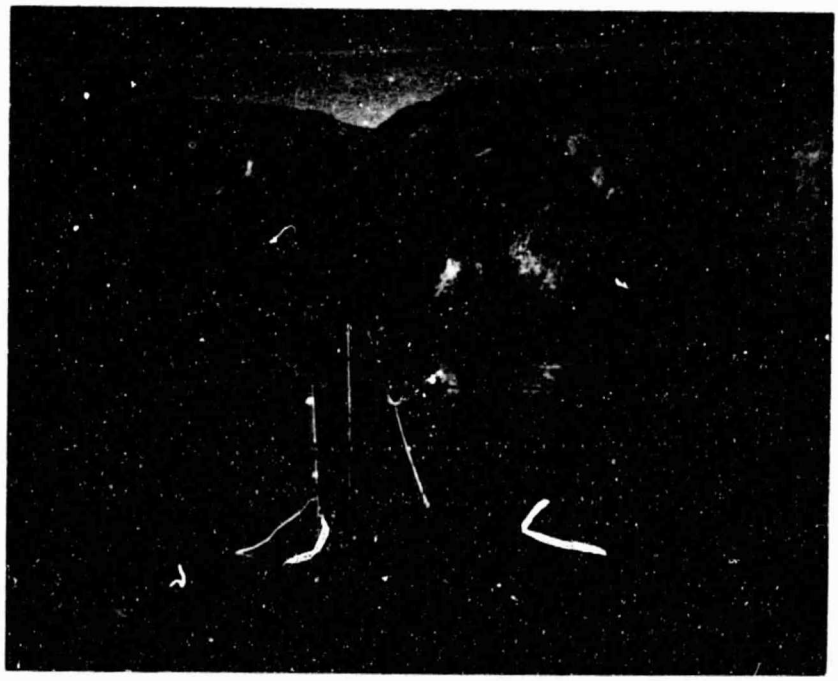

Figure 8b. A larger scale picture of the same fan showing the output line going to line 4. On line 4 the signal is directed north to an east-west phasing line which combines signals from pairs of columns.

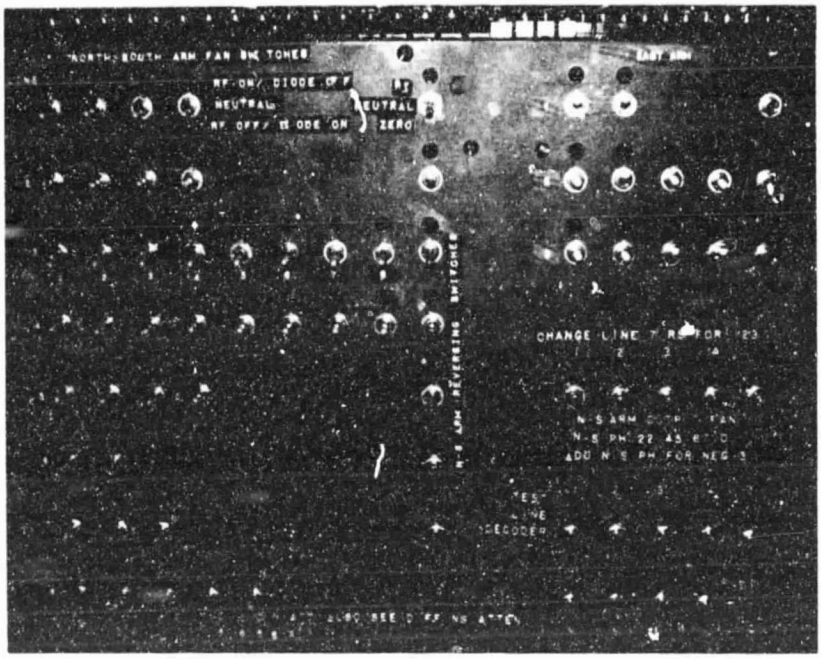

Figure 9. Manual Control Phase Switch Box. Each fan toggle switch controls all the diode switches (in its hierarchy) which are at the position indicated on the panel. Thus each NS arm line 1 toggle switch controls 64 diode switches. Also shown are the toggle switches for controlling NS steering of the EW arm (upper right), NS arm fine-phasing (middle), and test line switches. The on-off switches for the array amplifiers are on the bottom right. This manual switching system has been replaced by a card-reader-controlled system.

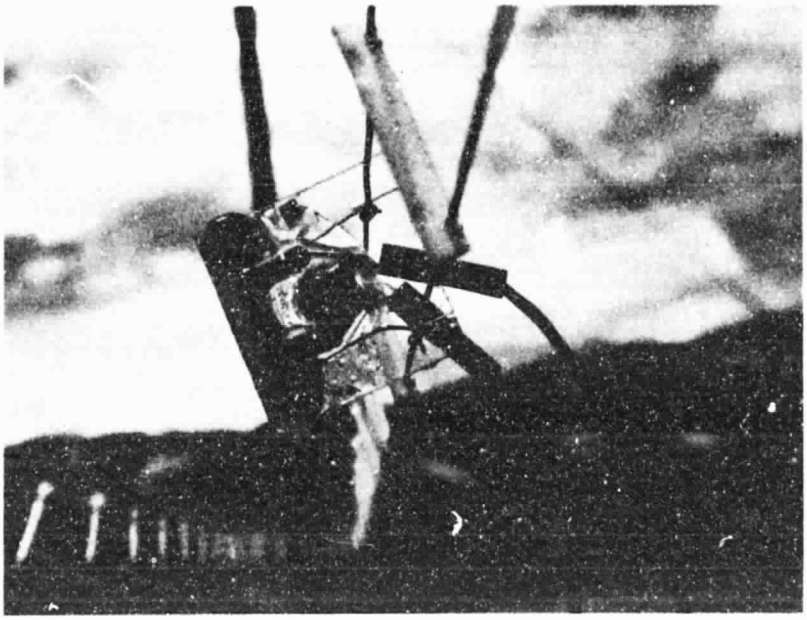

Figure 8d. Diode Switch Assembly. The switches are constructed and attached to precut ladder lines at the University of Iowa. The lines were installed at Clark Lake and the d.c. control wires crimped to the switch. Epoxy was applied to the crimp joint for additional mechanical strength at the joint. In more recent switch assemblies, leads several inches long were soldered to the switch assembly and then crimped to the d.c. control line cable wires, relieving the strain of crimping right at the switch itself.

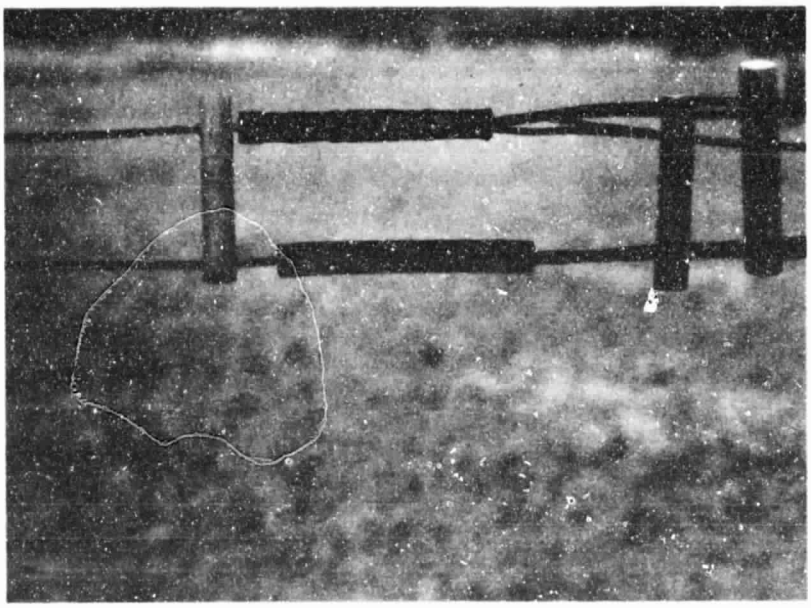

Figure 8e. Attachment of the output line to a 4-way fan. A 4:1 "Nicopress" reducing sleeve is used. Large numbers of "Nicopress" sleeves, ranging in size from 1:1 to 8:1 were used throughout the array.

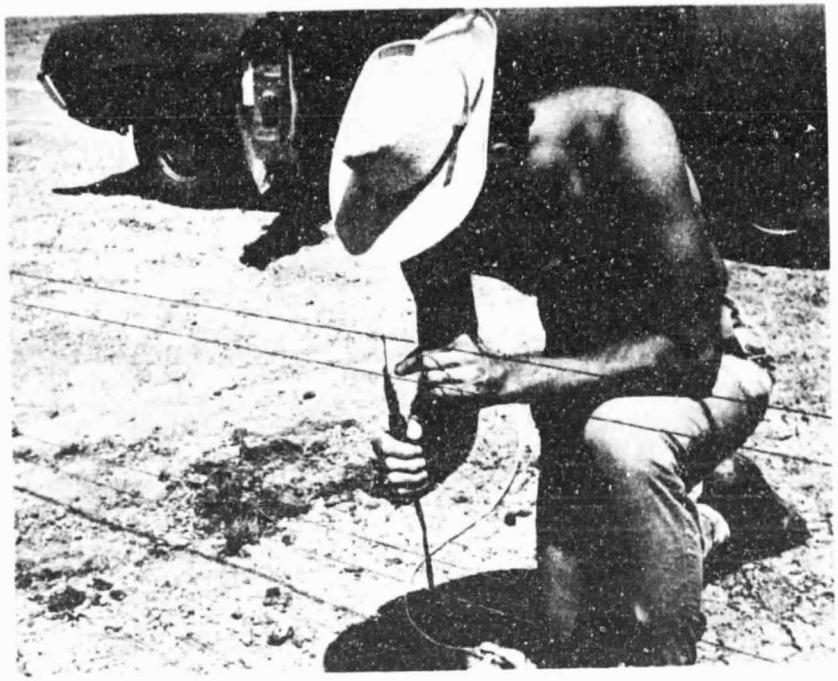

Figure 8f. Resistance soldering unit used for much of the field soldering on the transmission lines. The unit is a commercially available device which was operated off 12 volt vehicular power. "95/5" tin/silver solder was used throughout the array because of its far superior weathering resistance compared with ordinary tin/lead solder. Stan Shawhan is shown installing a short on one of the east-west open wire transmission lines.

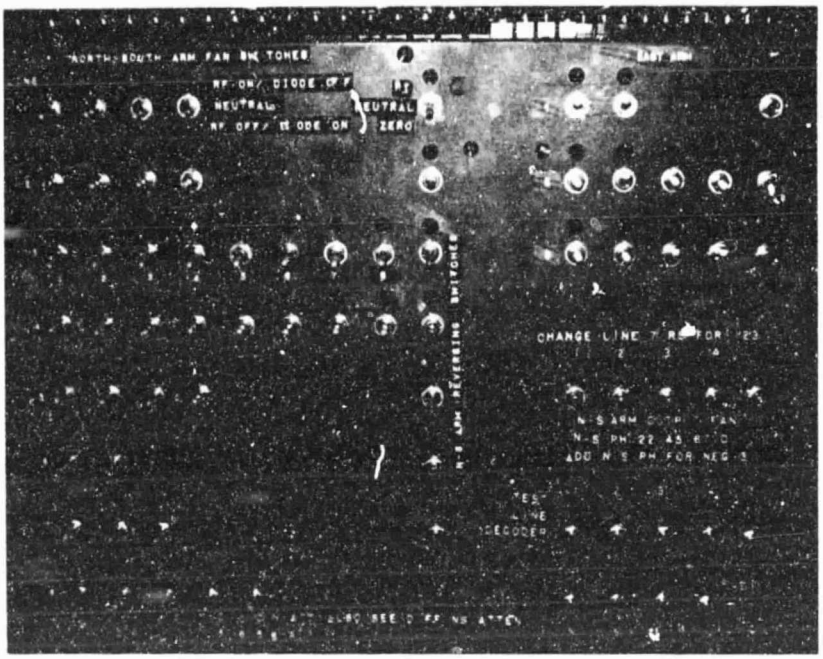

Figure 9. Manual Control Phase Switch Box. Each fan toggle switch controls all the diode switches (in its hierarchy) which are at the position indicated on the panel. Thus each NS arm line 1 toggle switch controls 64 diode switches. Also shown are the toggle switches for controlling NS steering of the EW arm (upper right), NS arm fine-phasing (middle), and test line switches. The on-off switches for the array amplifiers are on the bottom right. This manual switching system has been replaced by a card-reader-controlled system.

NUM	SOURCE ID	N-S PHASING N-S ARRAYS 1	2	3	4	5	6	7	8	NSOF	E-W ARRAY 1	2	3	1975.5 COORDINATES CELESTIAL R.A. HR.MN.SE (START LST)	DEC DG.MN	HORIZON ZENITH DG.MN	GALACTIC L	B	RESPONSE * PNS	REW SSR
										(FLUX)										
1	CAM *	3	3	-2	-8	-2	1	-1	1	2/90	1	3	-1	0. 5. 6	-0.09	-33.04	100.0	-60.8	0.82	0.83
	4C-00.01/3C 2				DIAM0.70FRAC0.90ELON35B							44		(23.57.54)					0.80	-0.01
2	CAM *	2	3	6	-1	-3	2	3	5	2/90	1	3	3	0.15. 5	79.07	45.36	121.3	16.6	0.70	0.76
	4C+78.01/3C 6.1				DIAM0.30FRAC0.45ELON65B							108		* 0. 6.41)					0.65	0.07
3	PARKES	1	-4	-3	3	1	-2	-1	1	1/ 0	-2	-4	-2	0.21.56*	-25.10	-57.36	51.6	-83.5	-0.51	0.48
	MSH 00-27											0		(0.20.45)					0.54	0.09
4	CAM *	-3	3	-1	-6	4	-1	2	3	2/ 0	-1	3	-1	0.32.55	39.16	6.02	119.6	-23.2	-0.93	0.90
	4C+39.01/3C 13				DIAM1.30FRAC0.55ELON35P							-57		(0.27. 0)					0.96	0.07
5	CAM *	4	-3	7	-2	-4	-1	2	-2	1/90	2	-3	4	0.59.29	17.40	-15.24	123.5	-44.9	0.86	0.95
	4C+17.07/3C 23				DIAM0.35FRAC0.50ELON35B							36		(0.42.36)					0.79	0.01
6	CAM *	4	-2	4	3	1	-2	-1	-2	4/ 0	2	-2	2	1. 7.35	13.13	-19.50	129.9	-49.1	0.91	0.89
	4C+13.07/3C 33				DIAM0.90FRAC0.70ELON35C							137		(0.59. 7)					0.84	-0.09
7	PARKES	1	-4	-5	7	-1	-2	1	1	3/90	1	-4	-3	1.15.39	-21.00	-53.33	147.9	-81.2	-0.58	0.56
	MSH 01-26											0		(1.11.32)					0.60	-0.05
8	CAM *	-4	-1	2	-7	-1	-2	-2	-4	1/ 0	-2	-1	1	1.25.51	49.40	16.22	120.1	-12.5	-0.95	0.95
	4C+49.06				DIAM0.95FRAC0.50ELON50C							-17		(1.19.50)					0.95	-0.05
9	PARKES	2	2	5	6	4	-1	1	-1	1/90	1	2	3	1.30.52*	-7.03	-39.52	150.9	-67.4	-0.77	0.84
	MSH 01-06											0		(1.28.53)					0.71	0.06
10	CAM *	-2	2	1	4	2	1	-2	3	3/90	-1	2	2	1.36.17*	33.01	-0.10	134.3	-28.5	0.97	1.00
	4C+32.08/3C 48				DIAM0.45FRAC1.00ELON35A							61		* 1.33.21)					0.93	0.05
11	PARKES	3	3	8	-5	3	2	-1	-1	1/ 0	1	3	4	1.45.32	-2.06	-34.59	152.6	-61.3	-0.87	0.87
	MSH 01-010											0		(1.41.19)					0.88	0.08
12	CAM *	-2	1	-8	-5	3	2	2	-3	2/90	-1	1	-4	1.55.47	28.43	-4.26	140.2	-31.6	0.89	0.96
	4C+28.05/3C 55				DIAM0.50FRAC0.25ELON35C							76		(1.50.19)					0.82	0.09
13	CAM *	-3	3	-2	-7	-1	-2	-2	-3	2/ 0	-1	3	-1	2.22.12	39.55	6.41	141.7	-19.3	0.91	0.90
	4C+39.07/3C 65/(CS)				DIAM1.20FRAC0.25ELON35C							55		(2. 8. 6)					0.97	-0.06
14	CAM *	-2	2	3	1	-3	2	-2	-3	2/ 0	-1	2	1	2.32.56	31.28	-1.42	147.6	-26.1	0.96	0.96
	4C+31.08/3C 68.2				DIAM0.90FRAC0.25ELON35C							63		(2.27.51)					0.95	-0.02
15	CAM *	3	3	-2	-8	-2	1	-1	1	3/90	1	3	-1	2.41.24	-0.06	-33.01	172.4	-51.6	0.83	0.83
	4C-00.13/3C 71				DIAM0.90FRAC0.33ELON35P							33		(2.37.30)					0.82	0.09
16	CAM *	-1	-3	8	-5	3	2	2	2	4/90	2	-3	4	2.53. 0	19.10	-13.56	159.2	-34.6	0.95	0.94
	4C+19.09/3C 74				DIAM0.50FRAC0.45ELON35B							0		(2.47. 2)					0.95	-0.03
17	4C16.07	4	-3	7	-1	-3	2	-2	2	4/ 0	2	-3	3	3. 8.38	17.00	-16.04	164.4	-34.2	0.88	0.94
	3C79													(3. 0.52)					0.82	-0.08
18	PKS0320-37	-4	-3	7	-2	-4	-1	1	-1	3/ 0	-2	-3	4	3.21.40	-37.20	-69.08	240.0	-56.5	0.26	0.27
	MSH03-301/C 23											0		(3.14.33)					0.25	-0.08
19	CAM *	-3	-1	-6	-1	-3	2	2	4	1/90	-2	-1	-3	3.28.39	45.37	12.21	150.0	-8.5	-0.84	0.89
	4C+45.05				DIAM0.40FRAC1.00ELON35B							-21		(3.24.56)					0.80	-0.06
20	CAM *	4	-2	4	3	1	-2	-1	-2	1/ 0	2	-2	2	3.35. 5*	12.56	-20.04	173.4	-33.0	0.98	0.98
	4C+12.15/3C 90				DIAM0.40FRAC1.00ELON35B							0		(3.32.23)					0.97	-0.08
21	CAM *	2	2	5	5	3	2	-1	1	4/ 0	1	2	2	3.51.14	-7.55	-40.44	197.5	-42.8	-0.80	0.84
	3C 94.				DIAM0.60FRAC0.60ELON35B							0		(3.43.13)					0.77	0.02
22	CAM *	2	2	4	3	1	-2	-3	-5	1/90	1	2	2	4. 0.14	74.53	41.24	134.6	16.8	0.77	0.85
	4C+74.07				DIAM0.20FRAC0.95ELON55B							35		* 3.53. 7)					0.70	0.03
23	CAM *	-3	4	-4	4	2	1	2	4	2/ 0	-2	4	-2	4. 6.21*	42.57	9.41	157.0	-6.3	0.91	0.86
	4C+42.11/3C103				DIAM0.70FRAC0.20ELON35C							88		(4. 4.51)					0.93	-0.05
24	CAM *	-2	3	8	-4	2	1	-2	-3	4/90	-1	3	4	4.16.44	37.58	4.44	161.9	-8.5	0.96	0.96
	4C+37.12/3C111				DIAM1.30FRAC0.08ELON35C							218		(4.11.44)					0.95	-0.09

Figure 10. Sample output from the "ALLIN1" computer program. Source information (especially from the Readhead and Hewish [1974] 80 MHz scintillation source survey) is inputted. This information along with the calculated beam steering, array response, and source coordinates is outputted.

Of course the toggle switches required an operator, were slow, and were prone to error. An automatic card-reader-controlled beam steering system has replaced the toggle switch system and greatly simplified the operation of the array, making it practical to observe at least one hundred and fifty sources/day. It greatly reduced the possibility of mistakes in beam setting.

Test and Calibration Lines. Although not included in the NASA proposal, we realized, particularly after some operational experience with the array, that it would be necessary to install both a test line system and a calibration line system.

The test line distributes 34.3 MHz from the equipment trailer to any selected line 3 fan in the north-south arm, or any selected column output in the east-west arm, that is, each point in the array at which the signals from eight elements are combined is a point at which a test signal can be injected through a directional coupler. The phase and amplitude of the test signal as it comes back through the main feed system can be measured to locate difficulties (such as short- or open-circuited transmission lines). The test-line system greatly simplifies routine array maintenance.

Since there are amplifiers located in each of the four arms, it is important to calibrate the gain and phase of each amplifier with the calibration signal system. This system makes it possible to inject a calibration signal into the input of each amplifier without ever having to disturb the main feed system. The test

line system starts at the trailer and carries the signal out to the center of the array. From this point it is distributed to each of the four arms. To keep the losses in front of the amplifier to a minimum, the test line signal is injected into the amplifier through the directional port on a directional coupler. The array connection is made through the input port, which has a loss of less than a few tenths of a decibel.

3.3 Electronics

3.3.1 RF-IF System

RF-IF system is block-diagrammed in Figures 11a and 11b; photographs are shown in Figures 12a and 12b. It features two stages of RF amplification (one in the array, the other in the equipment trailer), an RF pass band sharply defined by multi-section filters for maximum rejection of out-of-band interference and IF amplifiers which are under very strong AGC (automatic gain control). Correlation is done by high-level (~ +2dBm) multiplication at the output of the IF amplifiers; the AGC level is established by the requirement that it be in the middle of the linear power response region of the mixer. The measured response of the system for signal levels less than 10 percent of the background is plotted in Figure 13 and displays the accurate linear response over a wide dynamic range. At higher signal levels the departure from linear response has been measured and found to be in accordance with a response proportional to $x/(1 + x)$, where x is the ratio of

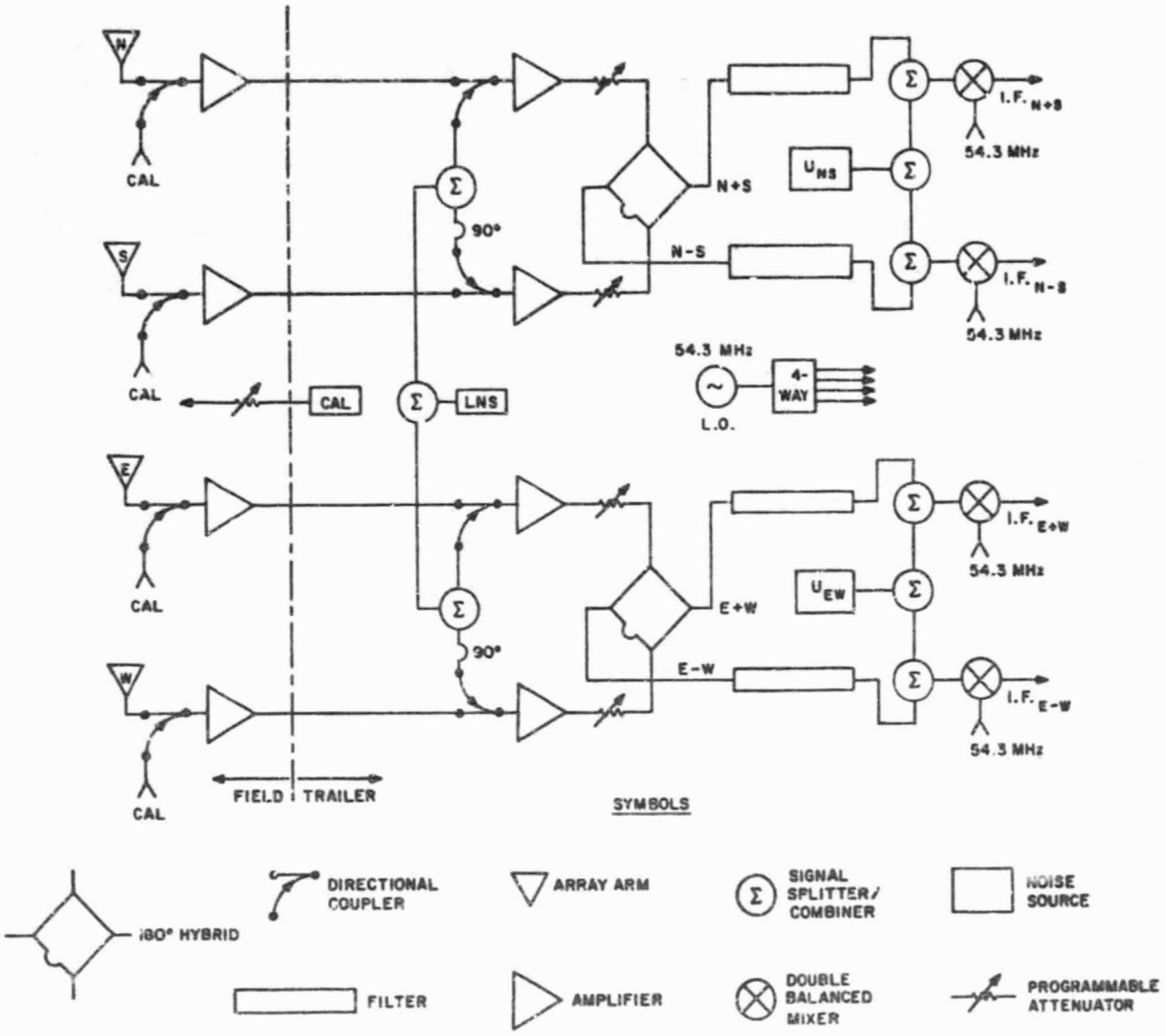

Figure 11a. Block diagram of the RF section of the receiver. LNS is a local noise source for calibrating the receiver response. U_{NS} and U_{EW} are uncorrelated (with respect to each other) noise sources used to inject high level noise to linearize the receiver response to strong sources. CAL is a calibration noise source for calibrating the amplitude and phase response of each preamplifier. IF is 20 MHz.

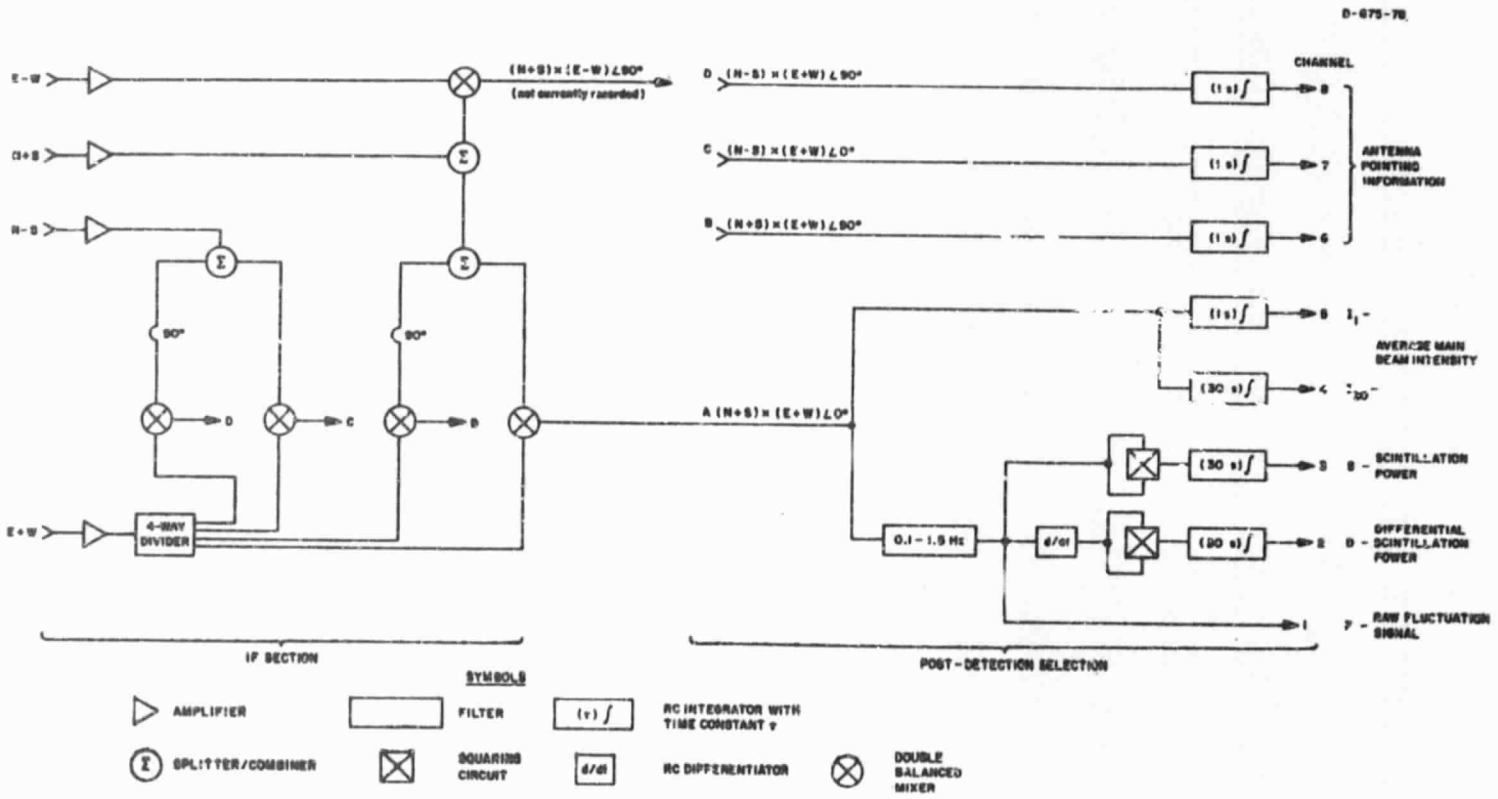

Figure 11b. Block diagram of the IF and post-detection sections of the receiver.

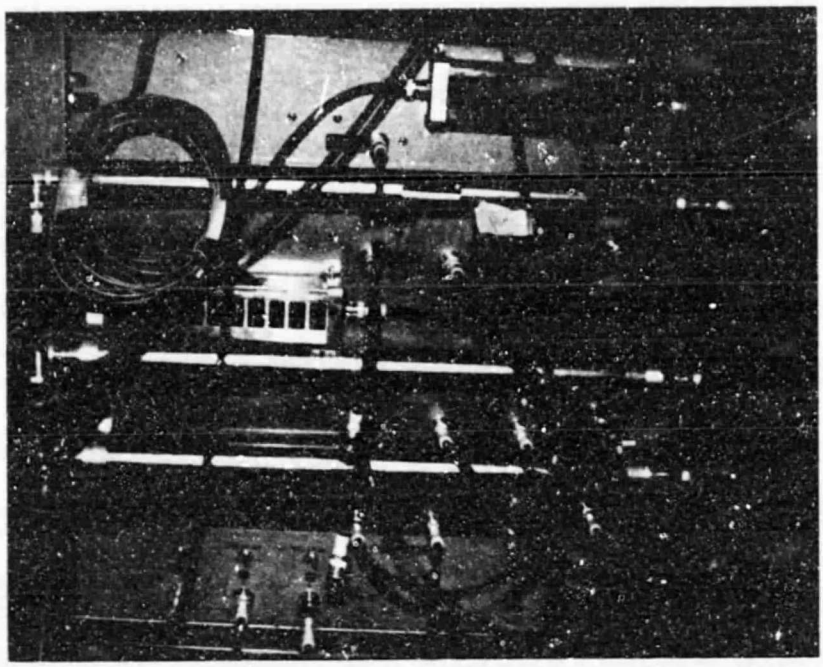

Figure 12a. RF Panel. Tubular structures are bandpass filters at 34.3 ± 0.25 MHz, one for combining outputs of E and W arms, one each for N and S arms which are brought together in a hybrid combiner (0° and 180° summing ports) to give NS beam pointing information.

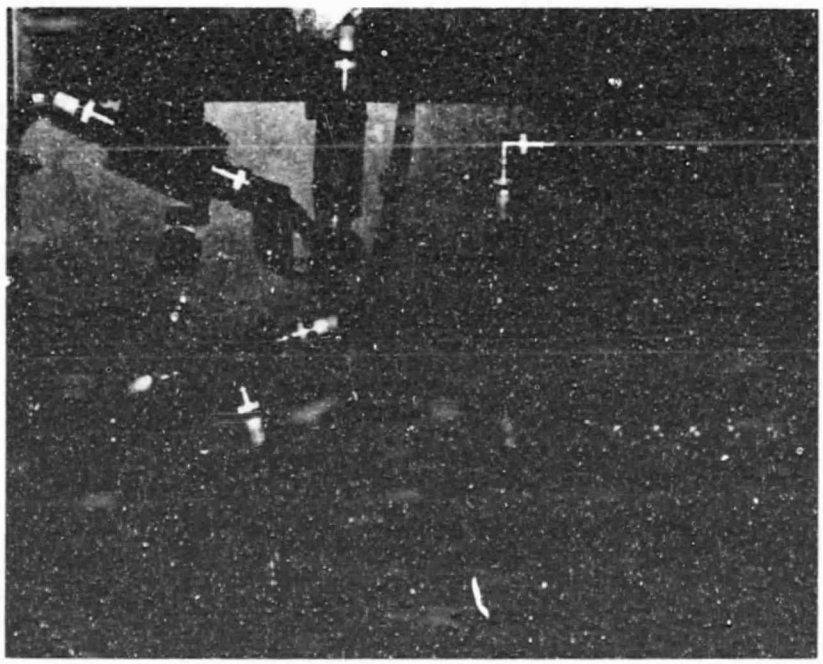

Figure 12b. IF Panel. Double-balanced mixer correlators, power splitters, local oscillator, IF phasing cables, and four-RHG IF amplifiers are mounted behind the panel.

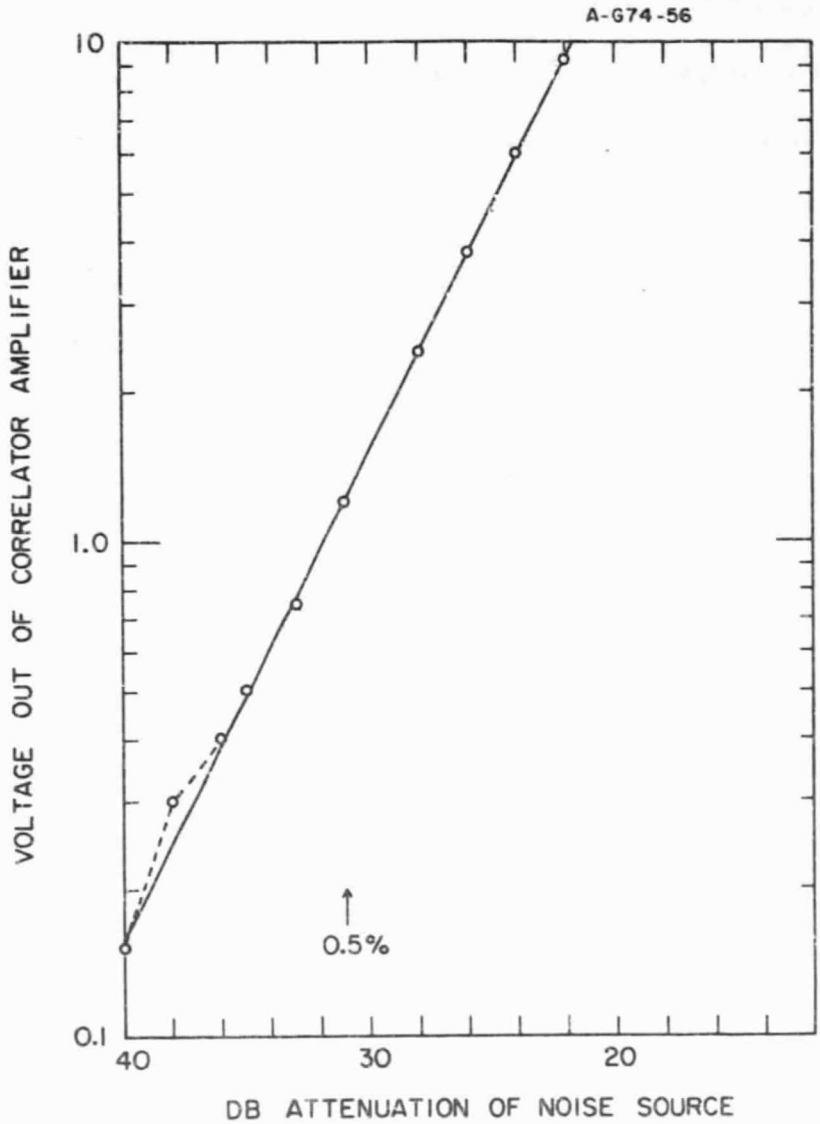

Figure 13. Measured response of correlation receiver to correlated power. Correlation of 0.5 percent typically corresponds to 3 flux units.

correlated antenna temperature to uncorrelated temperature. Obviously when x > a few percent there will no longer be a strictly linear relationship between x and system response. Thus for sources whose antenna temperature is more than a few percent of the background sky temperature, the system response must be linearized by adding uncorrelated noise. (A source of 60 flux units gives about 10 percent correlation so that for the nonlinearity to be no more than 10 percent, excess noise is added for all sources > 60 flux units. However, very few sources subject to IPS have > 60 flux units.)

The multiplying, AGC correlation receiver is essential for the following reasons:

(1) Stability. The system responds only to correlated noise temperature. Thus small changes in background noise temperature or preamplifier gain have essentially no effect on the AGC-controlled correlation receiver.

(2) Lack of Sensitivity to Interference. There are two major reasons for the greatly reduced sensitivity to interference, particularly wide band interference such as static charge precipitation or distant lightening discharges: (a) It is usually quite uncorrelated; therefore there will be no response over periods of time which are long compared with the receiver bandwidth correlation time. (b) The AGC will not allow the IF amplifier signal to rise. Thus, even if the signal is very high amplitude and

highly correlated, it can cause the correlation receiver to indicate nothing higher than 100 percent correlation.

(3) Operational Convenience. There is no need for an operator to be present to adjust buck-off controls to counteract the effect of large drifts in the system. Also, the system sensitivity automatically adjusts itself to whatever is appropriate for the background noise temperature; if it is low, the sensitivity is high and vice versa. The system fluctuation level is constant, which is extremely convenient for stable IPS observations.

3.2.2 Post Detection Circuitry

The post detection circuitry is block-diagrammed in Figure 11b. There are three different post detection channels:

(a) D.C. Response. Simply a time constant of 30 seconds or 1 sec for the correlation to give a smooth response proportional to source flux (assuming the correlation is no more than a few percent). Designated I_{30} and I_1.

(b) Scintillation Power. Before any significatn integration the correlation response is filtered by an audio band-pass filter with band edges at 0.1 and 1.5 Hz. The output of the filter is then squared (self-multiplied) in an analog multiplier and integrated for up to 30 seconds. The response is thus proportional to the relative fluctuation power between 0.1 and 1.5 Hz. The lower limit is set by the cut-off for ionospheric scintillation. There is rarely ionospheric activity about 0.1 Hz. The 1.5 Hz is determined by the fact that there is also very little IPS above 1.5 Hz. Thus a source subject to IPS will

display an increase in scintillation power as it passes through the beam of the telescope; a source subject only to ionospheric scintillation will have very little effect. Designated by S.

(c) Differential Power or Spectral Scale. The output of the audio filter is also differentiated, squared and integrated. For the same total fluctuation power between 0.1 and 1.5 Hz, the differential power channel will give approximately 15 times as much output if the spectral scale is about 1.5 Hz rather than 0.1 Hz. Designated D.

3.3.2 Data Acquisition System

The data acquisition system we have at the present time is an eight-channel Brush chart recorder, formerly part of the GSFC Jupiter monitoring network and now on loan to our project. In addition, for a cooperative Crab pulsar IPS study in 1973 with the IPS group at the University of California at San Diego, data were sent over a phone line for digitization and analysis at the U.C.S.D. data acquisition facility at La Jolla. In mid-1975 we shall be employing a Data General Nova 2/10 minicomputer to handle all data acquisition and processing (such as power spectral analysis).

3.3.3 Manual and Clock-Driven Observations

A UT/LST clock has been constructed with a variety of necessary features such as BCD output, UT/LST preset alarm, and input of preset UT. The UT clock is driven by a 1 kHz clock signal supplied from a University of Maryland high-stability oscillator.

The LST clock is driven by a 1 pulse per sidereal second signal derived through a precision UT/LST divider chain from the same Maryland oscillator.

3.3.5 Electronics Trailer

Presently the beam steering, receiving and data acquisition electronics equipment is located in a NASA instrumentation trailer which can be seen in the Frontispiece and Figure 5f. Figures 14a and b show the equipment inside this trailer.

3.4 General Facility and Equipment

3.4.1 Lab, Office, Observing Area, and Housing

Through cooperative and mutually beneficial arrangements between the University of Maryland, the University of Iowa, and NOAA, personnel associated with the NOAA/Iowa project have been provided with adequate lab, office, and conference facility space in the University of Maryland observatory building. Housing in both the Clark Lake house trailer and another Maryland trailer located in Borrego Springs has been made available.

3.4.2 Equipment and Tools

The University of Maryland has made available a variety of equipment ranging from hand tools to shop machinery to electronic test equipment. Through arrangements with the NOAA/ERL equipment rental service, we have acquired an oscilloscope, counter, function generator, gain/phase meter, and programmable desk calculator. We have also acquired our own inventory of common hand tools and some

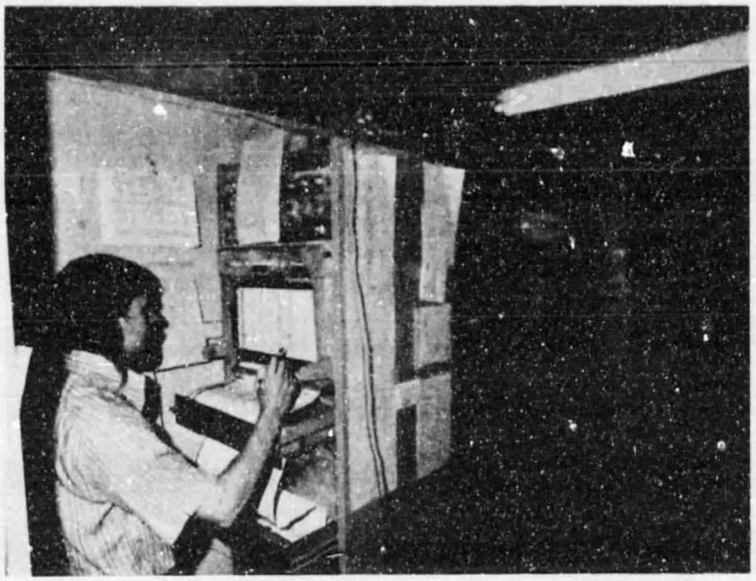

Figure 14a. View inside instrumentation trailer showing the eight channel chart recorder and the racks of receiver electronics. Fred Erskine is attending the equipment.

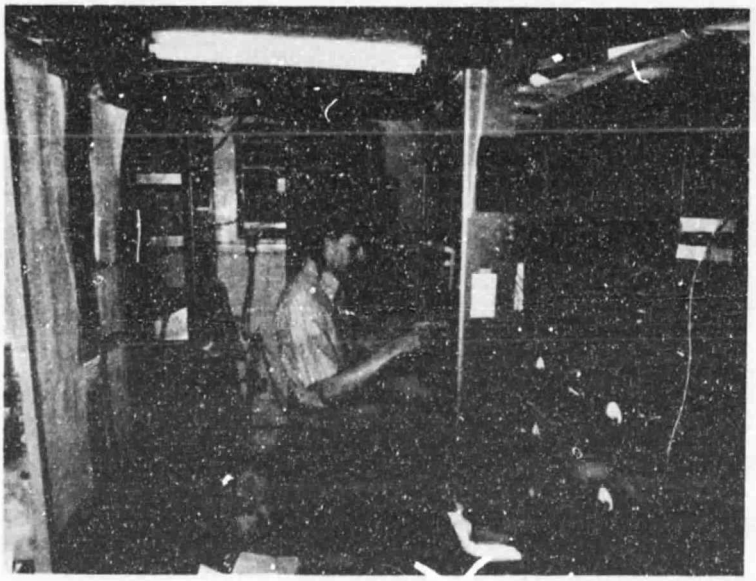

Figure 14b. View inside instrumentation trailer showing the equipment power supplies and racks of beam steering electronics. Fred Erskine is attending the equipment.

specialized equipment needed for field work such as a battery-powered electric drill, an inverter, and a resistance soldering unit which operates from a 12 volt car battery.

The University of Maryland has also made available a variety of vehicles including a ladder truck equipped with an air compressor and water dispensing system, a tractor, jeep, pick-up truck, and mobile jeep-pulled air compressor for an air hammar system. On a regular basis we have available an old University of Maryland pick-up truck suitable for on-site cartage and transportation and a GSA pick-up truck for transportation and cartage between the observatory and Borrego Springs or more distant points as needed.

4. OBSERVATIONS

The first observations made at Clark Lake with the NOAA/Iowa elements and phasing system are shown in Figure 15. They were made in August 1972, two months after array construction was begun and they verified the performance expected of the elements and phasing system. Tests of a single element by itself and electrical measurements on the phasing fan, both indicated that performance expectations would be met. However, one must always be wary of unpredictable or subtle interactions which do not manifest themselves when system components are used by themselves!

The first full array observations were made in February 1973 on the north-south arm and verified the full array performance. Tests were made to rock both the entire beam and the phase of individual hierarchies with respect to the nominal beam and phasing steps given by the theoretical beam steering calculations. In all cases, the nominal position was at least as good as adjacent positions or phases and was usually better.

The first IPS observation was made on the north-south arm March 15, 1973 as shown in Figure 16. The scintillating source flux is about 400 flux units which is about 15 percent of the total source flux. Total power channel (bottom) displays small, rapid

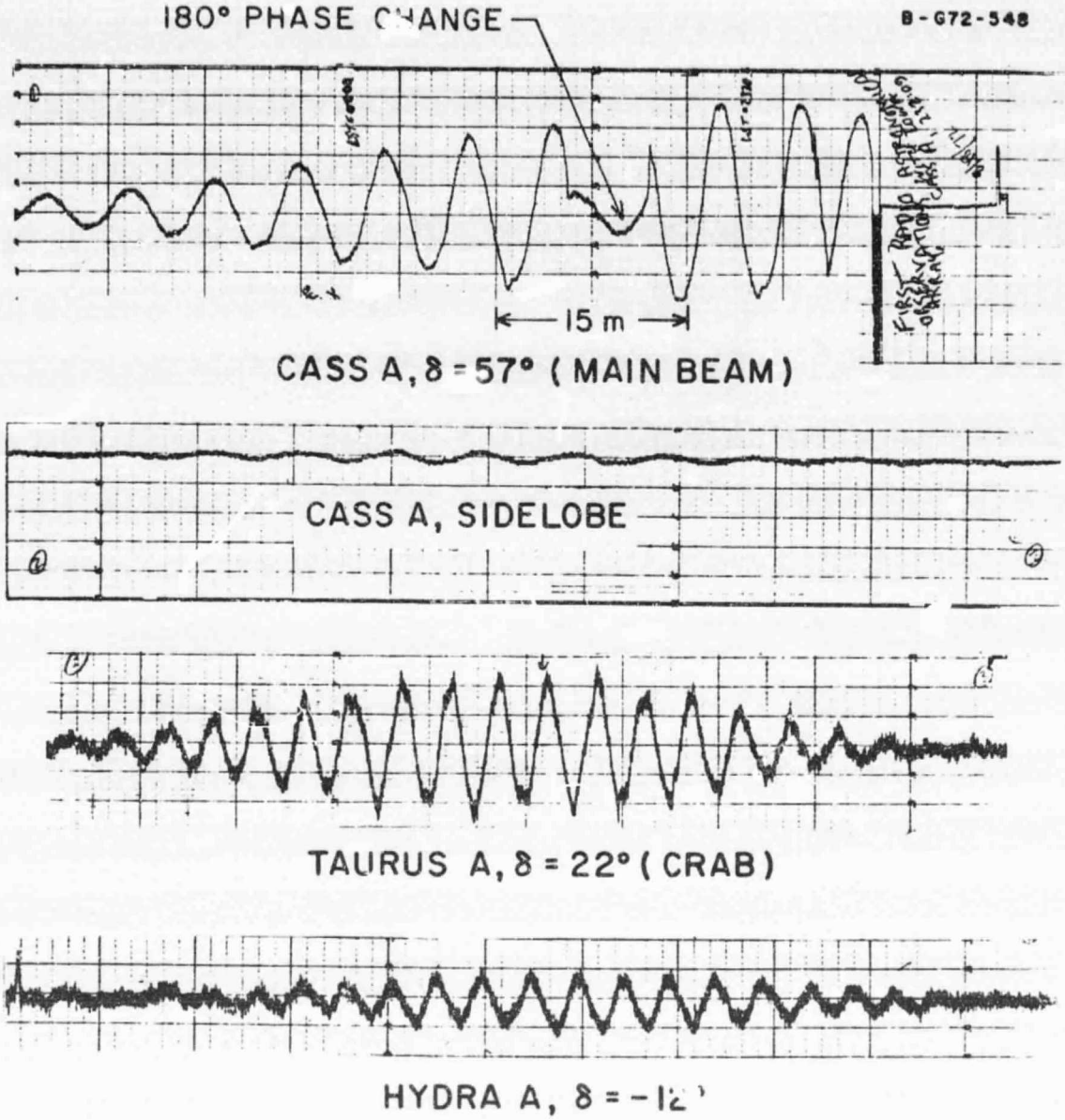

Figure 15. Interferometer fringes obtained for sources of widely different declinations using only 4 percent of the array collecting area. Eight elements of the north-arm and eight elements of the east-arm were operated as an interferometer to demonstrate the operation of the elements and the phasing scheme. Note that the fringes nearly disappear on Cass A when 180° phase reversal is inserted.

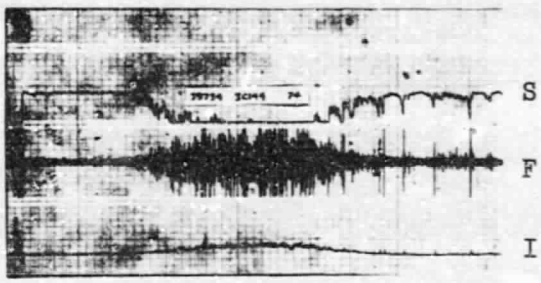

Figure 16. First IPS observation with NOAA/Iowa array. Taken in total power March 15, 1973. Total flux of the scintillating source is about 400 f.u. Total power channel (bottom) displays small, rapid intensity fluctuations which are accentuated by audio bandpassing the signal and increasing the gain (channel 2). Channel 3 displays the rectified, integrated fluctuation signal. Elongation $\epsilon \sim 90°$.

intensity fluctuations which are accentuated by audio bandpass filtering the signal and increasing the gain (channel F). Channel S displays the rectified and smoothed scintillation signal. The extremely large increase in fluctuation level as the source passed in and out of the beam is very obvious. It should be noted that these are total power, not correlation observations.

More examples are given in Figure 17. In this figure the gains of all channels relative to one another remain fixed for all sources and the channel identifications and functions correspond to those of Figure 11b. We should emphasize that over-all system gain is subject to very large source-to-source changes as a result of either changing background temperatures or deliberate additions of uncorrelated noise and front end attenuation.

The scintillation index is calculated from the data of Figure 17, for example, as $m = k_s \sqrt{S}/I$, where k_s is a rigidly fixed gain constant, S is the net source fluctuation power deflection on channel 3, and I is the absolute value of the channel 5 source deflection (the polarity of the channel 5 deflection being incidental to IPS measurements). Frequency scale is calculated as $f = k_D \sqrt{D/S}$, where k_D is another gain constant and D is the channel 2 deflection.

The contamination of IPS measurements by ionospheric scintillation, particularly at a frequency as low as 34.3 MHz, is an important consideration. However, the combination of

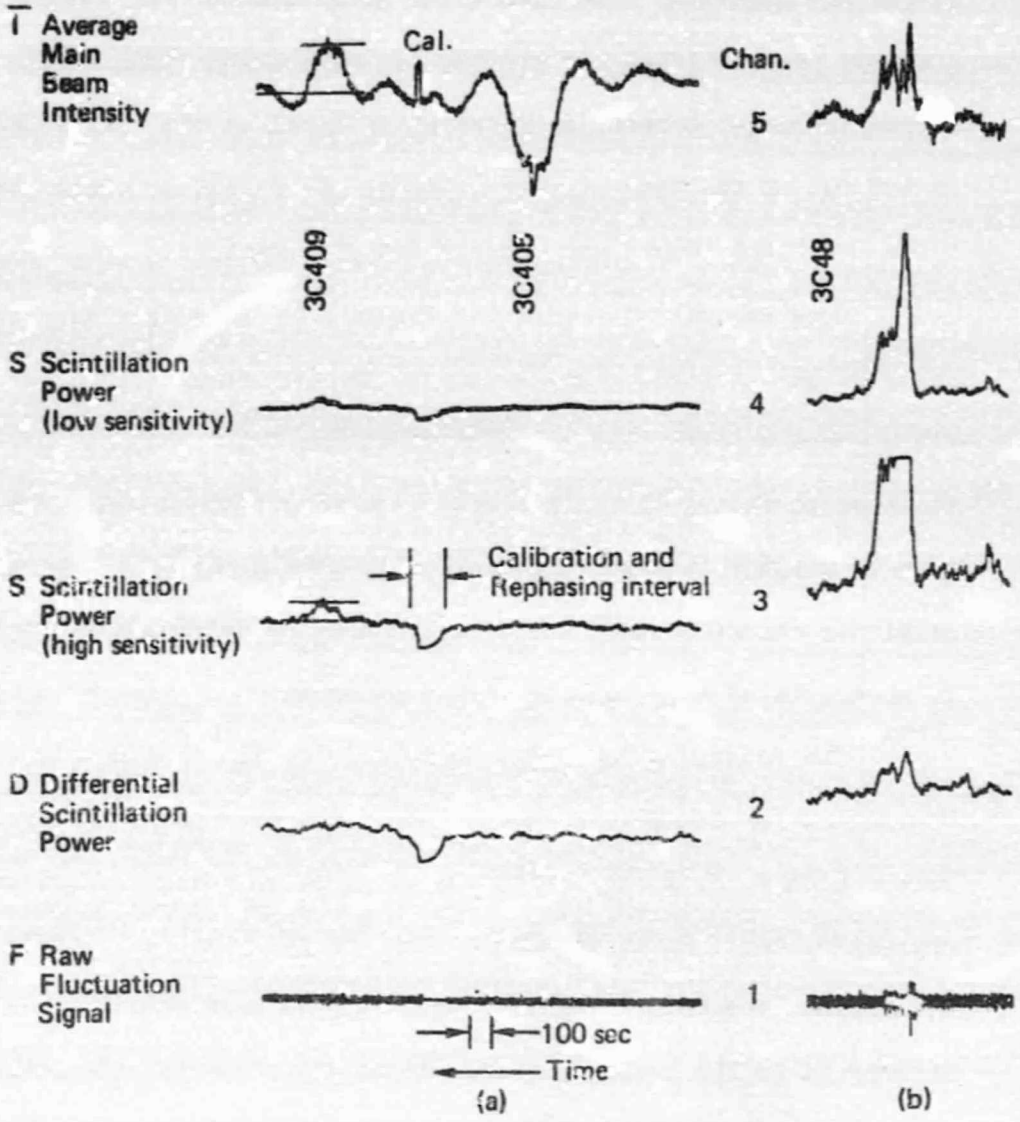

Figure 17. Sample Data. (a) A very strong, non-IPS source, 3C405, displaying no response on channels 1-4, followed by a source approximately 100 "times" weaker displaying IPS. The weaker source, 3C409, shows a significant increase in the S channel but no increase in the D channel. (b) A strongly scintillating source 3C48, showing large increases in all channels.

audio-bandpass filtering and the large spatial extent of the telescope result in severe attenuation of ionospheric components, as we shall show. Components less than 0.1 Hz are severely attenuated by the filter. Aperture filtering severely attenuates components greater than 0.1 Hz. The spatial extent L of frequency components greater than any frequency ν_o can be estimated from the relationship

$$L \leq U/2\pi\nu_o$$

where U is the ionospheric wind velocity. Using $U \leq 0.15$ km/sec, $L < 0.25$ km which is less than the 1 km spatial extent of the array so that for $\nu > 0.1$ Hz the array is averaging over a number of independent scintillation patches. The effectiveness of the ionospheric scintillation suupression has been confirmed by numerous observations of large angular diameter sources such as 3C405 which display strong ionospheric scintillation but no "IPS" (i.e., no channel 3 response as shown in Figure 17) except on rare occasions of extraordinarily strong ionospheric scintillation.

Examples of recent observational work are shown in Figures 18, 19, and 20. For convenience, a relative index m' is measured which assumes that the source deflection is the net difference between the minima of the first negative sidelobes and the peak of the main beam deflection (thereby underestimating the true index by ~ 20%). Source parameters for these observations are listed in Table 3.

A-G75-59

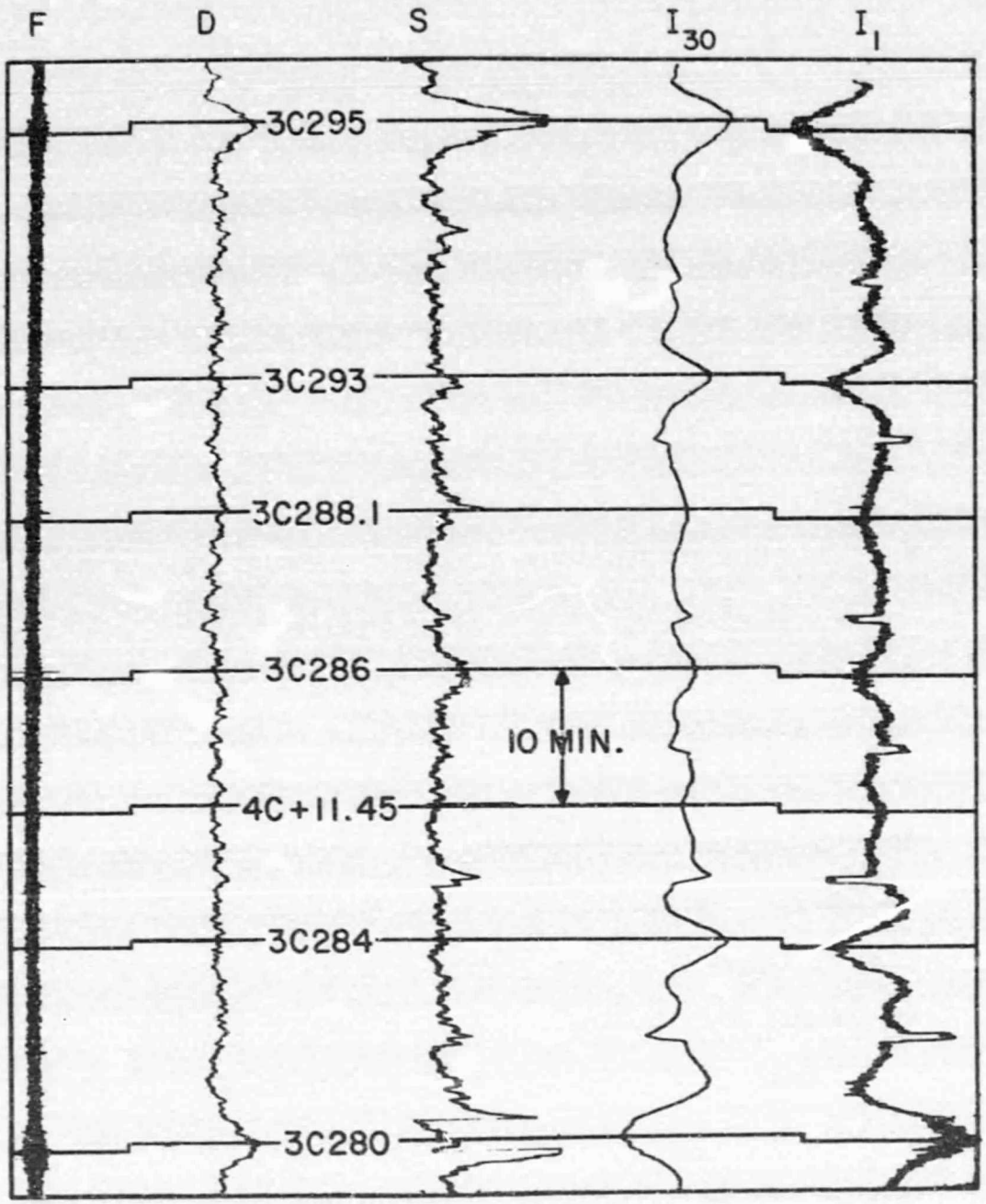

Figure 18. Observations taken on 5 October 1974. Data channels are identified as in Figure 11b. Relative sensitivity of channels is constant in time except on channel S which is reduced by 4 during transit of 3C280. Polarity of correlation response I can be either positive or negative. Channel F is the raw fluctuation power; channels D, S, and I_{30} have a 30 second time constant and are therefore delayed by 30 seconds with respect to channel I_1 which has a 1 second time constant. Rectangular spikes on I_1 are calibration signals after rephasing for the next source.

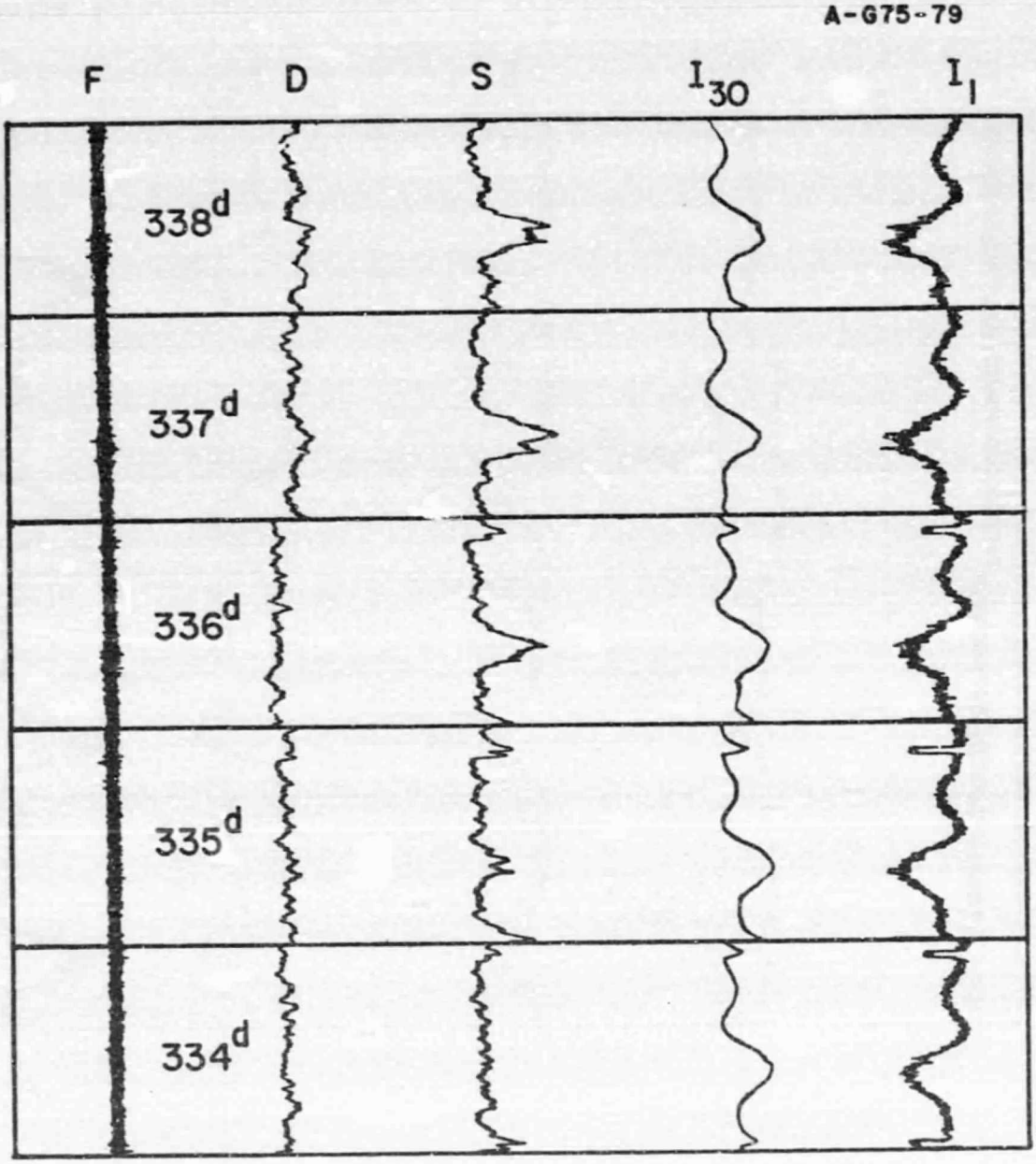

Figure 19. Observations of 3C13 taken between days 334 and 338 in 1974. Channels are identified as in Figures 11b and 18. Rectangular pulses before and after transit on channel I_1 are due to rephasing and calibration. Scintillation activity increases gradually over this five day period.

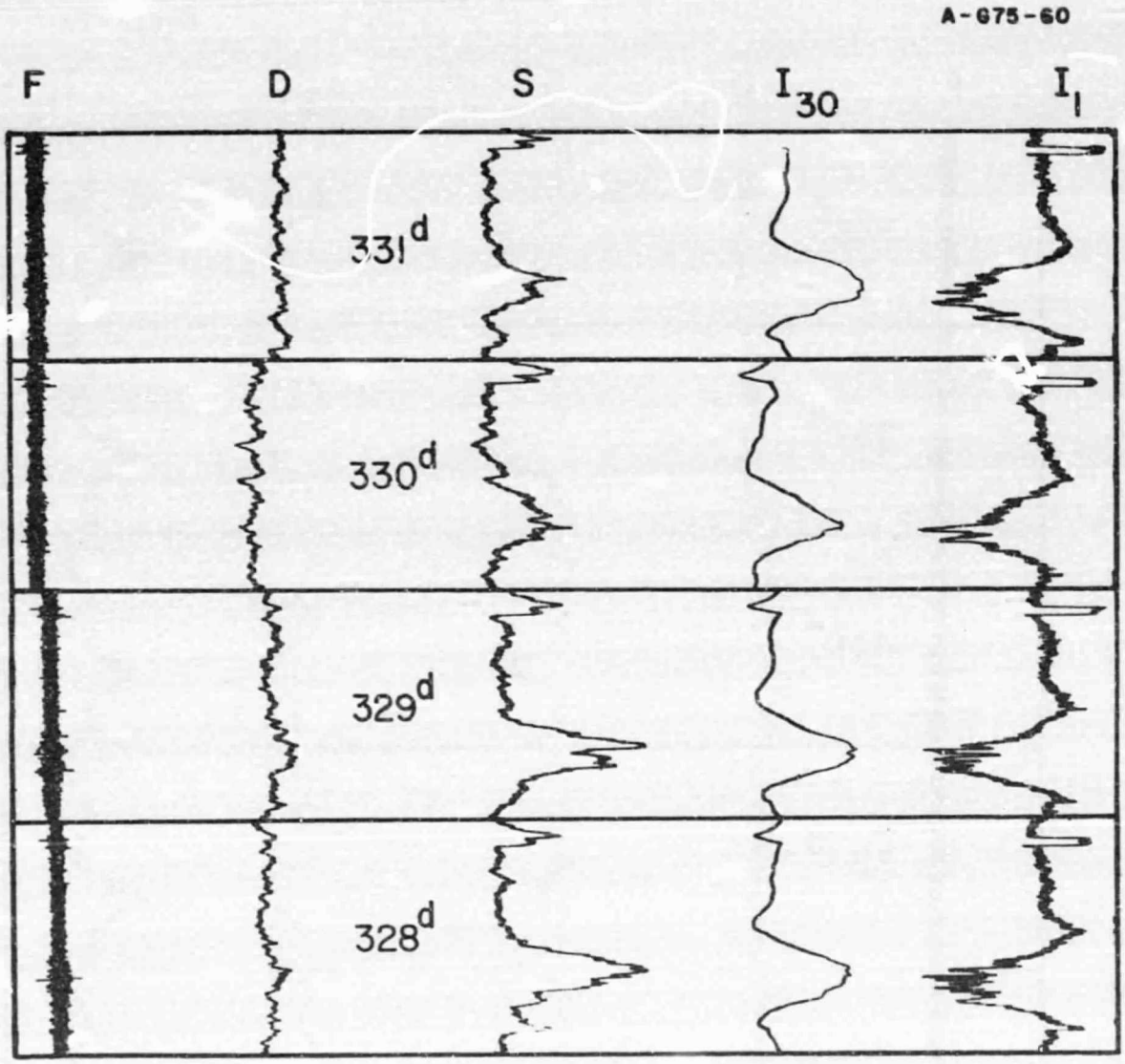

Figure 20. Observations of Quasar 3C186 taken between 24 and 27 November 1974. Channels are identified as in Figure 18. Rectangular pulse after transit on channel I_1 is rephasing and calibration. Scintillation activity changes significantly between days 329 and 330.

Table 3. Source Parameters for Observations in Figures 18, 19, and 20.

Source	Flux, f.u.*	Day	Solar Ecliptic Coordinates Longitude	Latitude	Elongation Angle	Index m′	Frequency Scale, f_o (Hz)
3C13	57	334	219	32	131	<.04	
		335	220		131	.09	.56
		336	221		130	.15	<.32
		337	222		129	.17	.52
		338	223		128	.13	.56
3C186	49	328	127	16	125	.12	.32
		329	128		126	.12	.42
		330	129		127	.07	<.36
		331	130		128	.07	<.39
3C275.1	40	278	5	19	20	.05	1.0
3C280	62	278	20	48	51	.17	.44
3C284	46	278	4	32	32	<.03	--
4C11.45	--	278	- 2	18	18	<.18	--
3C286	32	278	1	37	37	.20	<.50
3C288.1	23	278	- 31	62	66	.22	.74
3C293	42	278	- 4	40	40	.10	<.46
3C295	94	278	9	59	59	.16	.60
3C298	73	278	- 22	19	29	.11	.74

*At 38 MHz, from Williams, Kenderdine, and Baldwin (1966).

These data are illustrative of four important points about the telescope: (1) 3C298 (and possibly 3C275.1) is one of several sources which display IPS within 30° of the sun and is therefore useful in monitoring the sunward cone for scintillation activity arising from blast waves; (2) there is significant day-to-day variability in IPS activity even at large elongation angles; (3) there is a high density of scintillators which we can observe; and (4) the sensitivity and angular resolution of the array permits useful measurements of IPS parameters for sources whose flux is considerably less than 20 flux units. In addition, a number of IPS sources have been found at galactic latitudes less than 15°, demonstrating that the IPS-quenching effects of interstellar scattering are not strong enough to seriously reduce the number of usable scintillators.

In Table 4 we list all 66 sources which have displayed usable IPS. The list is by no means an indication of the ultimate number of usable sources we expect to compile because (1) systematic searches for IPS sources have not been carried out yet since we wanted to establish an initial grid against which to immediately observe IPS activity; (2) a substantial number of the sources included in our initial observational work were deliberately picked because they were <u>not</u> subject to IPS (i e., they were known not to have any small angular scale structure) and could therefore serve as a control group to evaluate ionospheric scintillation suppression; (3) at the present time a minimum of about ten

Table 4. Scintillators as of 10 December 1974

Source	Solar Coordinates		Galactic Coordinates	
	Ecliptic Longitude	Ecliptic Latitude	ℓ^{II}	b^{II}
3C2	1°.1	- 0°.6	100°	-60°.8
3C13	24.7	32.4	120	-23
3C23	18.5	11.3	123	-45
3C33	20.6	5.6	130	-49
3C48	34.7	21.3	134	-29
3C55	37.1	15.8	140	-32
3C65	46.8	24.3	142	-19
3C68.2	45.9	15.6	148	-26
3C103	68.0	21.6	157	- 6
3C111	69.0	16.4	162	- 9
3C123	71.6	7.5	171	-11
3C125	74.9	17.3	164	- 3
3C134	78.4	15.2	168	- 2
3C144	83.7	- 1.3	185	- 6
3C147	86.5	26.5	162	11
3C153	91.4	24.6	166	14
3C161	97.4	-29.1	216	- 8
3C171	99.0	31.2	162	22
3C175	107.8	-10.6	205	10
3C181	111.1	- 7.2	204	15
3C186	110.8	16.3	182	26
3C190	119.2	- 6.1	208	22
3C196	114.1	27.6	171	33
3C204	112.7	44.8	150	36
3C208	131.5	- 3.5	214	33
3C212	132.7	- 2.8	214	35

Table 4. Scintillators as of 10 December 1974 (Continued)

Source	Solar Coordinates		Galactic Coordinates	
	Ecliptic Longitude	Ecliptic Latitude	ℓ^{II}	b^{II}
3C216	126.3	25.2	178	43
3C225	142.8	0.0	220	44
3C230	149.8	-12.2	238	39
3C238	152	- 4.5	234	47
4C31.35	144.9	19.8	196	57
3C241	202.0	11.0	214	56
3C244.1	133.1	44.7	151	51
4C00.38	163.7	- 6.9	252	50
3C245	157.3	3.6	234	57
3C254	151.6	32.5	173	66
3C265	162.8	27.3	192	75
3C268.1	128.4	61.4	128	44
3C268.4	161.9	40.1	147	72
3C270.1	170.4	32.6	166	81
3C273	186.7	4.7	291	64
3C275.1	184.2	19.3	295	79
3C280	168.8	47.8	120	70
3C284	185.2	32.1	36	85
3C286	188.3	36.8	55	80
3C288.1	162.2	61.9	112	56
3C293	192.9	39.7	54	76
3C295	179.8	59.0	97	61
3C298	211	19.2	352	60
3C305	167.5	70.0	103	49
3C315	217.3	42.2	39	58
3C321	223.5	41.6	37	54
3C324	229.7	40.4	35	49

Table 4. Scintillators as of 10 December 1974 (Continued)

Source	Solar Coordinates		Galactic Coordinates	
	Ecliptic Longitude	Ecliptic Latitude	ℓ^{II}	b^{II}
3C330	171	79.0	99	41
3C336	239.5	44.6	41	42
3C352	247	68.5	72	36
3C356	250.4	73.8	78	34
4C+50.44	281.7	73.8	79	26
4C+48.45	275	71.9	76	27
3C380	286.6	71.8	77	23
4C21.53	300.9	42.2	58	0
3C409	314.0	42.1	64	- 6
3C438	350.1	46.6	89	13
3C459	352.5	8.1	84	-51

minutes must be allocated to the observation of each source to measure a deflection peak with respect to a baseline, whereas when the telescope is computer-controlled it will be possible to time share between sources; and (4) the telescope sensitivity will be increased by a factor of about 3 when additional preamplifiers are installed, thereby increasing the weak source scintillation power signal-to-noise ratio by a factor of almost 10.

5. SCIENTIFIC RESULTS

The 24-hour/day monitoring of IPS activity which began in May 1974 has yielded several interesting scintillation events. The most straightforward to deduce is the recurrent activity in which a large number of sources displayed enhanced IPS on or about June 26 and 2 x 27, 3 x 27, and 4 x 27 days later. (The array was not operating for several weeks in July which included the recurrence period.) In Figure 21 we show the initial and third 27-day recurrence. Note that although several sources display enhancements at times other than the recurrence time, the peak is exceptional in the number of sources partaking. We have no reliable observations of normal IPS sources not displaying the enhancement during these two enhancement periods. Note the increased geomagnetic indices peaking 2-4 days after the scintillation peaks.

The event has been analyzed in detail [Cronyn et al., 1975a] and is included as an appendix item in this report. We feel we have demonstrated the capacity to predict terrestrial effects of a flare-associated shock wave with a significant degree of confidence and lead time. Of course, such predictions will not be realized until the data acquisition and reduction can be done on-line.

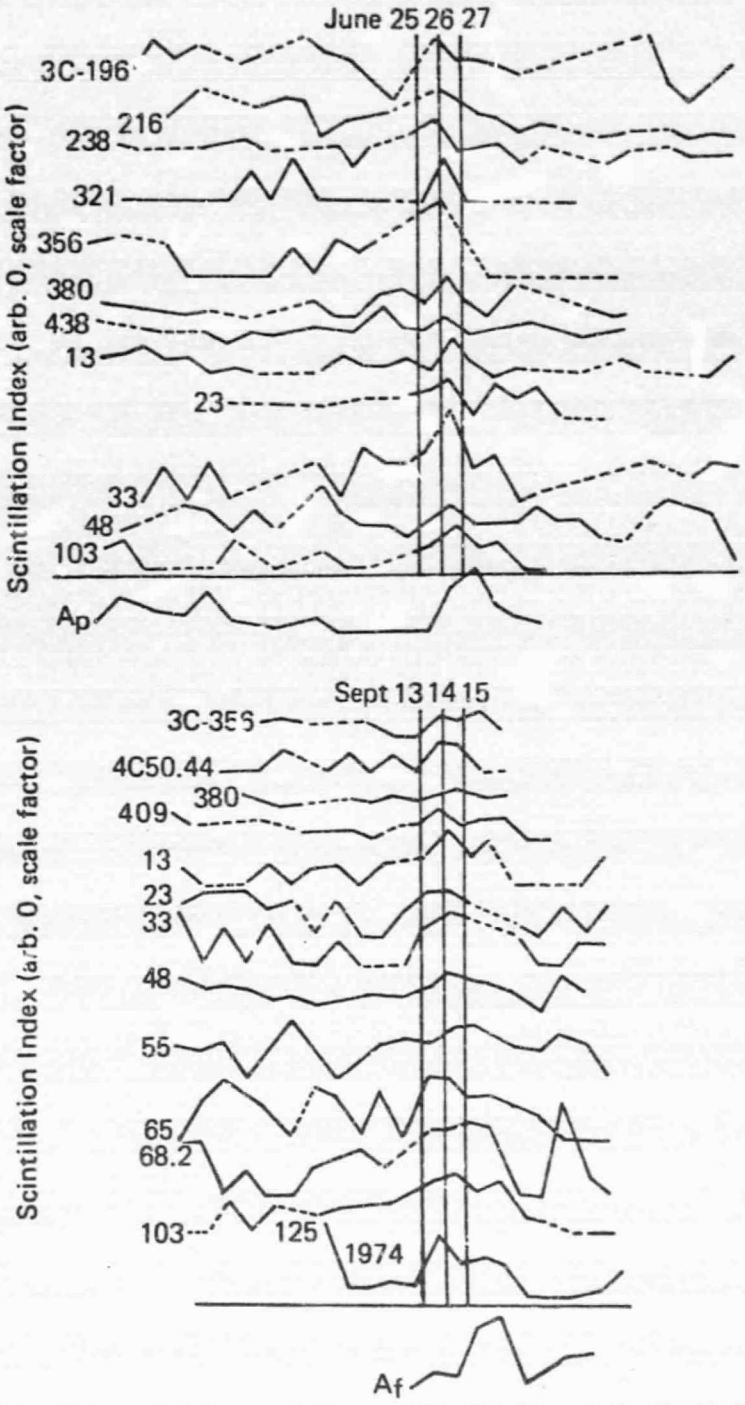

Figure 21. Initial and third 27-day recurrence of interplanetary scintillation activity associated with a recurrent series of geomagnetic disturbances (indicated by the Ap index in June and the Af index in September). Sources are labeled with their Third Cambridge (3C) Catalog number except if otherwise noted.

A brief description of the array and a discussion of the initial observations have been prepared [Cronyn et al., 1975b].

6. COLLABORATION

A number of individuals are involved in collaborative work with us. Messrs. Fred Erskine and Don Mitchell, doctoral candidates in physics from the University of Iowa and the University of New Hampshire, respectively, have been involved in much of the initial construction and operation of the telescope, and Erskine has been taking thesis observations on it.

The electron density irregularity structure we shall be observing via the IPS technique which should serve to complement the observations of magnetic field irregularity structure made with spacecraft magnetometer experiments such as those carried out by Dr. Norman F. Ness.

Dr. Ed Roelof, Johns Hopkins Applied Physics Laboratory (Mr. Mitchell's thesis advisor), is using our observations for correlative studies with other types of solar and solar wind observations. Dr. Murray Dryer (NOAA/SEL) is hoping to exploit the forecast potential of the observations to watch for comet brightenings at optimum times. We expect to be furnishing data to SEL's Space Environment Forecast Center. We have commenced joint scintillation studies with the IPS solar wind group at U.C.S.D., under Dr. William Coles.

7. ACKNOWLEDGMENTS

Support and funding for the major construction phase of the telescope was provided by Dr. Norman F. Ness (NASA/GSFC) through NASA Purchase Request S-57016-A to whom we are extremely grateful. Continued support has been provided through the University of Iowa under NSF grant DES73-06559. Dr. Donald Williams and Professor James A. Van Allen have been unstinting in the enthusiastic support and encouragement of the project through the Space Environment Laboratory, NOAA, and the Department of Physics and Astronomy, University of Iowa (under NASA grant NGL-16-001-002), respectively.

We owe a special debt of gratitude to Professor William C. Erickson and the University of Maryland staff under Mr. John Hubbard at the Clark Lake Radio Observatory for the space, equipment, advice, and assistance they have made available to us.

A large number of individuals endured atrocious living and working conditions and unmitigated by even financial amenities to contribute to the construction and operation of the telescope. Besides Messrs. Erskine and Mitchell, we would particularly like to cite Mr. Al Huneke, who directed the construction of the antenna elements and phasing lines at the University of Iowa and their

installation at Clark Lake, and designed and constructed the automatic beam steering system, the UT/LST clock, and much of the other digital circuitry; Mr. Kerry Neal, SEL/NOAA, who designed the phasing switch, built most of the RF preamps, and participated in much of the initial construction work; and Mr. Stig Johansson, a University of Maryland staff employee who designed and built a superb ladder-line making machine when it was discovered that suitable ladder type transmission line was no longer commercially available.

We would also like to thank Messrs. John Benson, Dale Rupert, Dave Sentman, Bill Taylor, Joel Weisberg (all of whom were Iowa graduate students), and Jonathan Throne (a Boulder, Colorado high school student) who carried out the most arduous part of the array construction work during the Summer of 1972; Mr. Austin Hearst, who carried out much of the cabling and construction, Fall 1972 -- Spring 1973; Mr. William Stoertz, an Antioch College work-study student, who carried out construction, testing, and observational work, Spring-Summer 1973; Ms. Julie Johnson, U.C.S.D. student, who directed much of the cabling and much of the observational work; Mr. Scott Scheuerman, Borrego Springs High School graduate, who was in charge of much of the array maintenance and observational work; Ms. Lynne Cronyn who carries out a variety of construction and observational work and is in charge of all current data scaling, RF cabling, and secretarial work; Mr. Harold Young, Antioch College, who performed

drafting and construction work; and Mr. Dick Farrell who has been in charge of various technical and maintenance operations. We would like to thank all those who have served in recent observing and data scaling, including Messrs. Ted Dart, Ruben Garcia, Jeff Johnson, Dave Kulbarsh, Mike Maas, Ms. Carol Seidel, and Ms. Nan Roach. We would also like to thank a number of others who have assisted us in the construction and/or operation of the array; Howard Thomson, Steve Odam, Dave and Liz Carr, Joey Rivera, and Wayne Dooley, Borrego High School students; Robin and Terry Hubbard and a number of their Escondido High School friends; James Munroe, Antioch College; and Mike Thorne and Steve Williams, students from Boulder, Colorado.

REFERENCES

Armstrong, J. W., W. A. Coles, J. K. Harmon, S. Maagoe, B. J. Rickett, and D. G. Sime, Radio scintillation measurements of the solar wind following the flares of August 1972, World Data Center A for Solar-Terrestrial Physics, Report UAG-28, 371, July 1973.

Balsley, B. B., and W. L. Ecklund, A portable coaxial colinear antenna, IEEE Trans. Ant. Prop. 20, 513, 1972.

Burnell, S. J., Enhancements of interplanetary scintillation, corotating streams and Forbush decreases, Nature 224, 356, 1969.

Coles, W. A., B. J. Rickett, and V. H. Rumsey, Interplanetary scintillations, Solar Wind Three, ed. C. T. Russell, Institute of Geophysics and Planetary Physics, University of California (Los Angeles), 351, 1974.

Coles, W. A., and S. Maagoe, Solar wind velocity from IPS observations, J. Geophys. Res. 77, 5622, 1972.

Cronyn, W. M., Density fluctuations in the interplanetary plasma: Agreement between space probe and radio scattering observations, Ap. J. 171, L101, 1972.

Cronyn, W. M., F. Erskine, S. D. Shawhan, B. L. Gotwols, and E. C. Roelof, Prediction of ionospheric effects associated with solar wind disturbances using interplanetary scintillation observations at 34.3 MHz, Applied Physics Lab/Johns Hopkins U. Preprint Series, January 1975 and to be published Proceedings of Ionospherics Effects Symposium, Crystal City, Va., 20-22 January 1975a (included in Appendix).

Cronyn, W. M., S. D. Shawhan, F. T. Erskine, and D. G. Mitchell, Interplanetary scintillation observations with the Cocoa Cross radio telescope, Dept. Physics and Astron., U. of Iowa Research Report 75-1, 1975b.

Dennison, P. A., and A. Hewish, The solar wind outside the plane of the ecliptic, Nature 213, 343, 1967.

Hewish, A., P. F. Scott, and D. Wills, Interplanetary scintillation of small diameter radio sources, Nature 203, 1214, 1964.

Houminer, Z., Corotating plasma streams revealed by interplanetary scintillation, Nature 231, 165, 1971.

Houminer, Z., Enhanced scintillation sectors outside the plane of the ecliptic, Planet. Space Sci. 21, 1367, 1973a.

Houminer, Z., Power spectrum of small-scale irregularities in the solar wind, Planet. Space Sci. 21, 1367, 1973b.

Houminer, Z., and A. Hewish, Long-lived sectors of enhanced density irregularities in the solar wind, Planet. Space Sci. 20, 1703, 1972.

Matheson, D. N., and L. T. Little, Radio scintillations due to plasma irregularities with a power law spectra, the interplanetary medium, Planet. Space Sci. 19, 1615, 1971.

Ochs, G. R., National Bureau of Standards Technical Report No. 8772, 1965.

Readhead, A. C. S., and A. Hewish, Fine structure in radio sources at 81.5 MHz III, Mem. R. Astr. Soc. 78, 1, 1974.

Rickett, B. J., Power spectrum of density irregularities in the solar wind plasma, J. Geophys. Res. 78, 1543, 1973.

Sharp, L. E., and D. E. Harris, Enhanced interplanetary scintillations associated with solar flares, Nature 213, 377, 1967.

Ward, B. D., Detection of the June 15th disturbance by interplanetary scintillation, Compilation of Solar Particle and Interplanetary Measurements Acquired During the Campaign for Integrated Observations of Solar Flares (CINOF), ed. M. A. Shea and D. F. Smart, Air Force Cambridge Research Laboratories Special Report No. 177, AFCRL-TR-74-0271, 53, 1974.

Watanabe, T., and T. Kakinuma, The recurrent solar wind streams observed by interplanetary scintillation of 3C48, Pub. Ast. Soc. Japan 24, 459, 1972.

Watanabe, T., T. Kakinuma, M. Kojima, and K. Shibasaki, Observations of the solar wind by interplanetary scintillation of radio sources in early August 1972, Report of Ionospheric and Space Research in Japan 27, 158, 1973a.

Watanabe, T., T. Kakunuma, M. Kojima, and K. Shibasaki, Solar wind disturbances detected by the interplanetary scintillation of radio sources in early August 1972, J. Geophys. Res. 78, 8364, 1973b.

Williams, P. J. S., S. Kenderdine, and J. E. Baldwin, A survey of radio sources and background radiation at 38 Mc/s, Mem. R. Astr. Soc. 70, 53, 1966.

Wiseman, M., and P. A. Dennison, Flare induced shocks and co-rotating streams in the interplanetary medium, Proc. Ast. Soc. Australia 2, 64, 1972.

APPENDICES

APPENDIX A

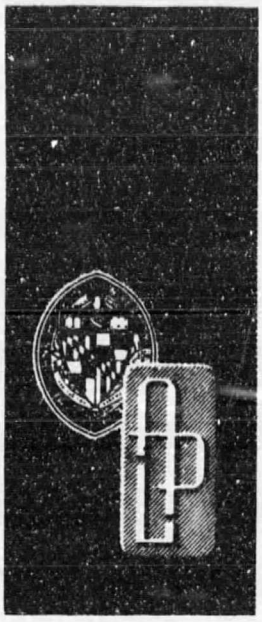

Preprint Series Jan. 1975

PREDICTION OF IONOSPHERIC EFFECTS ASSOCIATED WITH SOLAR WIND DISTURBANCES USING INTERPLANETARY SCINTILLATION OBSERVATIONS AT 34.3 MHZ

W. M. CRONYN
NOAA/ERL, Boulder, Colorado

F. ERSKINE and S. D. SHAWHAN
University of Iowa, Iowa City, Iowa

B. L. GOTWOLS and E. C. ROELOF
Applied Physics Laboratory

Presented to the Ionospheric Effects Symposium,
Crystal City, Virginia, January 20-22, 1975

THE JOHNS HOPKINS UNIVERSITY • APPLIED PHYSICS LABORATORY
8621 Georgia Avenue • Silver Spring, Maryland • 20910
Operating under Contract N00017-72-C-4401 with the Department of the Navy

PREDICTION OF IONOSPHERIC EFFECTS ASSOCIATED WITH SOLAR WIND DISTRUBANCES USING INTERPLANETARY SCINTILLATION OBSERVATIONS AT 34.3 MHz

W. M. Cronyn
NOAA/ERL, Boulder, Colorado

F. Erskine and S. D. Shawhan
University of Iowa, Iowa City, Iowa

B. L. Gotwols and E. C. Roelof
Applied Physics Laboratory
The Johns Hopkins University
Silver Spring, Maryland

Precis. In May 1974, observations at 34.3 MHz of interplanetary scintillations (IPS) of radio sources commenced using the NOAA/University of Iowa COCOA-Cross radio telescope (co-linear dipoles of coaxial cable in a Mills cross). The arms of the array are 0.8 and 1.2 km yielding a collecting area of 72,000 m^2. The 1/2° x 3/4° beam is steerable in the meridian, allowing viewing of > 200 sources per day covering the entire northern ecliptic hemisphere and extending into portions of the southern hemisphere as far as 45° south ecliptic latitude. We present an analysis of daily IPS observations of 28 selected sources during June 20-30, 1974. This period contains the sudden commencement of a geomagnetic storm (SSC) at 2330 UT, June 25 which was accompanied by 2 days of disturbed ionospheric conditions as indicated by a drop from 6 to 2 in the radio propagation quality indices in the band 2-26 MHz between Luchow (Germany) and Halifax (Canada). The SSC also marked the onset of a delayed solar particle event as measured on the APL/JHU experiment on IMP-7 (protons > 0.3 MeV, electrons > 0.2 MeV) with proton intensities > 200 $(cm^2\text{-sec-ster-MeV})^{-1}$ persisting until June 29. The source of the solar wind disturbance (inferred from the SSC) and the delayed particle event is identified as a 2B flare at ∿ 0500 UT, June 23. Two-dimensional analysis of the latitude-longitude grid of daily IPS observations of June 24 - June 27 indicate the earliest detection of the flare-associated solar wind blast wave at ∿ 1900 UT June 24. The blast wave appears in all sources within 60° of the sun, beginning ∿ 1500 UT June 25, more than 8 hours before the SSC and commencement of ionospheric effects. We can recast our analysis as a simulated prediction of the SSC, assuming that we had realtime data such as is currently available: 1) daily IPS observations from the COCOA-cross grid; 2) satellite measurements of low-energy (∿ 1 MeV) protons and relativistic (∿ 100 keV) electrons; and 3) solar synoptic charts of large-scale chromospheric magnetic polarity regions constructed continuously from Hα patrol photographs at NOAA/ERL (Boulder, Colorado). The Hα synoptic charts indicate coronal magnetic structures that often affect the emission of particles and solar wind. We conclude that we could have predicted with high reliability the SSC, delayed solar particle event (and hence the ionospheric disturbances) at least 6 hours before their occurrence.

INTRODUCTION

We are presently monitoring interplanetary scintillation (IPS) on a 24-hour basis of more than 150 radio sources distributed over the entire northern ecliptic hemisphere as well as a portion of the southern hemisphere extending as far as S45° ecliptic latitude. We believe that these observations literally add another dimension to the analysis of interplanetary disturbances and the prediction of geomagnetic storms and solar particle events.

It has been known for about ten years (Hewish, et al., 1964) that small angular diameter natural radio sources display intensity fluctuations on a time scale of about one second. The intensity fluctuations develop because of random diffraction arising from scattering by irregular variations in the interplanetary electron density, and are termed IPS (interplanetary scintillation).

Detailed analyses of day-to-day changes in IPS activity have revealed associations between the activity and other solar wind phenomena. The emphasis to date in IPS observations oriented towards studies of the solar wind has been on three areas: (1) statistics of dynamical features, i.e. auto-correlation analyses of scintillation activity to find 27 day synodic periodicities, cross-correlation of solar wind velocity (as deduced from IPS measurements) and IPS activity, cross-correlation of IPS data with solar disc, space probe and terrestrial data (Burnell, 1969; Houminer, 1971; Houminer and Hewish, 1972; Watanabe and Kakinuma, 1972; Houminer, 1973; Coles et al.,

1974); (2) detailed analyses of specific solar wind events, in which IPS data contribute to a self-consistent description involving a variety of solar-terrestrial and space probe data (Sharp and Harris, 1967; Wiseman and Dennison, 1972; Rickett, 1973; Watanabe et al., 1973; Armstrong et al., 1973; Ward, 1974); and (3) analyses of ambient solar wind parameters such as plasma density spectrum and solar wind speed dependence on solar latitude (Dennison and Hewish, 1967; Matheson and Little, 1971; Coles and Maagoe, 1972; Cronyn, 1972; Houminer, 1973; Rickett, 1973; Coles et al., 1974).

With our instrument we are emphasizing the second area of IPS studies: locating, mapping and tracking co-rotating streams and blast waves, with a view towards predicting the interception of these structures by Earth and space probes. Perhaps the best example to date of this technique is described by Wiseman and Dennison (1972). Using the Culgoora (Australia) radio telescope, they were able to follow the origin and evolution of both a radial blast of turbulent plasma and two separate co-rotating solar wind streams. The shape and extent of these large scale structures, as inferred from the sequential variations in scintillations activity across a grid of 14 sources, were consistent with, and were complemented by, observations of solar flare activity, velocity streaming, sudden commencement geomagnetic storms and Forbush decreases.

In May, 1974, a large electronically steerable decametric wavelength Mills Cross radio telescope with a collecting area of over 7.2 x 10^4 m^2 (one of the largest in the world) began regular observations as a joint undertaking by the Space Environment Laboratory of the National Oceanic and Atmospheric Administration and the Department of Physics and Astronomy of the University of Iowa. It has been specifically designed for, and dedicated to, IPS observations at solar elongation angles ranging from 20° to 180°. It is located at the University of Maryland Clark Lake Radio Observatory south of the Santa Rosa mountains, in the eastern desert country of San Diego County, an isolated site well-suited for such sensitive studies. The extremely large collecting area and low operating frequency makes possible a unique capability of being able to observe a large number of IPS sources even at source-sun elongation angles approaching 180°.

The observational and interpretational techniques we are currently using are a generalization of those used previously, made possible by the dense grid of sources that can be observed. The scintillation activity of a grid of more than 100 small angular diameter sources, distributed more or less at random over the sky at solar elongation angles greater than 20° and celestial declinations north of -25°, are being monitored daily and the scintillation index m ($m = \Delta I/\bar{I}$, ΔI = rms intensity fluctuation, $\bar{I}$ = average intensity) measured for each source. Thus, each day of observations, we monitor IPS activity in the entire northern ecliptic hemisphere, and in the southern hemisphere at ecliptic latitudes ranging from ~0° to -45°, subject only to a cone of avoidance of 20° radius centered on the sun.

Steering in the N-S direction is accomplished automatically with electrical phase shifters, while the rotation of the earth provides the E-W steering. A schematic diagram of the antenna geometry is given in Figure 1. The reason for the unusually thick arms of the cross is to provide a very large collecting area, in order to obtain adequate sensitivity with the very short effective time constant required for IPS observations. The antenna array has been named the COCOA-Cross, where COCOA is an acronym which stands for the individual element type, Balsey and Ecklund (1972), which are colinear dipoles fashioned out of coaxial cable. Cross stands for the type of array, which is a Mills Cross.

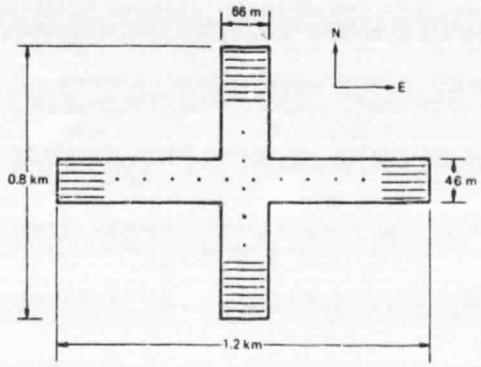

Fig. 1 Overall geometry of the COCOA-Cross Array

Extraction of useful information from the main beam signal is accomplished with analog circuitry and the resulting processed signals are plotted on a multi-channel chart recorder. A 0.1 - 1.5 Hz bandpass filter is used to isolate the signal fluctuations which are due to IPS. Thus, the lower cutoff of 0.1 Hz has been chosen to minimize the contribution of ionospheric scintillation, whereas the upper cutoff of 1.5 Hz is about the upper limit of the IPS frequency components. The output of the bandpass filter, called the raw fluctuation signal, is then subjected to further processing in order to obtain its average power as well as a rough estimate (the second moment) of the shape of its frequency spectrum. The average power (called the scintillation power, S) is obtained by squaring and integrating with a relatively long time constant (30 s). The spectrum estimate (called the differential scintillation power, D) is obtained by differentiating the raw fluctuation signal with a

short time constant, and then squaring and integrating. The average main beam intensity, $\bar{I}$, is obtained simply by integrating the main beam signal (prior to S and D), with a time constant long enough to filter out the IPS (i.e., 1 s).

Calculation of the scintillation index straight-forward matter, since $m = \sqrt{S/\bar{I}}$. For the stronger sources, it is also possible to obtain an idea of the relative distribution of high vs. low frequency scintillations by calculating the frequency scale, $f = \sqrt{D/S}$.

In the initial group of nearly 100 sources we have observed, in which about 80 were known from higher frequency (≥ 80 MHz) observations by others (Harris, et al., 1969; Little and Hewish, 1968; Readhead, 1974) to be subject to IPS, 60 have displayed IPS. Since there are over 900 catalogued IPS sources, the initial observations indicate that the number of sources on which we will be able to take synoptic observations will be limited solely by declination limits on the array (-25°), solar elongation angle (>20°) and observing time needed to get adequate source and baseline data (~6 minutes).

The current observing list consists of 154 sources. As some of the newly observed sources will undoubtedly prove to be unreliable scintillators, they will be dropped from the observing list. However, there are many more sources to choose from, so the observing list will actually be expanded until it ultimately contains a grid of about 200 reliable IPS sources which will be monitored on a daily basis.

EVENT OF JUNE 26, 1974

We can now turn to the event which we shall use as an example for the prediction of upper-atmospheric and ionospheric disturbances associated with solar particle events and geomagnetic storms. Continuous monitoring of about 90 radio sources on a regular 24-hour basis was carried on during June, 1974 with the COCOA-Cross array. The largest event in that month occurred on June 26. It is of considerable interest for four reasons:

(1) There was a geomagnetic storm sudden commencement (SSC) observed by 19 stations (from 64.6° N to 46.7° S geomagnetic latitude) at 2329 UT, June 25, with 3-hour values of Kp = 5 for the next two days;

(2) The SSC was accompanied by a decrease ~ 5% in the galactic cosmic ray intensity (CRD) as measured by high-latitude neutron monitors, with recovery 3 days later;

(3) Within 12 hours of the SSC the flux of low-energy solar protons (0.3-0.5 MeV) had exceeded 100 $(cm^2\ sec\ ster\ MeV)^{-1}$ and remained above this level for 3 days, while the flux of relativistic solar electrons (> 220 keV) rose some 3 hours after the protons, reaching a peak flux above 10 $(cm^2\ sec\ ster)^{-1}$ by June 28;

(4) An ionospheric disturbance followed the SSC; its recovery began on June 27 and lasted until June 30.

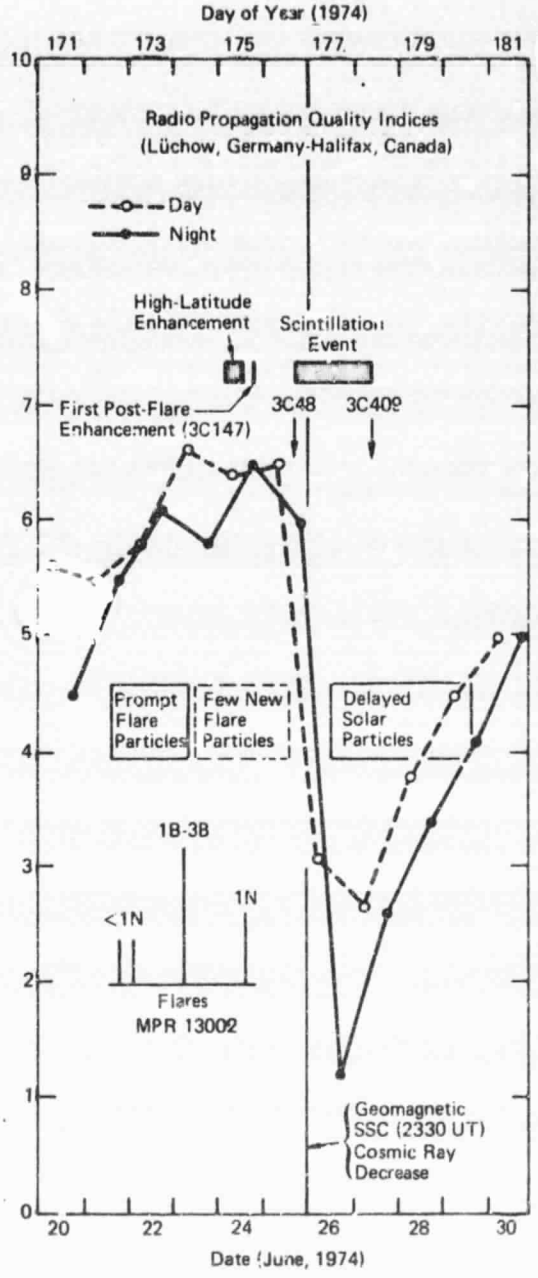

Fig. 2 Radio propagation quality indices for transmission in the band 2-26 MHz between Lüchow (Germany) and Halifax (Canada), June 20-30, 1974. Times of significant flares from MPR 13002 and the SSC on June 25 are indicated, as well as the IPS events that could have led to the prediction of the geomagnetic storm and associated solar particle event on June 26.

Figure 2 shows the radio propagation quality indices for transmission between Lüchow (Germany) and Halifax (Canada) over frequencies in the band 2-26 MHz appropriate for day or night at both stations during June 20-30. The drop in the field strength for the first observation (day) after the SSC is apparent, and it is also clear that the observation (night) between the beginning of the scintillation event and the SSC was in the range of average propagation conditions (index ~ 6). Also summarized in Figure 2 are the solar flares from the McMath Plage Region (13002) responsible for the disturbance, the COSPA-Cross IPS events and solar particle observations for the period. Since we know that solar and interplanetary data complement IPS observations and thereby enhance prediction reliability, let us first present the solar and spacecraft data before proceding to the IPS observations. Since all data discussed is actually available on a real-time basis, they can be incorporated into our prediction simulation based on IPS observations.

McMath Plage Region 13002 began optical flare activity soon after its central meridian passage (CMP June 20) with small flares (< 1N) at ~1800 UT, 21 June and ~ 0330 UT, June 22. The only prior flares in June at this importance level had been in two other regions (12972, CMP June 3 and 12993, CMP June 14), all before June 15. The last flare ≥ 1N from MPR 13002 before it went over the west limb on June 26, was at ~ 1500 UT on June 24. The only other flare activity was from MPR 13043 (CMP July 3) on June 29-30 (after limb passage of MPR 13002 on June 26). Therefore MPR 13002 dominated solar activity from its CMP until its limb passage.

A striking signature of this active region transit June 20-30 is found in the 0.3-0.5 MeV proton and > 0.22 MeV electron fluxes measured by the APL/JHU experiment on IMP-7, shown in Figure 3. The times and optical importance of all flares from MPR listed in Solar-Geophysical Data (Prompt Reports) are indicated on the figure, as well as the position of IMP-7 along its ~ 34 R_e near-circular orbit relative to the magnetotail and Earth-Sun line.

The first small flare (~ 1800 UT, June 21) resulted in a prompt relativistic electron event as well as a characteristically rapid and strongly anisotropic rise in the low-energy protons. The second small flare (~ 0330 UT, June 22) produced a small electron enhancement. It therefore appears paradoxical that the larger and brighter flare (importance ~ 2B, with decimeter type III as well as meter and dekameter type II radio emission) at ~ 0500 UT, June 23 did not produce any significant prompt enhancement of either proton or electron fluxes. Nor for that matter did the 1N flare at ~ 1515 UT, June 24.

It then appears that the interplanetary magnetic "connection" between the acceleration site and the earth was much "poorer" during

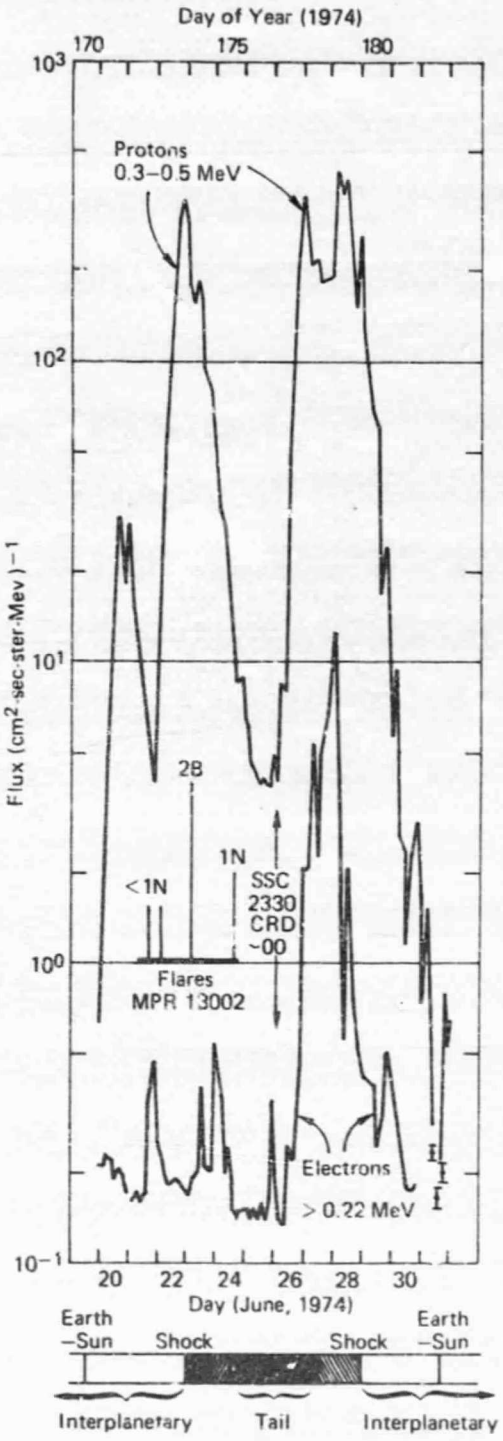

Fig. 3 Solar energetic particle fluxes measured by the APL/JHU experiment on IMP-7, June 20-30, 1974. Location of the spacecraft (near-circular orbit ~ 34 R_e) relative to the magnetotail and Earth-sun line is shown below the figure. Times are indicated for all significant flares from McMath Plage Region 13002 as well as the sudden commencement of the geomagnetic storm (SSC) and associated decrease in cosmic ray intensity (CRD) at the end of June 25.

June 23-25 than it was on June 21 and 22, since we know that these small gyro-radius particles cannot appreciably cross field lines in interplanetary space (Lin et al., 1968; Krimigis et al., 1971; Roelof and Krimigis, 1973). This inference is strongly supported by the particle event of June 26, when it appears that the interplanetary magnetic "connection" moved to coronal regions where particle injection was greatly enhanced. It seems very unlikely that the onsets on June 26 were due to new acceleration because the relativistic electron rise is abnormally slow, and the low-energy proton rise precedes that of the electrons by more than 6 hours. Rather it is likely that the higher solar wind velocities behind the shock (which we infer from the SSC at 2230 UT on June 25), resulted in the earth being re-connected into a new region of the equatorial corona an appreciable distance further east ($\geq 30°$) on June 26 than it was on June 25. Just such an effect was recently documented during the August, 1972 activity from Earth and Pioneers 9 and 10 by Roelof et al., (1974). MPR 13002 released 0.3 MeV protons and > 0.2 MeV electrons into interplanetary space for two additional days (June 27-28) without appreciable decrease in intensity, with similar > 0.2 MeV electron injection for more than a day. Long-lived injections earlier in the solar cycle have been analyzed by Roelof and Krimigis (1973).

We therefore are led to the conclusion that the protons and electrons were being accelerated well before the interplanetary shock allowed the them to reach earth, perhaps as early as the ~ 2B flare on June 23. The abrupt decrease of the proton intensity beginning June 29 may then simply be explained by the magnetic "connection" longitude moving further eastward after the decay of the solar wind event.

The inter-relationships of the flares, scintillation enhancements and solar particle events observed from Earth become more clearly ordered when we quantitatively estimate the Earth's coronal magnetic connection longitude and compare the events with low-coronal magnetic structure.

That quantitative estimates of equatorial high-coronal connection longitude of interplanetary magnetic field lines can be made using observed solar wind velocities has been justified theoretically for both quiet and disturbed interplanetary conditions (Nolte and Roelof, 1973a; 1973b). Observational verification has been presented by Krieger et al., (1973; 1974) of the tracing back of recurrent solar wind streams to magnetically open coronal structures (coronal "holes") seen in x-ray images obtained from the American Science and Engineering Telescope on a rocket flight and throughout the Skylab mission. A recent multispacecraft observational calibration of the precision of the mapping (Gold and Roelof, 1975) has yielded a mean error of $< 10°$ in solar longitude over 6 months of observations in 1967. The mapping simply assumes that the interplanetary magnetic field is "frozen-in" the solar wind plasma whose velocity is assumed to be radial and constant after it leaves the outer corona.

As an indicator of coronal magnetic structure, we have chosen to use Hα Synoptic Charts, since it has been established that absorption features in solar Hα photographs (filaments, filament channels, fibril patterns, etc.) delineate neutral lines for large-scale chromospheric polarity regions (McIntosh, 1972a; 1972b). Moreover we have shown that the equatorial crossings of Hα neutral lines often correspond to spatial discontinuities in interplanetary energetic particle fluxes when they are mapped back to the corona along large-scale interplanetary field lines deduced from observed solar wind velocities (Roelof and Krimigis, 1973; Gold et al. 1974; Roelof et al. 1974; Nolte, 1974; Roelof, 1973a; 1973b; 1974).

Figure 4 shows an annotated version of the preliminary (real-time) Hα Synoptic Chart for Carrington Rotation 1616 (June-July, 1974), published by P.S. McIntosh in Solar Geophysical Data (Prompt Reports) (August, 1974). Hα filaments are cross-hatched, and magnetic neutral lines are solid if inferred from Hα structure, but dashed if inferred from continuity. Sunspots are solid dots and Hα emission plages are stippled. McMath Plage Region 13002 is centered at 350° longitude $\leq 20°$ latitude. Magnetic polarities (±) have been checked with solar magnetoheliograms.

The time history of terrestrial observations is shown on the "time line" below the Central Meridian Date on the upper border. The estimated high-coronal connection longitudes for the interplanetary magnetic field are shown by arrows above the equator for the indicated dates and times (e.g., 21:18 is 1800 UT, June 21). Since solar wind velocity measurements are not available at the time of writing, we have made the following estimates. The period June 21-25 was very quiet geomagnetically (three-hour $Kp \leq 3$), so we have assumed a velocity of 350 km/s, except for July 23 when there was a small storm ~ 0800 UT when we chose 600 km/s. Immediately after the SSC, we have assigned a velocity from the June 23 flare, and assumed that the stream velocity decayed to 350 km/s by June 29. It will be seen from the following discussion that the arguments will still hold even if our estimates are not too accurate.

The prompt low-energy protons and relativistic electrons from the June 21 flare were injected onto interplanetary field lines ~ 30° west of the flare site in MPR 13002. Even though the estimated connection longitude is over the flare site on June 23, few new particles were seen at earth. We have observed such behavior before and concluded that the magnetic structure immediately over a flare site may sometimes be relatively closed. One such case, MPR 8942 in August 1967, was extensively

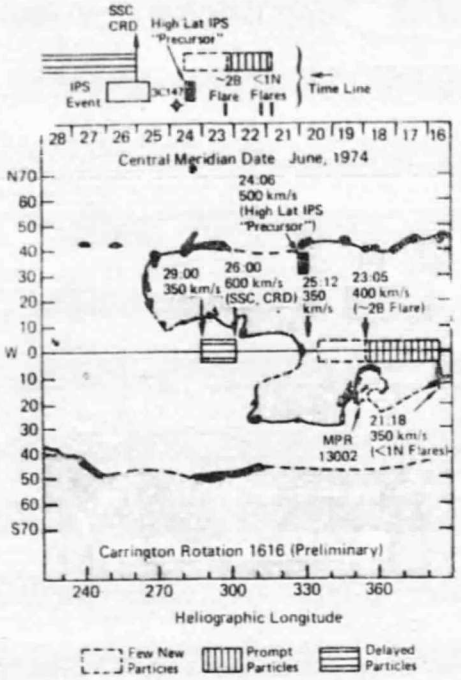

Fig. 4 Large-scale chromospheric magnetic field polarities (shaded, out of the sun) deduced from Hα photographs. Dark filaments (filled with heavy stipple), filament channels and fibril patterns delineate neutral lines between polarity regions. Open stipple patterns are Hα emission plage. Time line (above figure) summarizes IPS and energetic particle events (see legend below figure). High coronal equatorial connection longitudes (estimated from indicated solar wind velocities) for interplanetary injection of solar particles (Figure 3) are marked along the heliographic equator. Time indications (arrows) are in day and hour; for example the connection longitude at 1200 UT on June 25 (25:12) was 330°, estimated on the basis of a solar wind velocity of 350 km/s.

documented for > 40 keV electrons by Lin (1970) and for > 0.3 MeV protons by Roelof and Krimigis (1973).

On the other hand, the onset of the "delayed" particle event of June 26 apparently was the result of the connection longitude being switched ~ 30° eastward (from 330° at 1200 UT, June 25 to 300° at 0000 UT, June 26) by the increased solar wind velocity behind the interplanetary shock inferred from the SSC. If the solar wind velocity did then steadily decay to something like 350 km/s by June 29, then the coronal injection longitudes for most of the delayed particle event were between 275°-300°. The decay of the particle fluxes beginning June 29 may then have been due to the combination of the resumption of the eastern motion of the connection longitude (13.2° per day at a constant solar wind velocity) and a western gradient of the coronal injection profile for > 0.3 MeV protons. It is therefore possible that the magnetic coronal structure above the inferred neutral-line which crosses the equator ~ 295° served to "compartment" the energetic particles in the high corona, with enhanced interplanetary access for particles outside the eastern boundary of the large negative polarity region west of 270°. A similar case, where particles preferentially occurred outside the polarity region containing the flare site (MPR 8905 in August, 1967) was documented by Roelof and Krimigis (1973), using these same techniques with three spacecraft separated over 0.5 AU (Mariners 4 and 5 and Explorer 35).

SIMULATED PREDICTION OF IONOSPHERIC DISTURBANCE

Let us now construct a scenario for an attempted prediction of the June 26 disturbances. With all due disclaimers for the superior acuity of hindsight, we believe that the IPS observations of June 20-25, when combined with other routinely available real-time data, would have allowed a probable prediction of disturbance. We shall assume for this exercise that we have available on a daily basis only the data presented in the previous section, namely:

(1) IPS monitored on a 24-hour basis from a grid ~ 100 sources;

(2) Optical and radio flare observations;

(3) Hα Synoptic Chart in progress for the current solar rotation (i.e., completed to heliographic longitudes at least as far east as E30° on each day of observations);

(4) Low-energy (≤ 1 MeV) proton and near-relativistic (≥ 50 keV) electron measurements with time resolution ≤ 1 hour;

(5) Geomagnetic and ionospheric activity indices.

It will be noted that all five classes of data are currently available. In addition (although we shall not make use of it here), solar wind velocity measurements with a significant sample in intervals ≤ 3 hours would considerably augment the prediction reliability.

With a grid of ~ 90 sources, two-dimensional analysis of a scintillation event is possible. After all, there is no a priori reason that the spatial dependence of events should be confined to the ecliptic; indeed, a variety of complex three-dimensional configurations may be anticipated on the most simple physical grounds.

Therefore we selected 28 sources from the 90 being monitored in late June that exhibited consistent patterns of scintillation activity over the first 60 days of observations. These are listed in Figure 5 by their Third Cambridge Catalog number, right ascension (epoch 1974.5) and ecliptic latitude. Note that the sources are somewhat uniformly distributed in right ascension, but range from +5° to -12° ecliptic latitude. Their scintillation indices for each day of the period June 20-30 are indicated by

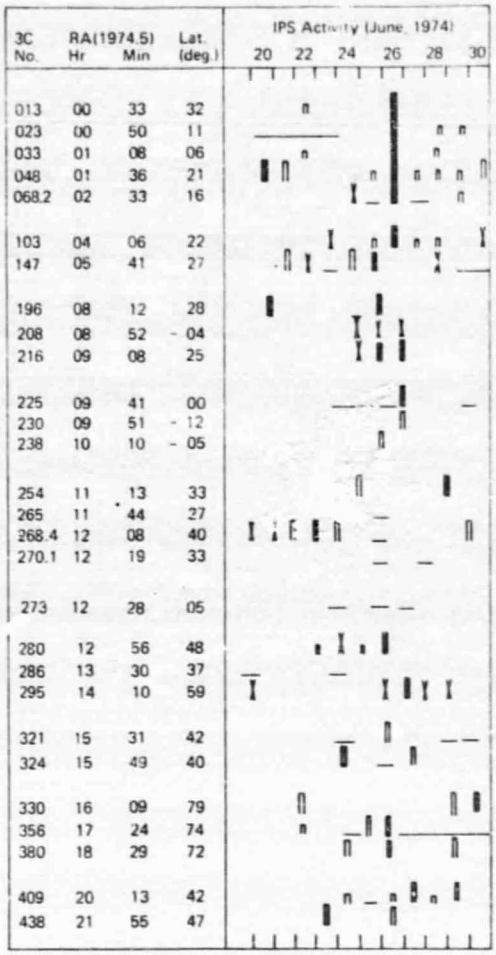

Fig. 5. Sources exhibiting consistent interplanetary scintillation activity during May-June 1974, listed by Third Cambridge Catalog number, right ascension (epoch 1974.5) and ecliptic latitude. During June 20-30, source transit time was approximately $10^h\ 30^m$ less than right ascension. Activity symbols for each day's observations: open bars, moderate; solid, high; none, low; dash, no observation; cross, radio frequency interference.

the following symbols: open bars (half and full height, moderate activity; solid bars, high activity; no bars, low activity; dash, no observation; and cross, radio frequency interference (RFI) placing an upper bound on scintillation index.

Even cursory examination of Figure 5 immediately reveals the scintillation event of June 26 following the SSC of 2330 UT June 25. However, since UT at Clark Lake for source observations is about $10^h\ 30^m$ less than their right ascension, the chart reveals that several sources showed high activity on June 25, up to 12 hours before the SSC, while others showed activity the following day (June 27). Moreover, activity in a cluster of sources (e.g., 3C23, 3C33, 3C48, 3C68.2, 3C103 and 3C409), persists until June 30. In addition, there appears to be a weak "precursor" event in the higher latitude sources on June 24.

We can now begin our scenario by simulating, on a day-by-day basis, the COCOA-Cross IPS observations and complementary solar, geomagnetic and energetic particle data.

June 20 – The first indication of subsequent solar activity would have been the small proton event (see Figure 3) ever though it had no flare association, since we know that protons at these energies are often associated with the disc transit of an active region with no required flare association. However, with MPR 13002 just past central meridian passage and having shown no previous significant optical activity, the small proton even would not have done much more than suggest that activity in MPR 13002 might be on the increase.

June 21-22 – The prompt relativistic electrons and low energy protons from the small (< 1N) flares in MPR 13002 would establish the region as a significant acceleration of particles. The sharpness of the intensity rises, combined with the interplanetary magnetic connection longitude being $\sim 30°$ west of MPR 13002 assuming a quiet solar wind based on Kp < 3 (see Figure 4), would have suggested that a subsequent large flare might have produced an intense particle event. Also, the sunward cone of IPS sources would be watched closely on June 23 for a small interplanetary disturbance from the ≤ 1N flares.

June 23 – The picture would change dramatically on this day. Firstly, the anticipated large flare ($\sim$ 2B at W50° with type II and III radio emission) does not produce any prompt significant enhancements of relativistic electrons or low energy protons (see Figure 3), implying that either the flare produced considerably fewer particles than would have been expected from the June 21-22 activity in MPR 13002, or that the Earth-corona magnetic connection was strikingly different from what it had been during those earlier flares. Since geomagnetic activity was still low, the latter implication would have to be interpreted as a relatively closed coronal magnetic structure over MPR 13002, since it now lay under the estimated connection longitude (using a nominal 400 km/s solar wind velocity).

Examination of the Hα neutral-line structure (Figure 4) might then have suggested that the bulk of the accelerated particles may have been preferentially injected to the east of the equator crossing of the neutral line through MPR 13002 at $\sim 330°$. We would then anticipate that if the low-energy proton injection continued for another day or two, the protons could reach the Earth after the magnetic connection crossed that line. With an undisturbed solar wind, that would be no later than sometime June 26. There is still no evidence in the IPS observations for an interplanetary plasma disturbance. It would appear that no significant one

had been generated by the small flares of June 21-22, and it would still be too early for anything but a very fast blast wave to be seen by the small-elongation sources.

June 24 -- The continued decay of the low-energy proton fluxes is still consistent with either the absence of particles from the June 23 flare or their preferential release elsewhere in the corona. However, the persistence of the relativistic electrons (even increasing on this day) suggests that particle injection is continuing.

It is the IPS pattern that would tip the balance toward the possibility of a delayed event in the making.

These patterns, although somewhat ordered in right ascension (as in Figure 5), become considerably clearer and more amenable to physical interpretation when presented in latitude as well as longitude. We therefore present the data of Figure 5 using "all-sky" plots for four 24-hour periods in Figure 6 beginning at 00 UT: (a) June 24; (b) June 25; (c) June 26; and (d) June 27. The longitude coordinates are λ_{177}, the solar ecliptic longitude at 00 UT, June 26 (just after the SSC). The ecliptic latitude is plotted as the polar coordinate from +90° to -10°. Thus any localized region (less than 30° by 30°) shows the relative positions of the sources therein with only slight distortion (very similar to the image from the all-sky cameras used in auroral studies). As in Figure 5, sources are labeled by their Third Cambridge Catalog number, and the level of scintillation activity is indicated by the symbols given in the legends.

In interpreting the 24-hour, all-sky plots, it is essential to bear in mind the time of observation of the sources (see Figure 5 for right ascension). For instance, since all the plots begin at 00 UT (Figures 6a-6d), the earliest source observed during the 24 hours was 3C254, while a neighboring source at nearly the same ecliptic longitude (3C238) was observed almost one day later.

The major interplanetary activity in late June was initiated by a flare with optical importance ~ 2B at ~ 0500 UT on June 23 at W50° S16° in McMath Plage Region (MPR) 13002. Figure 6a reveals that about 38 hours later, on June 24, 3C147 (solar elongation angle ≈ 25°) exhibited a moderate enhancement in scintillation index. Although confirmation is not obtained from the other western source at small elongation (3C103), nor from a source north-east of the sun (3C196) because of no observation, the mean minimum transit velocity for a disturbance to cross the line of sight to 3C147 is ≥ 550 km/s and to 3C103 is ≤ 800 km/s (a reasonable velocity range for flare-associated plasma flow 0.5-0.7 AU of the sun). The lack of enhancement of the source 3C103 at small elongation is therefore not inconsistent with the possibility that the enhancement of 3C147 was due to outgoing plasma from the June 23 flare.

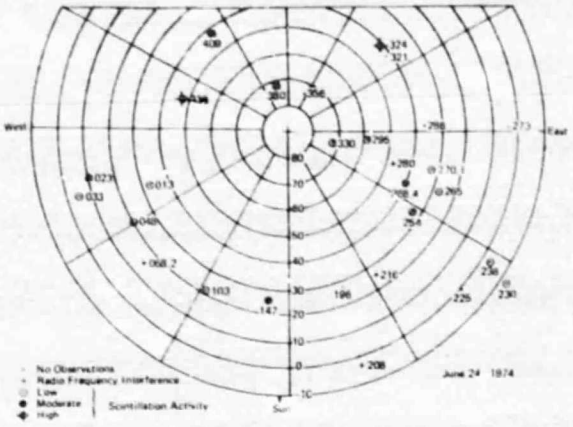

Fig. 6a "All-sky" plot of scintillation activity. Note first source observed during indicated 24-hour period is 3C254 and last is 3C238. Ecliptic latitude is plotted linearly as polar coordinate, and ecliptic longitude on day 177, 1974 (June 26) is the azimuthal coordinate. Data are plotted from Figure 5 and symbols identified in legends. High latitude "precursor" and first sunward scintillation enhancement (3C147 following the ~ 2B flare, 0500 UT June 23.

It is striking, however, that the only other scintillation activity on June 24 in Figure 6a appears exclusively in the northern mid-to-high-latitude sources (> 40°): 5 out of the 7 observations show enhancements, two of which (3C324 and 3C438) are significantly high. It is not unusual that two sources show low activity (3C295 and 3C330); we have found that high latitude scintillation events are often "patchy". Therefore, this pattern raises the possibility that a co-rotating solar wind disturbance well north of the ecliptic swept over the earth at this time. Three additional facts are consistent with this suggestion. The high latitude disturbance is unlikely to have the form of a blast wave, since it was not seen at lower latitudes on June 22 or 23 (see Figure 5). Moreover, the only flares prior to June 23 are at 0310 UT, June 22 and 1800 UT, June 21, both from MPR 13002, but both of optical importance < 1N. Thirdly, the inferred co-rotating stream would emanate from a northern coronal latitude at a position nearly due north of MPR 13002 (which was ~ W40° at the time of the observations). The high-latitude "precursor" event observed from 0600-1200 UT with an estimated source location (assuming a typical stream velocity of 500 km/s) in the large unipolar region north-east of MPR 13002 would be the first evidence that high velocity plasma had been emitted from the vicinity of the active region for several days prior to the ~ 2B flare on June 23 and therefore that MPR 13002 might also generate a large temporal disturbance in the solar wind. There have been cases of co-rotating solar wind streams emanating from open magnetic structures no closer than ~ 60° in longitude to active regions (Krieger et al. 1973; 1974), so it is quite reasonable that such a stream is inferred

~ 60° northeast of MPR 13002 in a unipolar, and hence possibly magnetically open coronal region.

In the light of the high latitude "precursor" associated with MPR 13002, the solitary scintillation enhancement of 3C147 at ~ 1900 UT (the source at smallest observable elongation angle and slightly to the west of the sun), would take increased significance, raising the possibility that a disturbance was propagating outward at > 550 km/s at ~ 1500 UT, June 24. This conservative lower bound implies an arrival at Earth no later than mid-day, June 26, along with an eastward shift of coronal connection longitude into a new region which may contain the energetic particles "missing" from the June 23 flare, thus producing a "delayed" particle event following an SSC of a geomagnetic storm.

June 25 – The scintillation activity on June 25 (Figure 6b) is very suggestive of an outward moving blast wave from the large flare of June 23. All observing sources with elongation ≤ 60° showed either moderate or high scintillation indices, while no sources outside of this sunward cone (with the sole exception of moderate activity in 3C356) showed any enhancements. The timing of the observations is critical here, since the enhancement in 3C48 (at the western edge of the sunward cone) was observed ~ 1500 UT, more than 8 hours before the solar wind disturbance caused the SSC at 2330 UT, and all but one (3C230) of the 8 observations subsequent to 3C48 (i.e., through 3C254), show enhancements; the three closest to the sun are significantly high (3C147, 3C196 and 3C216).

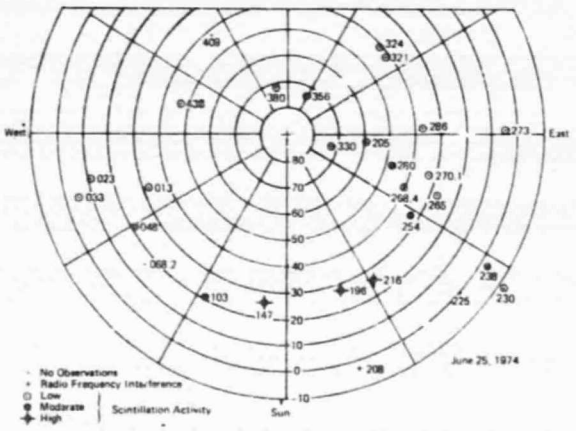

Fig. 6b IPS signature of flare-associated disturbance which caused SSC at 2330 UT, June 25. See Figure 6a.

As the low-altitude sunward sources, beginning with 3C48 at ~ 1500 UT, sequentially show enhanced scintillation indices, we would find our previous conjectures supported and conclude that the arrival of a geomagnetic storm and a possible delayed solar particle event were imminent. It seems reasonable to say that we would have reached these conclusions at least 6 hours before the SSC at 2330 UT, and that we would have been alerted to the possible arrival of the SSC and solar particles on the previous day (see discussion of June 24).

June 26 – The scintillation event is immediately evident in Figure 6c, implying that the turbulent solar plasma from the June 23 flare was enveloping the Earth beginning with the SSC at 2330 UT on June 25 and continuing throughout June 26. The SSC time implies a mean transit velocity for the plasma of 620 km/s, consistent with the strong decelerations deduced for blast waves. Closer examination of Figure 6c shows a significant bias toward the westward enhancements: 7/10 high (vs. 4/12 for the east); 2/10 moderate (vs. 2/12 for the east); and only 1/10 low (vs. 6/12 for the east). The difference is unlikely to be due to the timing of the observations of the eastern sources; those following 3C268.4 were within the first 6 hours immediately after the SSC. The three-dimensionality of the interplanetary disturbance is apparent not only in the strong western enhancements of 3C013 through 3C103, (a reasonable IPS response for plasma ejected at W50° if its axis of symmetry lies above the flare site), but can also be seen in the lack of enhancement in the sources with smallest elongation angles (3C147 and 3C196) which exhibited high activity on the previous day before the disturbance reached the earth. These sources would not see appreciable turbulence near the earth-sun line as the disturbance swept over the Earth.

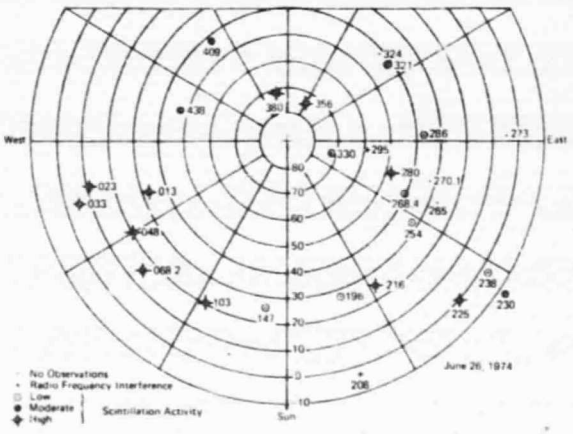

Fig. 6c IPS event as disturbance sweeps over Earth, with westward sources responding to distant plasma from flare longitude (W50°). See Figure 6a.

Even after the SSC arrives, the IPS and energetic particle observations enable us to anticipate the future history of the event. The steady rise of the low-energy protons and relativistic electrons after the SSC (with no prompt flare association), imply that this is the beginning of an extended delayed particle event. The scintillation observations for the day (see Figure 6c) revealed that the centroid of the

turbulence was to the west of us (in agreement with the flare location), so that if this solar wind disturbance followed the pattern of many others, the velocity would begin to decay, possibly on June 27, and continue to decay until reaching its average value. Such a decay usually takes 1-2 days, so around June 28 the connection longitude (having remained around ~ 300° because of the decay), should begin drifting eastward again (at its normal 13° per day).

The result would be that even if the solar proton injection from MPR 13002 were to continue after June 28 (which it well could since the delayed particles were observed already three days after the large flare), the particle fluxes would then likely begin to drop because the coronal connection longitude would rapidly leave the complex of coronal magnetic fields associated with MPR 13002 whose extent was probably roughly indicated by the equator-crossing neutral line (see Figure 4) which extends no further east than 270°.

June 27 – The persistance of the low-energy proton intensity at high flux levels would reinforce the above conjecture about the nature of the termination of the particle event. The anti-solar and weak westward scintillation activity (see Figure 6d) would be interpreted as the passing of the turbulent front beyond the Earth and subsequent over-the-limb activity of MPR 13002. Further particle or plasma disturbances would be unlikely for the next few days.

If the turbulent plasma was no longer enhanced along the line of sight for 3C147 and 3C196 in the inner forward cone on June 26, Figure 6d then suggests that it may have been observed moving away from the Earth on June 27, since the two sources closest to the anti-solar direction (3C324 and 3C409) showed significant enhancements. Aside from 3C295, the only other enhancements were those of 3C48 and 3C103, looking well west of the sun at low latitudes. These enhancements may well be responding to additional solar wind disturbances generated by activity in MPR 13002 after it has passed over the west limb of the sun early on June 26. This hypothesis is supported by the continued activity up to June 30 exhibited by the westward-looking sources (3C23-3C103) that is evident in Figure 5.

June 28-30 – The continued scintillation enhancements of the westward sources (3C23-3C103, Figure 5) would raise the possibility that the successor of MPR 13002 on the next rotation might be the source of a recurrent solar wind stream and geomagnetic disturbance some 27 days after the longitude of the June stream (~ 300°) again reached W60°. Since the next CMP of this longitude would be early July 20, the recurrent storm could be expected about July 23.

Such a storm (with 3-hour Kp > 7) did occur, with 10 stations reporting an SSC ~ 0100 UT, July 23. Of course, there was much intervening geomagnetic activity and high energetic particle fluxes during the period July 3-8. These events

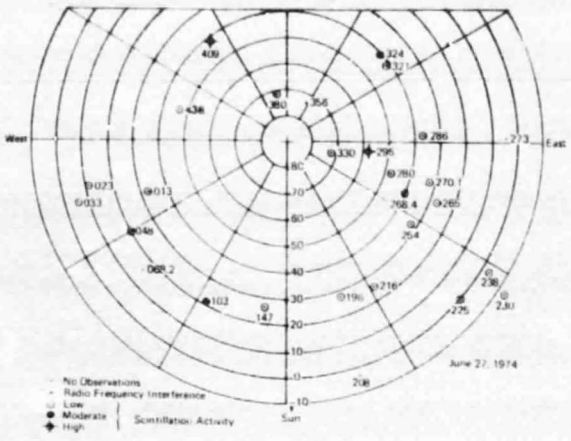

Fig. 6d IPS activity in anti-solar direction (as disturbance passes beyond Earth and westward direction (from over-the-west-limb active region). See Figure 6a.

were from MPR 13043, some 180° east of MPR 13002, and hence quite independent. There was also a scintillation event July 4-6 in conjunction with a large geomagnetic storm, but this happened in a period of sparse observations, precluding an analysis (or prediction) as complete as that given for the June 26 event.

To summarize our interpretation of the IPS observations of Figures 6a-d:

(a) A "precursor" co-rotating solar wind stream emanating from north of MPR 13002 may have been observed by high latitude sources, 0600-1200 UT, June 24. The blast wave from the flare at 0500 UT, June 23 (W50°) may have been detected at small westward elongations (< 30°) as early as 1900 UT on June 24;

(b) The blast wave appears in scintillation in all sources within the sunward cone containing elongation angles ≤ 60° beginning more than 8 hours before the SSC at 2330 UT on June 25;

(c) The turbulent flare plasma sweeps over the Earth on July 26, but the centroid of the interplanetary disturbance appears to be well west of the Earth;

(d) The disturbance may have been detected in the anti-solar direction, having passed beyond the Earth on June 27. At the same time, there is evidence from westward looking sources that MPR 13002 continued to generate interplanetary disturbances up to 4 days after west-limb passage.

In summary, we have attempted to demonstrate the possibilities for prediction that result from the combination of existing daily IPS, Hα, solar particle and geomagnetic (solar wind) observations, the bulk of which are already available through our programs at Clark Lake and Boulder. The reader may draw his own conclusion as to the verisimilitude of our prediction scenario, but

the arguments used are based on our experience in analyzing solar plasma and energetic particle events throughout the last Solar Cycle. Clearly, therefore, the prediction technique as it now stands cannot be carried out by an untrained observer, nor have we made sufficient observations to evaluate the reliability of our approach. Nonetheless, we believe the availability of synoptic monitoring of the interplanetary medium by the COCOA-Cross array adds a new and incisive diagnostic for the solution of the solar-terrestrial prediction problem.

ACKNOWLEDGMENTS

The initial design and construction of the COCOA-Cross array was funded by a grant to NOAA from Dr. Norman Ness at NASA/GSFC. Current support is provided by the Atmospheric Sciences Branch of NSF, the University of Iowa, NOAA, and Applied Physics Laboratory/The Johns Hopkins University.

REFERENCES

Armstrong, J. W., W. A. Coles, J. K. Harmon, S. Maagoe, B. J. Rickett, and D. G. Sime, Radio scintillation measurements of the solar wind following the flares of August 1972, World Data Center A for Solar-Terrestrial Physics, Rept. UAG-28, 371, July 1973.

Balsley, B.B. and W.L. Ecklund, A portable coaxial collinear antenna, IEEE Trans. Ant. Prop., 20, 513, 1972.

Burnell, S. J., Enhancements of interplanetary scintillation, corotating streams and Forbush decreases, Nature 224, 356, 1969.

Coles, W.A., B.J. Rickett and V.H. Rumsey, Interplanetary scintillations, Solar Wind Three, ed. C.T. Russell, Institute of Geophysics and Planetary Physics, University of California (Los Angeles), 351, 1974.

Coles, W.A. and S. Maagoe, Solar wind velocity from IPS observations, J. Geophys. Res., 77, 5622, 1972.

Cronyn, W.M., Density fluctuations in the interplanetary plasma: Agreement between space probe and radio scattering observations, Astrophys. J., 171, L101, 1972.

Dennison, P.A. and A. Hewish, The solar wind outside the plane of the ecliptic, Nature, 213, 343, 1967.

Gold, R.E. and E.C. Roelof, Inference of the equatorial high coronal magnetic field polarity from interplanetary measurements, submitted to Solar Phys., 1975.

Gold, R.E., J.T. Nolte, E.C. Roelof and R. Reinhard, The influence of coronal magnetic structure on low-energy solar proton events, Space Research XIV, (ed.) A.C. Strickland, Akademie Verlag, Berlin, in press, 1974.

Harris, D.E. and E.G. Hardebeck, Interplanetary scintillations V, A survey of the northern ecliptic, Astrophys. J. Suppl., 19, 115, 1969.

Hewish, A., P.F. Scott, and D. Wills, Interplanetary scintillation of small diameter radio sources, Nature, 203, 1214, 1964.

Houminer, Z., Corotating plasma streams revealed by interplanetary scintillation, Nature, 231, 165, 1971.

Houminer, Z., Power spectrum of small-scale irregularities in the solar wind, Planet. Space Sci., 21, 1367, 1973.

Houminer, Z., Enhanced scintillation sectors outside the plane of the ecliptic, Planet. Space Sci., 21, 1617, 1973.

Houminer, Z. and A. Hewish, Long-lived sectors of enhanced density irregularities in the solar wind, Planet, Space Sci., 20, 1703, 1972.

Krieger, A.S., A.F. Timothy and E.C. Roelof, A coronal hole and its identification as the source of a high velocity solar wind stream, Solar Phys., 23, 123, 1973.

Krieger, A.S., A.F. Timothy, G.S. Vaiana, A.J. Lazarus, and J.D. Sullivan, X-ray observations of coronal holes and their relation to high velocity solar wind streams, Solar Wind Three, ed. C.T. Russell, Institute of Geophysics and Planetary Physics, University of California (Los Angeles), 132, 1974.

Krimigis, S.M., E.C. Roelof, T.P. Armstrong and J.A. Van Allen, Low energy ($\geq$ 0.3 MeV) solar particle observations at widely separated points (> 0.1 AU) during 1967, J. Geophys. Res., 76, 5921, 1971.

Little, L.T. and A. Hewish, Radio source structure derived from interplanetary scintillation, M.N.R.A.S., 138, 393, 1968.

Lin, R.P. S.W. Kahler and E.C. Roelof, Solar flare injection and propagation of low energy protons and electrons in the event 7-9 July, 1966, Solar Phys., 4, 338, 1968.

Lin, R.P., The emission and propagation of $\sim$ 40 keV solar flare electrons, 2. The electron emission structure of large active regions, Solar Phys., 15, 453, 1970.

Matheson, L.N. and L.T. Little, Radio scintillations due to plasma irregularities with a power law spectra, the interplanetary medium, Planet. Space Sci., 19, 1615, 1971.

McIntosh, P.S., Inference of solar magnetic polarities from H-alpha patterns, in Solar Activity Observations and Predictions, ed. P. McIntosh and M. Dryer, MIT Press (Cambridge), 65, 1972a.

McIntosh, P.S., Solar magnetic fields derived from hydrogen alpha filtergrams, Rev. Geophys. Space Phys., 10, 837, 1972b.

Nolte, J.T. and E.C. Roelof, Large-scale structure of the interplanetary medium. I: High coronal source longitude of the quiet-time solar wind, Solar Phys., 33, 241, 1973a.

Nolte, J.T. and E.C. Roelof, Large-scale structure of the interplanetary medium. II: Evolving magnetic configurations ded from multi-spacecraft observations, Solar Phys., 33, 483, 1973b.

Nolte, J.T., Inter-relationship of energetic particles, plasma and magnetic fields in the inner heliosphere, Ph.D. Dissertation, University of New Hampshire, 1974.

Readhead, A.C.S., Fine structure in radio sources at 81.5 MHz III. M.N.R.A.S., 78, 1, 1974.

Rickett, B.J., Power spectrum of density irregularities in the solar wind plasma, J. Geophys. Res., 78, 1543, 1973.

Roelof, E.C., Coronal propagation of energetic charged particles, Proceedings of the Symposium on High Energy Phenomena on the Sun, (ed.) R. Ramaty and R. G. Stone, National Aeronautics and Space Administration SP-342, 1973a.

Roelof, E.C., Coronal magnetic fields and the structure of low-energy solar charged particle events, Proc. of the Solar-Terrestrial Relations Conference, University of Calgary, Canada, 341, 1973b.

Roelof, E.C., Coronal structure and the solar wind, Solar Wind Three, ed. C.T. Russell, Institute of Geophysics and Planetary Physics, University of California (Los Angeles), 98, 1974.

Roelof, E.C. and S.M. Krimigis, Analysis and synthesis of coronal and interplanetary energetic particle, plasma and magnetic field observations over three solar rotations, J. Geophys. Res., 78, 5375, 1973.

Roelof, E.C., J.A. Lezniak, W.R. Webber, F.B. McDonald, B.J. Teegarden and J.H. Trainor, Relation of coronal magnetic structure to the interplanetary proton events of August 2-9, 1972, in Proc. of the Seventh ESLAB Symposium on Correlated Interplanetary and Magnetospheric Observations, (ed.) D.E. Page, D. Reidel (Holland), 563, 1974.

Sharp, L.E. and D.E. Harris, Enhanced interplanetary scintillations associated with solar flares, Nature, 213, 377, 1967.

Ward, B.D., Detection of the June 15th disturbance by interplanetary scintillation, Compilation of Solar Particle and Interplanetary Measurements Acquired During the Campaign for Integrated Observations of Solar Flares (CINOF), ed. M.A. Shea and D.F. Smart, Air Force Cambridge Research Laboratories Special Report No. 177, AFCRL-TR-74-0271, 43, 1974.

Watanabe, T. and T. Kakinuma, The recurrent solar wind streams observed by interplanetary scintillation of 3C48, Pub. Ast. Soc. Japan, 24, 459, 1972.

Watanabe, T., T. Kakinuma, M. Kojima, and K. Shibasaki, Solar wind disturbances detected by the interplanetary scintillation of radio sources in early August 1972, J. Geophy. Res. 78, 8364, 1973.

Wiseman, M. and P.A. Dennison, Flare induced shocks and corotating streams in the interplanetary medium, Proc. Ast. Soc. Australia, 2, 64, 1972.

APPENDIX B

Interplanetary Scintillation Observations with the Cocoa Cross Radio Telescope*

by

W. M. Cronyn, S. D. Shawhan,
F. T. Erskine, A. H. Huneke,
and
D. G. Mitchell

Department of Physics and Astronomy
THE UNIVERSITY OF IOWA
Iowa City, Iowa 52242

Interplanetary Scintillation Observations with the Cocoa Cross Radio Telescope*

by

W. M. Cronyn, S. D. Shawhan,
F. T. Erskine, A. H. Huneke,
and
D. G. Mitchell

W. M. Cronyn
Space Environment Laboratory/ERL
National Oceanic and Atmospheric Administration
Boulder, Colorado 80302

S. D. Shawhan, F. T. Erskine, A. H. Huneke
Department of Physics and Astronomy
University of Iowa
Iowa City, Iowa 52242

D. G. Mitchell
Department of Physics
University of New Hampshire
Durham, New Hampshire 03824

February, 1975

Submitted as a Letter to Nature-Physical Sciences.

*Located at the University of Maryland Clark Lake Radio Observatory, Borrego Springs, CA 92004. Research supported by NSF Grant (Atmos. Science Section) DES73-06559A01, NASA Purchase Request S-57016A, NASA Grant NGL16-001-002 and NOAA Contract 04-3-022-28.

ABSTRACT

Physical and electrical parameters for the 34.3 MHz Cocoa Cross Radio Telescope are given. The telescope is dedicated to the determination of solar wind characteristics in and out of the ecliptic plane through measurement of electron density irregularity structure as determined from IPS (interplanetary scintillation) of natural radio sources. The collecting area (7.2×10^4 m^2), angular resolution (.4° EW x .6° NS) and spatial extent (1.2 km EW x 0.8 km NS) make the telescope well suited for measurements of IPS index and frequency scale for hundreds of weak radio sources without serious confusion or ionospheric scintillation effects.

INTERPLANETARY SCINTILLATION OBSERVATIONS WITH THE COCOA CROSS RADIO TELESCOPE

We report the first IPS (interpla tary scintillation) observations made with the 34.3 MHz Cocoa Cross radio telescope, a joint project of the National Oceanic and Atmospheric Administration and the University of Iowa. The instrument has one of the largest effective collecting areas of any radio telescope in the world, more than 7×10^4 m^2 (approximately equal to the geometric area of the 300m Arecibo reflector). It has been specifically designed for synoptic IPS observations of large numbers of radio sources at source-sun elongation angles of 20° to 180° covering southern ecliptic latitudes of 0° to 45° (depending on ecliptic longitude) and the entire northern ecliptic hemisphere. Observing this grid of sources daily we intend to locate, map and track co-rotating and transient solar wind features such as streams, blast waves and plasmoids as identified by associated IPS activity[1-5]. These observations are being correlated with measurements of interplanetary magnetic fields, solar wind velocity, electron number density and energetic particles as well as H_α maps and geomagnetic activity.

Technical parameters of the Cocoa Cross radio telescope are given in Table 1. A simplified block diagram of the receiver electronics is presented in Figure 1. To obtain the main beam response the North and South arm signals are amplified, filtered and summed at 34.3 MHz,

down-converted to 20 MHz, amplified under strong automatic gain control and correlated against the East-West arm signals using a double-balanced mixer. Other correlation products are also measured to provide beam pointing and array performance information. The resultant normalized main beam correlation product is then smoothed to give the total power of the source, I, and is also bandpass filtered in the range 0.1 to 1.5 Hz giving the fluctuation power, F, and squared (self-multiplied) and smoothed to give the scintillation power, S; the 0.1 - 1.5 Hz signal is also differentiated, squared and smoothed to give the "differentiated power", D. The scintillation index is then estimated as $m = k_m \sqrt{S}/I$, and the frequency scale of the scintillations (square-root second moment of the power spectrum) is $f = k_f \sqrt{D/S}$, where k_m and k_f are gain constants. These and other receiver outputs are presently displayed on a multichannel paper chart recorder (see Figure 2). All necessary telescope and receiver functions such as beam steering, calibration and gain changes are card reader controlled allowing unattended operation. (Further details are given in a NOAA/SEC technical report in publication.)

The three characteristics of the telescope which make it particularly well suited for the measurement of IPS index and frequency scale for large numbers of sources are: (1) large collecting area, (2) relatively high angular resolution, and (3) large spatial extent. Feature (1) is necessary for measurements of IPS parameters of weak sources ($\geq$ 10 f.u.); (2) is necessary to avoid serious confusion problems and to make possible the determination of normalized IPS index for every source without consideration of array response variation,

ionospheric effects or source intensity variability. With regard to feature (3), ionospheric scintillation frequencies $\lesssim$ 0.1 Hz are eliminated by the bandpass filter while frequency components above 0.1 Hz are severely attenuated by aperture filtering[7]. The spatial extent, L, of ionospheric frequency components greater than frequency ν_c can be estimated from the relationship

$$L \leq U/2\pi\nu_c$$

where U is the diffraction pattern speed. For ν_c = 0.1 Hz and using U < 0.15 km/sec (appropriate for ionospheric wind speeds), L $\lesssim$ .25 km which is less than the 1 km spatial extent of the array, resulting in averaging over several independent scintillation patches. By contrast, for solar wind velocities of 400 km/sec and ν_c = 1.5 Hz, the spatial extent of components for $\nu < \nu_c$ is L $\geq$ 40 km $\gg$ 1 km. Beyond 1.5 Hz there is no significant IPS energy for most sources at 34 MHz. Typical data records are shown in Figure 2. Source solar ecliptic coordinates range in longitude between 22°W and 12°E, in latitude from 19°N to 59°N, and in elongation angle from 32° to 60°. The increase in raw fluctuation signal F can be seen clearly for 3C280 and 3C295. Measurable scintillation indicies are 0.1 (3C293) to 0.2 (3C286); frequency scales are 0.4 Hz (3C280) to 0.6 Hz (3C295). In Figure 3 we show observations of a source taken on four successive days at solar ecliptic longitude 128°E, latitude 16°, elongation angle of 126°. Scintillation index is 0.11 for days 328 and 329; 0.07 for 330 and 331. It is illustrative of both daily index variability and IPS at large elongation angles.

The effectiveness of the ionospheric scintillation suppression has been confirmed by numerous observations of large angular diameter sources such as 3C405. These sources display strong ionospheric scintillations but not within the frequency range of 0.1 to 1.5 Hz on the Cocoa-Cross telescope (except during extraordinary ionospheric activity).

Interpretation of the observations to date have revealed recurrent scintillation activity displaying a 27 day periodicity over a seven month period as well as a scintillation event on 26 June which was probably associated with a blast wave, a geomagnetic storm sudden commencement, and a solar particle event (papers presented at Fall 1974 URSI and AGU meetings and in preparation for J. Geophys. Res.).

From our initial IPS observations at 34.3 MHz we make the following general conclusions: (1) even though IPS-quenching interstellar scattering effects are more pronounced at our observing frequency[8-10], we have observed more than 65 scintillating sources (some at less than 15° galactic latitude) out of approximately 100 sources, implying a larger number of decametric wavelength sources with second-of-arc structure; (2) IPS activity is highly variable even at large solar elongation angles; (3) IPS activity is sometimes observed at high ecliptic latitudes which has no apparent correlation with low latitude activity; (4) IPS can be observed on some sources to within less than 20° of the sun; (5) ionospheric scintillation effects can be suppressed by a combination of bandpass and aperture filtering.

In addition to the IPS studies, observational programs dealing with planetary sources, pulsars, flare stars and x-ray sources are underway.

We acknowledge the encouragement of Dr. Norman F. Ness, Dr. Donald J. Williams, and Prof. James A. Van Allen and the support of NASA, NOAA, and the Atmospheric Science Section of NSF.

TABLE 1

PARAMETERS OF THE COCOA-CROSS RADIO TELESCOPE

A.	Array Type:	Mills Cross	135.5λ EW x 95.25λ NS
B.	Linear Dimensions	NS Arm	66m EW x 832m NS
		EW Arms	1184m EW x 46m NS
C.	Antenna Elements:	Type	Balsley-Ecklund[6] Colinear-Coaxial
		Polarization	East-West
		Length	NS Arm 7.2λ EW Arm 3.8λ
		EW Beamwidth	NS Arm 8° EW Arm 15°
D.	Element Organization:	NS Arm	128 elements spaced 0.75λ NS
		EW Arm	256 elements in 32 banks spaced 4λ EW with 8 elements per bank spaced 0.75λ NS
E.	Feed and Phasing:	Branch feed, diode-switch-controlled tapped phasing lines with real-time delay control for wideband coherence.	
F.	Steering:	NS	$\pm$ 60° from zenith, 33° $\pm$ 60° in declination.
		EW	meridian transit $\pm$ 10 minutes
G.	Beamwidth:	NS Arm	8° EW x 0.6° secant (z) NS
		EW Arm	0.4° EW x 11° NS
		Composite	0.4° EW x 0.6° secant (z) NS

TABLE 1 (continued)

H.	Collecting Area:	NS Arm	3.5×10^4 m^2
		EW Arm	3.7×10^4 m^2
		Total	7.2×10^4 m^2
I.	Array Response:	$26\,^{\circ}K/10^{-26}$ W/m^2-Hz	(uniform illumination)
J.	Center Frequency:	34.3 MHz	(λ = 8.75 meters)
K.	Bandwidth:	1 MHz maximum	

REFERENCES

[1]Burnell, S. J., Nature, 224, 356-357 (1969).

[2]Sharp, L. E. and Harris, D. E., Nature, 213, 377-378 (1967).

[3]Wiseman, M. and Dennison, P. A., Proc. Ast. Soc. Australia, 2, 79-82 (1972).

[4]Ward, B. D., Compilation of Solar Particle and Interplanetary Measurements Acquired During the Campaign for Integrated Observations of Solar Flares (CINOF), ed. M. A. Shea and D. F. Smart, Air Force Cambridge Res. Lab, AFCRL-TR-740271, 43-47 (1974).

[5]Dennison, P. A. and Wiseman, M., Proc. Ast. Soc. Australia, 1, 142-145 (1968).

[6]Balsley, B. B. and Ecklund, W. L., IEEE Trans. Ant. Prop., AP-20, 513-516 (1972).

[7]Tatarskii, V. I., The Effects of the Turbulent Atmosphere on Wave Propagation, (Israel Program for Scientific Translation), U. S. Dept. of Commerce; U. S. National Technical Information Center, 272-277 (1971).

[8]Readhead, A. C. S. and Hewish, A., Nature, 236, 440-443 (1972).

[9]Lovelace, R. V., Saltpeter, E. E. Sharp, L. E., and Harris, D. E., Astrophys. J., 159, 1047 (1970).

[10]Harris, D. E., Harvard College Obs. Center for Astrophysics Preprint Series No. 129, submitted to Astron. J. (1974).

FIGURE CAPTIONS

Figure 1 Simplified block diagram of RF, IF and post detection circuitry. Symbols:  amplifier;  iso-T;  double balanced mixer;  analog multiplier;  30 second RC time constant;  RC differentiator. L. O. frequency is 54.3 MHz, IF is 20 MHz. Not shown are additional amplifiers and filters, and circuitry for measuring additional correlation products.

Figure 2 Observations taken on 5 October 1974. Data channels are identified as in Figure 1. Relative sensitivity of channels is constant in time except on channel S which is reduced by 4 during transit of 3C280. Polarity of correlation response I can be either positive or negative. Channel F is the raw fluctuation power; channels D, S and I_{30} have a 30 second time constant and are therefore delayed by 30 seconds with respect to channel I_1 which has a 1 second time constant. Rectangular spikes on I_1 are calibration signals after rephasing for the next source.

Figure 3 Observations of Quasar 3C186 taken between 24 and 27 November 1974. Channels are identified as in Figure 2. Rectangular pulse after transit on channel I_1 is re-phasing and calibration. Scintillation activity changes significantly between days 329 and 330.

A-G75-2

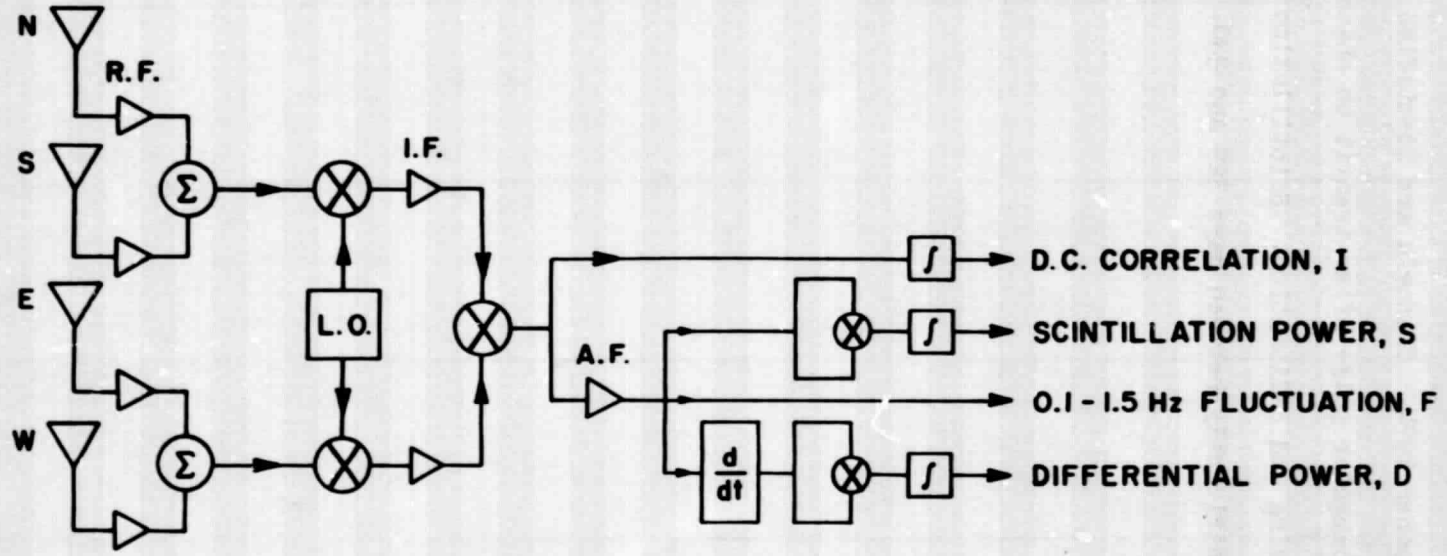

Figure 1

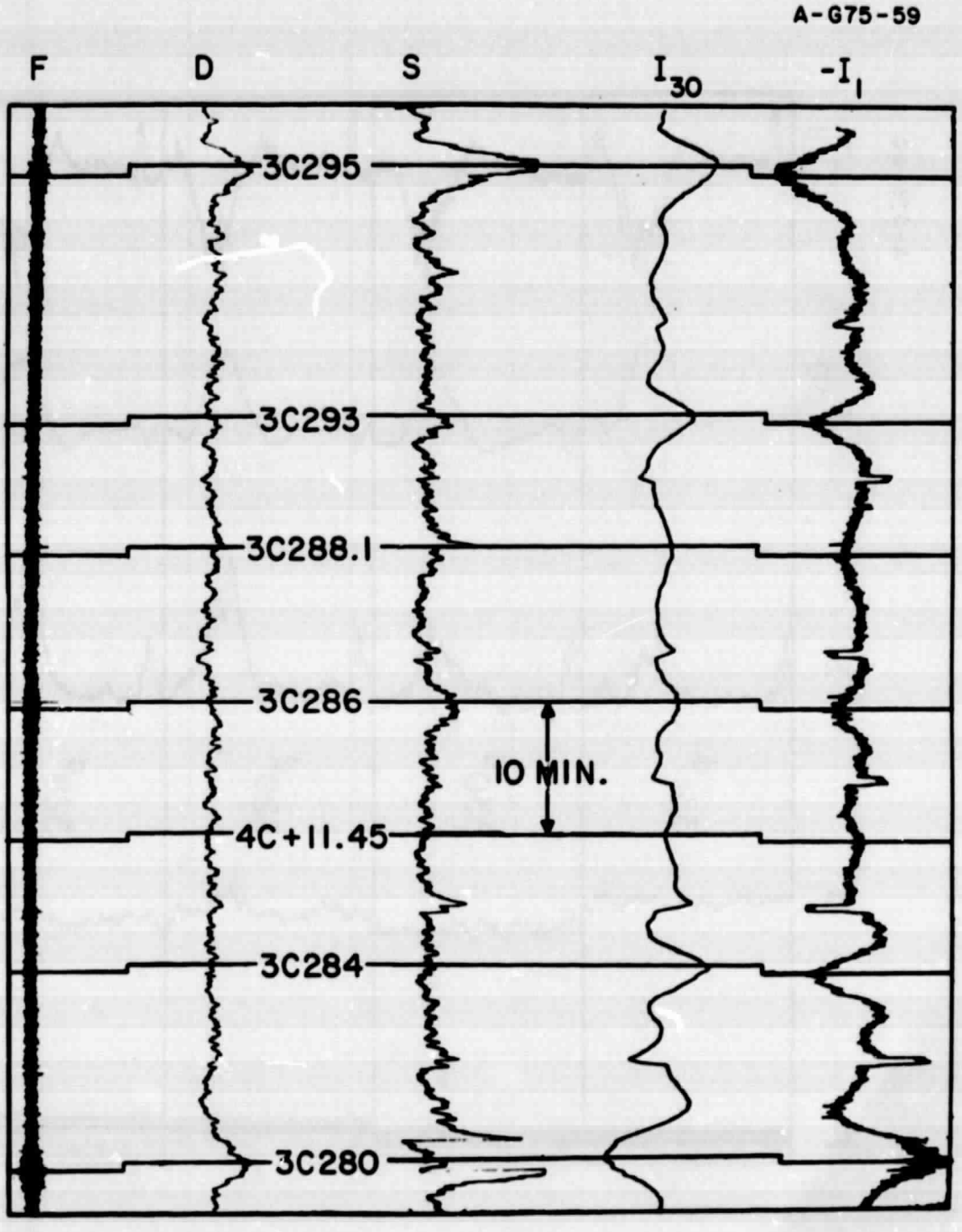
A-G75-59
F
D
S
I_{30}
$-I_1$
3C295
3C293
3C288.1
3C286
10 MIN.
4C+11.45
3C284
3C280

Figure 2

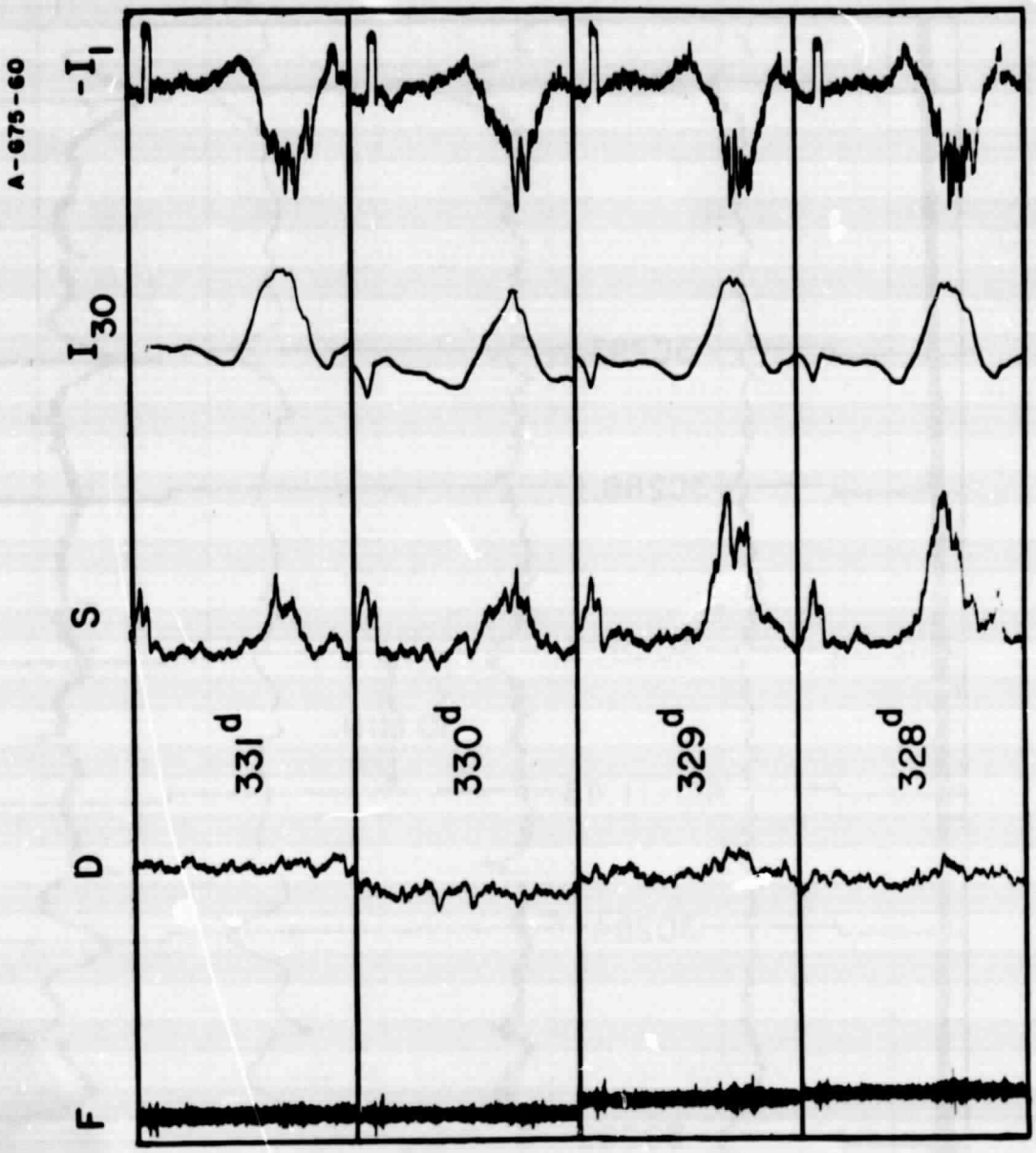

Figure 3